Ca²⁺-signalling in *C. intestinalis* notochord cells during embryonic development

by

Morsal Saba

This thesis is submitted in partial fulfilment of the requirements for the degree of Master of Science

Sars International Centre for Marine Molecular Biology, University of Bergen

&

Department of Biological Sciences, University of Bergen

April 2018

Acknowledgments

The work presented in this thesis was completed at Sars International Centre for Marine Molecular Biology, through the Department of Biological Sciences (BIO), at University of Bergen from spring 2017 to spring 2018.

First and foremost I would like to thank my main supervisor, Marios Chatzigeorgiou, for his immense support, tremendous guidance, constructive feedback and encouragement during the course of my thesis. I would also like to thank my co-supervisor, Riccardo Esposito, for his supervision and advice in the lab, who was always there to help whenever it was needed. It is safe to say that I have been challenged in many ways throughout this year, but never without support from my supervisors to help me achieve my goals, for which I am forever grateful.

I am additionally thankful for all the help I got from Daniel Dondorp, who accelerated my data-analysis process with his impressive programming skills. Furthermore, I would like to thank the rest of my dear S13 lab members, especially Felicia Keulder, Jerneja Rudolf and Zonglai Liang, and the rest of Sars, for making me feel as part of the team.

I also would like to express my appreciation to my study supervisor, Lill K. Knudsen, for her quick thinking and solution-oriented mind-set. Compliments should also be given to the rest of the staff at Molecular Biology section of BIO, such as Grethe Aarbakke, who has always helped to assist and support me when needed. It might have been small deeds for them, but it meant the world to me. I would also like to thank my fellow students at Molecular Biology brance, and of course Helix, for establishing a cozy student environment.

Lastly, I would like to express my gratitude to my family and friends for their loving support throughout my education. I sincerely appreciate all the love and care.

Bergen, April 2018

Morsal Saba

Table of Contents

IV

V

List of Abbreviations

Abbreviation	Full words
2APB	2-aminoethyl diphenylborinate
BCIP	5-Bromo-4-Chloro-3'-indolyphosphate p-toluidine salt
Cah3	Carbonate anhydrase III
Calmodulin	Calcium-modulated protein
DABCO	1,4-diazabicyclo[2.2.2]octane
EtBr	Ethidium Bromide
FASW-T	Filtered artificial seawater buffered with TAPS
Gado^{3+}	Gadolinium (III) chloride hexahydrate
GB	Glycine in PBT
GCaMP6s	Ultrasensitive protein calcium sensors
HB	Hybridization buffer
IP$_3$R	Inositol triphosphate receptor
IVT	In-vitro transcription
LB-Medium	Lysogeny broth medium
LB-Medium-AMP	Lysogoney broth medium with ampicillin
MEM-PFA	MOPS-EGTA-Magnisium sulphate- -paraformaldehyde
NaOAc	Sodium Acetate
NaTIO	Sodium Thioglycolate
NBT	Nitro-blue tetrazolium chloride
NFAT5	Nuclear Eactor of Ectivated T-cells 5
PBS	Phosphate buffered saline
PBT	Polybutylene terephthalate
PFA	Paraformaldehyde
PreHB	Pre-hybridization buffer
RNAi	RNA interference
ROI	Region Of Interest
SERCA	Sarco/endoplasmic reticulum calcium ATPase
shRNA	Short hairpin RNA
snRNA	Small nuclear RNA
SOCE	Store-Operated Calcium Entry
TAE buffer	Tris-Acetate-EDTA buffer
TMN	Tris-MgCl$_2$-NaCl
TNB	Trinitrobenzene
TNT	Trinitrotoluene
Tween-20	Polyoxyethylene (20) sorbitan monolaurate

Abstract

C. intestinalis notochord is an essential structure during embryonic development, conveying position and fate information, in addition to serving as a structural support and enabling locomotion during larval stage. Researchers have previously presented Ca^{2+}-signalling as a key element in development of many organisms, but few have performed detailed studies on *C. intestinalis*. This thesis aimed to elucidate the mechanism underlying Ca^{2+}-signalling in developing *C. intestinalis* notochord, through four sub-aims: 1) Determine whether the notochord cells exhibit Ca^{2+}-signalling activity during development, 2) Determine the contribution of various subcellular compartments, known to store/release Ca^{2+}, to the observed Ca^{2+}-signalling activity, 3) Study the mechanisms underlying Ca^{2+}-signalling in the notochord cells, and 4) Study the effects of calcium pathway on the actomyosin network, which mediates cell motility and cell shape changes.

The results present evidence of Ca^{2+}-signalling in *C. intestinalis* notochord cells at all studied developmental stages; as continues blips, waves, and short/long lasting blinks in individual cells, and/or blinks travelling in-between cells. Waves seem to dominate stages 22-24, whereas blinks appear to dominate stages 24-26. For the sake of simplicity, the Δ used in this context stands for "change in". There is a significant difference in terms of number of peaks, (Δ) peak intensity and (Δ) duration, between stage 22 and 23, and from stage 24 and onwards, but not between stage 23 and 24. The number of peaks appears to depend on cation channels and gap junctions, whereas the (Δ) signal intensity seems to rely on cation channels, gap junctions, IP_3R and SOCE. As for (Δ) signal duration, it might depend on IP_3R and SOCE as well. Furthermore, calmodulin is indicated to be important during stage 23 but not during stage 22, insignificant for number of peaks except for stage 23, and its significance various from stage 24-26. With regards to SERCA, stage 22, and 24-25 suggest independence, whereas stage 23 and 26 seem to depend to some degree. Calmodulin and SERCA data also indicate cell non-autonomous behaviour, as it is hinted in calmodulin RNAi with regards to differences in both AP and M compared to wild type. Ca^{2+}-signalling inhibition also affects the notochord actomyosin network. Specifically, $Gado^{3+}$ and 2APB affect the cell structures and protein expression already from 3hpi and onwards. Carbenoxolone inhibition, on the other hand, leads to visually different protein expression and cell shape from 6hpi and onwards. Lastly, this study further presents Ca^{2+}-signalling in epidermal and muscle cell, implying importance in tail relaxation, twitching, and movement during embryonic development.

1. Introduction

1.1 Origins of the notochord

1.1.1 Notochord development

The notochord is one of the defining structures of chordates, where it has previously been described to originate in, and plays an important role in chordate development. This embryonic midline structure exists transiently in higher vertebrates during embryogenesis. It is positioned in the centre of the embryo with respect to the dorsal-ventral (DV) and the left-right (LR) axes. During early gastrula stage, the dorsal midline mesoderm, which is the direct precursor of the notochord, becomes morphologically and molecularly distinct from the rest of the mesoderm. The dorsal midline mesoderm is then forced into an elongated stack of cells by cellular rearrangements. These cellular rearrangements involve the mediolateral intercalation and convergence of cells towards the dorsal midline. The dorsal midline mesoderm cells then obtain a thick extracellular sheath and a vacuole, where osmotic pressure within the vacuole acts against the sheath. This leads to the characteristic rod-like structure of the notochord. The pressure between the sheath and vacuole also provides the notochord with essential mechanical properties for embryonic elongation and locomotion. (Stemple, D. L. 2005)

1.1.2 Notochord function

The notochord can have a range of signalling functions depending on the organism. In terms of the notochord's function in signalling, it produces secreted signalling factors to the surrounding tissues. The signalling factors convey position and fate information, such as midline patterning cues involved in neural tube patterning and mediolateral patterning of vertebrate somites. The notochord has additionally an essential structural role in the developing chordates as well. The latter is due to the notochord being closely related to, and likely representing a primitive form of, cartilage. The notochord thus serves as an axial skeleton for the embryo, until other elements such as the vertebrae form. In higher vertebrates, the notochord ossifies in regions of forming vertebrae, and contributes to the centre of the intervertebral discs. In invertebrate chordates, the notochord exists during the embryonic and larval free-swimming stages, and provides an axial structural support that is necessary for locomotion. (Stemple, D. L. 2005)

1.2 *Ciona intestinalis* notochord

1.2.1 *C. intestinalis* notochord development

The existence of a group of animals, resembling present day ascidian larvae, has been described to diverge into two great branches. One of the branches is stated to further develop into present day class of Ascidians, with the other leading to the Vertebrata. The ascidian tunicate, *C. intestinalis*, is therefore regarded as closely related to vertebrates in terms of development, the relative position of the nervous system, and possession of a structure that resembles vertebrate *chorda dorsalis*. (Annona, G., N.D. Holland, and S. D'Aniello. 2015) But while the notochord ossifies in regions of forming vertebrae in vertebrates, it exists transiently during the embryonic and larval free-swimming stages in *C. intestinalis* (Stemple, D. L. 2005). The notochord of the latter lies in the centre position of the tail with muscles flanking on both sides, providing structural support and enabling locomotion in the larva free-swimming stages (**Figure 1.1**) (Denker, E., and D. Jiang. 2012).
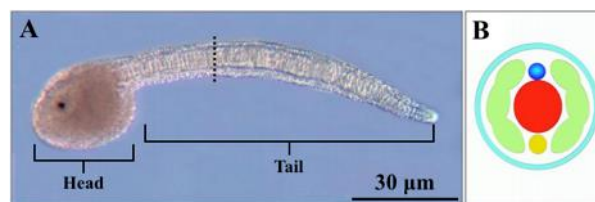
Figure 1.1 Late tailbud C. intestinalis notochord. The notochord is illustrated in side view, with the head and tail indicated in **A**. The diagram of the cross section in **B**, through the dotted line in the side view (**A**), depicts the nerve code (blue), notochord (red), axial muscles (green), and endoderm (yellow). (Modified from; Annona, G., N.D. Holland, and S. D'Aniello. 2015)

The *C. intestinalis* notochord structure resembles a straight tube closed at both ends, and its development can be divided into distinct stages. The development starts when the notochord cells are first induced at the blastula stages, which then becomes committed before gastrulation commences. During gastrulation, the notochord cells divide twice in a coordinated manner, where the resulting 40 cells are organized as a monolayer sheet (**Figure 1.2**, **Stage I**). The subsequent developmental stages include morphogenetic events involving cell shape changes, lumen formation, and tissue reconfiguration. During **Stage II**, invagination of the sheet of notochord cells leads to formation of a rod of notochord cells. The cells then intercalate radially and medio-laterally during neurula and early tailbud stages,

through the process of convergent extension (**Figure 1.2, Stage III**). The latter results in the formation of a columnar notochord consisting 40 cells, in a "stack of coin configuration". This marks the initial status before the onset of tubulogenesis. (Denker, E., and D. Jiang. 2012)

Stages I-III: Commitment, divisions, and intercalation of notochord cells to form a rod-like structure   A↔P
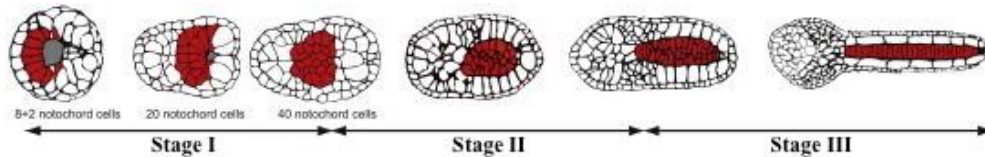
Figure 1.2 Embryonic notochord development stages I to III and their morphogenesis. The developmental stages are indicated in the figure, in addition to illustration of notochord morphogenesis within each stage. Notochord cells are coloured in red, and the embryos anterior-posterior (A↔P) part marked. Stages I-III here represent Hotta stages 10-22. (Modified from; Denker, E., and D. Jiang. 2012).

Tubulogenesis starts during **Stage IV** (**Figure 1.3**), where individual notochord cells are elongated along the anterior-posterior axis. During this stage, the diameter of each notochord cell decreases while its length increases, leading to transformation of notochord cells from the coin-shape into cylindrical shape. Equatorial contractile actomyosin rings, and other actin-binding proteins mediate this elongation process (Denker, E., and D. Jiang. 2012). The apical/luminal domains, and the extracellular lumen, thereupon emerge at the opposite ends of each cell during **Stage V**. Each notochord cell then initiates a bidirectional movement during **Stage VI**. The latter movement leads to the merge of two apical domains (except for the anterior- and posterior-most notochord cells), the morphology of the cell converting to endothelial-like shape, and the neighbouring lumen pockets being fused together. The tubulogenesis in *C. intestinalis* has been described to depend on exocytosis-based extracellular lumen formation. (Denker, E., and D. Jiang. 2012).

Stages IV-VI: Notochord tubulogenesis   **A↔P**
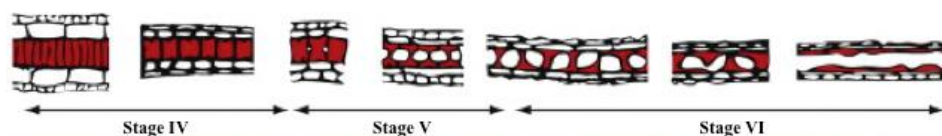
Figure 1.3 Embryonic notochord development stages IV to VI and their morphogenesis. The developmental stages are indicated in the figure, in addition to illustration of notochord morphogenesis within each stage. Notochord cells are coloured in red. Lumen formation, starting at Stage V, is depicted as the white area in-between the red coloured notochord cells. The notochords anterior-posterior (A↔P) part is also marked. Stages IV-VI here represent Hotta stages 23-26. (Modified from; Denker, E., and D. Jiang. 2012).

1.2.2 *C. intestinalis* notochord function

The transportation of gases, fluids, and cells throughout the whole organism and its tissues, is essential for *C. intestinalis*. Such transport, in addition to providing structural support, enabling locomotion during larvae stage, and signalling functions as stated in section **1.1.2**, is facilitated by its notochord. The process of its notochord tubulogenesis includes cellular processes such as cell shape change, cell proliferation, mesenchymal-epithelial transition, cell polarization, cell migration, and lumen formation. Disruption in any of these processes can lead to diseases. (Denker, E., and D. Jiang. 2012).

1.2.3 Study of notochord in *C. intestinalis*

C. intestinalis has emerged as an ideal system to better understand chordate development, genome organization, and notochord function. Genes involved in its notochord development have been characterized by taking advantage of its simple organ development, well-characterized genome, and high quantity transcriptome data. (Satoh, N., et al. 2014)

One of the first genes to be identified is a member of the T-box transcription factor family, called *Brachyury*. This gene is shown to play a major role in *C. intestinalis* notochord development. The expression of the *Ci-Bra* gene takes place from the 64-cell stage and onwards in notochord precursor cells. Moreover, approximately 400 genes have been characterized as *Brachyury* downstream cascade genes. Furthermore, maternally expressed genes such as *β-catenin* and *P60*, and zygotically expressed genes *FoxD, FoxA, FGF9/16/20*, and *ZicL*, have also been described to be involved in the upstream cascade of *Ci-Bra* transcriptional activation. (Satoh, N., et al. 2014) The transcriptional cascade starts with *β-catenin.* If the latter is supressed, it can lead the inhibition of notochord cell differentiation. (Yagi, K., Satou, Y., Satoh, N., 2004) This effect is mediated by the interactions between *β-catenin* and *FoxA*. Suppression of *FoxA* can lead to abolishment of *Ci-Bra* gene expression (Passamaneck, Y. J. et al. 2009), which in return can result in failure of notochord cell differentiation (Satoh, N., et al. 2014).

Several microarray studies have also been performed on the notochord, making it an interesting model used for linking genes to function (Takahashi, H., et al. 1999; Hotta, K., et al. 2000). *C. intestinalis* notochord also serves as an interesting model to study its morphological properties, due to the abundance of biological tubes in different organisms

(Andrew, D.J. and A.J. Ewald. 2010; Lubarsky, B. and M.A. Krasnow. 2003). Biological tubes have distinct origins, morphogenesis and functions, but different cells and tissue types still use some conserved set of tools to undergo branching morphogenesis. (Andrew, D.J. and A.J. Ewald. 2010; Lubarsky, B. and M.A. Krasnow. 2003; Lu, P.F. and Z. Werb. 2008)

1.3 Calcium signalling and ion channels in embryonic development

1.3.1 Calcium as an important second messenger

Biological systems adapt to changing environments by means of cell signalling, where the concentration of the cell signalling messengers varies with time. Calcium ions, as one of these messengers, have an important role in mediating such cell signalling. Ca^{2+} ions thus influence nearly every aspect of cellular life, by taking part in processes such as changes in protein conformation, and control of calcium concentration in cytoplasm and organelles. Additionally, Ca^{2+}-mediated signal transduction is involved in excitability, exocytosis, motility, apoptosis, and transcription. (Clapham, D.E. 2007)

Ca^{2+} binding can also alter protein shape and charge, thus regulating protein function. A conformational change as such is one of the universal tools of signal transduction in cells. For example, calmodulin is a Ca^{2+} adaptor protein that changes in shape upon Ca^{2+} binding. This conformational change then triggers the adaptor protein's function in relieving protein autoinhibition, active site remodelling, and protein dimerization. But since Ca^{2+} is regarded as a risky divalent that cannot be altered, it has to be chelated, compartmentalized or extruded by the cells. (Clapham, D.E. 2007)

ATPase pumps facilitated extrusion of Ca^{2+} into the endoplasmatic reticulum (ER) via sarcoendoplasmic reticular Ca^{2+} ATPases (SERCA pumps), or out of the cells via plasma membrane Ca^{2+} ATPases (PMCA pumps) (**Figure 1.3**). There are also other mechanisms to extrude Ca^{2+}, such as; the Na^+/Ca^{2+} exchangers (NCX), Na^+/Ca^{2+}-K^+ exchangers (NCKX), or cotransport of one K^+ with one Ca^{2+} in exchange for four Na^+ (NCKX) (**Figure 1.4**). Moreover, the PMCAs maintain low internal Ca^{2+} concentrations over long periods. The NCX and NCKX, on the other hand, enable rapid concentration adjustments needed during e.g. generation of action potentials in neurons. An increase in PMCA Ca^{2+} affinity, and ATPase pump rate, can also be facilitated by calmodulin adaptor protein. (Clapham, D.E. 2007)
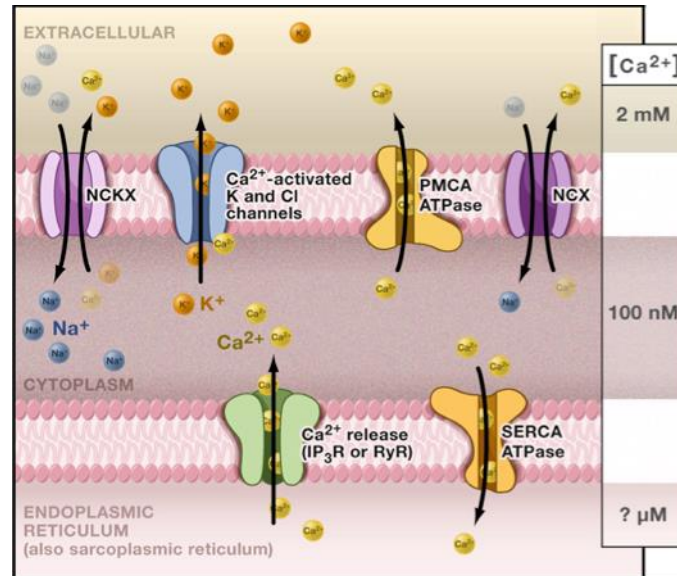
Figure 1.4 Maintaining Ca^{2+} levels for signalling. Extrusion by plasma membrane Ca^{2+}ATpase (PMCA) and sarcoendoplasmic reticular Ca^{2+} ATPases (SERCA pumps) maintain low cytoplasmic Ca^{2+} concentration, at ca. 100 nM, in resting cells. Ca^{2+} is released from ER by inositol-1,4,5-trisphosphate receptor (IP$_3$R), or ryanodine receptors (RyR), into cytoplasm. Na/Ca exchanger (NCX), and K+ channels or Cl- channels activated by intercellular Ca^{2+}, serve as secondary Ca^{2+} concentration regulators. Coloured spheres are Na$^+$ (blue), K$^+$ (orange), and Ca^{2+} (yellow). (Modified from; Clapham, D.E. 2007)

Furthermore, dramatic changes within a cell can be initiated through rapid Ca^{2+} signalling proteins such as voltage-gated Ca^{2+} channels (CaV) (**Figure 1.5**). Transient receptor potential (TRP) ion channels can also increase intercellular Na$^+$ and Ca^{2+} ions. Many of the latter channels are potentiated by phospholipase C (PLC) activation through G protein-coupled (GPCR) or tyrosine-kinase receptors (RTK). GPCRs mediate Ca^{2+}-signalling through Ca^{2+} release from intracellular compartments. Through a chain reaction, GPCRs activate PLCβ, and RTK activates PLCγ, which results in phosphatidylinositol-4,5-bisphosphate (PIP$_2$) being cleaved into inositol-1,4,5-trisphosphate (IP$_3$) and diacylglycerol (DAG). Binding of IP$_3$ to the IP$_3$R ER-channel then allows Ca^{2+} diffusion from ER to increase intracellular Ca^{2+} concentration. Flow of ER Ca^{2+} is also mediated by other receptors such as ryanodine receptors (RyR). (**Figure 1.5**) When the ER Ca^{2+} concentration is depleted, a store operated mechanism, known as Stim/Orai channel (SOC), is activated. The latter leads to a Ca^{2+}-release activated current (CRAC) that replenishes the ER with Ca^{2+} again. (**Figure 1.5**) (Clapham, D.E. 2007)
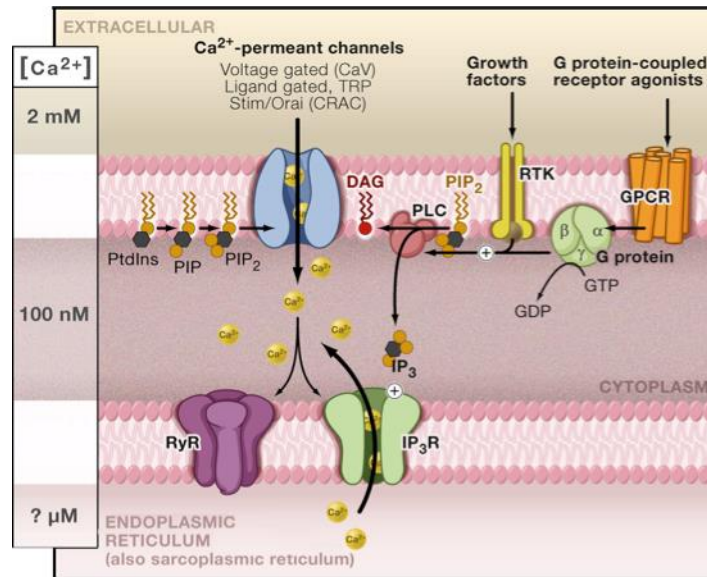
Figure 1.5 Excitatory signalling enabled by using Ca^{2+} gradients. The plasma membrane ion channels are opened due to change in voltage, or binding of extra- or intracellular ligands. G protein coupled receptor (GPCR) or tyrosine receptor kinase (RTK) mediates activation of PLC, resulting in cleavage of phosphatidylinositol-4,5-bisphosphate (PIP$_2$) into inositol-1,4,5-trisphosphate (IP$_3$) and diacylglycerol (DAG). IP$_3$ then binds to IP$_3$R ER-channel and allows Ca^{2+} diffusion from ER to intracellular matrix. PLCβ activation by GPCR is enabled by conversion of GTP to GDP. PLCγ activation occurs by dimerization of RTKs upon ligand binding, followed by autophosphorylation and interaction with other signalling proteins. Ca^{2+} diffusion is also mediated by ryanodine receptors (RyR). Ca^{2+} is depicted as yellow spheres. (Modified from; Clapham, D.E. 2007)

1.3.2 Calcium signals described as waves, puffs, quarks and sparks

Ca^{2+} signals have been described as intracellular Ca^{2+} waves, i.e. Ca^{2+} signals resulting from neighbouring receptors that excite each other and produce Ca^{2+}-induced Ca^{2+}-release waves (Bootman, M. and M.J. Berridge. 1996), in addition to blips, puffs, quarks and sparks (Webb, S.E. and A.L. Miller. 2003). A blip can be defined as a signal resulted from opening of on an individual IP$_3$R, whereas a puff would describe a signal resulted due to a group of IP$_3$Rs opening (Bootman, M. et al. 1997; Yao, Y., J. Choi, and I. Parker. 1995; Webb, S.E. and A.L. Miller. 2003). As for quark, it is a signal cause by opening of an individual RyR. A signal due to opening of a group of RyRs would then be described as a spark. (Lipp, P. and E. Niggli. 1998; Cheng. H., W.J. Lederer, and M.B. Cannell. 1993; Webb, S.E. and A.L. Miller. 2003)

1.3.3 Calcium signalling during embryonic development

Previously described Ca^{2+}-signalling features in mature cells and tissues, are now being found during embryonic development as well (Clapham, D.E. 2007; Webb, S.E. and A.L. Miller. 2003). Intracellular Ca^{2+}-signalling during fertilization and early zygotic developmental stages, are suggested to form the groundwork for majority of subsequent intra- and inter-cellular signalling events, which occur as the embryonic development proceeds. As the development proceeds, the increase in amount of embryonic cells becomes inversely proportional with the size of the cells. This results in individual cells being surrounded by an increasing amount of neighbouring cells. An increase in cell behaviour and cell signalling complexity, accompanied by initiation of developmental events requiring coordinated activity, initiates localized intercellular Ca^{2+}-signalling. Coordination on a broader scale is then required during widespread cellular rearrangements occurring during gastrulation, germ-layer formation, and body axes establishment. The intracellular signalling events afterwards become more localized again, in addition to reappearance of intracellular signalling from individual cells, associated with embryonic organogenesis. (Webb, S.E. and A.L. Miller. 2003)

Calcium waves have for example been studied in fertilized Ascidians eggs. In *P. mammillata*, and in a similar manner in *C. intestinalis*, a large calcium pulse starts at sperm entry point and then spreads like a wave across the egg. This activating pulse is followed by a series of 12-25 periodic pulses in *P. mammillata*, which occur during between fertilization and completion of meiosis. (Speksnijder, J.E., C. Sardet, and L.F. Jaffe. 1990) Gradients of intracellular Ca^{2+} and IP_3 have also been suggested to help with establishing the dorsal-ventral (DV) axis of a variety of developing embryos. In *D. rerio*, the ventral region of its blastoderm has shown prolonged intracellular Ca^{2+} concentration rise at shield stage. During gastrulation, several rapid axial intercellular Ca^{2+} waves have been described to move up the trunk towards the embryos anterior part. The cells have been suggested to sense the latter waves through cell-adhesion molecules, which are Ca^{2+} sensitive, and thus might modulate cell behaviour in accomplishing convergent extension. (Gilland, E., et al. 1999; Reinhard, E., et al. 1995; Webb, S.E. and A.L. Miller. 2003) Furthermore, intracellular Ca^{2+} and IP_3 gradients have also been suggested to take part in establishing DV axis in Xenopus for example. Similar axial waves have additionally been suggested to function in Xenopus neural ectoderm specification.

(Webb, S.E. and A.L. Miller. 2003) Cytosolic Ca^{2+} signalling has as well been studied in *D. melanogaster* development, where generation of Ca^{2+} gradients was shown along the DV axis. Gradients formed during blastoderm cellularization were stated to be the most pronounced, due to high a Ca^{2+} concentration in the dorsal region. The latter study suggested Ca^{2+} as an important player in specification of embryonic dorsal region. (Webb, S.E and A.L. Miller. 2003; Creton, R., J.A. Kreiling, and L.F. Jaffe. 2000)

1.3.4 Calcium signalling in vertebrate organogenesis

Accumulative lines of research also suggest that Ca^{2+}-signalling plays an important role in vertebrate organogenesis. During nervous system development, Ca^{2+}-signalling has for example been stated to take part in varying processes ranging from neural induction to neuronal differentiation, including neural tube formation from the neural plate. Ca^{2+}-signalling is also indicated to be crucial for brain development, by being involved in differentiating and regionalizing the central nervous system. (Webb, S.E. and A.L. Miller. 2003) During eye development, formation of the optic cup through optic vesicle invagination has been reported to be under Ca^{2+} regulation as well. (Webb, S.E. and A.L. Miller. 2003) The involvement of Ca^{2+}-signalling stretches further to heart formation, in addition to regulating normal heart activity (Creton, R. and K.E. Speksnijder. 1998; Linask, K.K. and K.A. Knudsen. 1997), muscle (Ferrari, M.B and N.C. Spitzer. 1999; Kelu, J.J. et al. 2017) and kidney formation (Seville, R.A. et al. 2002; Lederc, C. et al. 2008).

1.3.5 Calcium signalling in invertebrate organogenesis

The contribution of Ca^{2+}-signalling in *C. intestinalis* embryogenesis and organogenesis has been known for some time. Some of the earlier studies focused on how the signal was induced in the egg upon fertilization with sperm. (Webb, S.E. and A.L. Miller. 2003; Hackley, C., et al. 2013) More recent studies have focused on involvement of Ca^{2+}-signalling in anterior neural plate development, where a connexin gene is transiently expressed. The latter study was performed by electroporating the embryos with GCaMP5 Ca^{2+} indicators, which resulted in Ca^{2+} transients expressing the Ca^{2+} indicator in the neural plate. (Hackley, C., et al. 2013) T-type calcium channels (TTCC) have also been hypothesized as necessary for proper anterior neural tube closure. This is because a loss of TTCC can lead to failure in sealing the anterior neural folds. (Abdul-Wajid, S., et al. 2015) More recent studies have also focused on embryo-wide calcium activity. In relation with the latter, Ca^{2+} transients were detected in;

muscle cell precursors at late gastrula stage, left and right neurogenic cells repetitively at neurula stage, differentiating nerve code neuron precursors at early tailbud stage, and in a wide area of epidermal cells at mid tailbud stage. The transients in the latter stage increased both in terms of number and frequency, and coincided with relaxation of the tail bending. (Akahoshi, T., K. Hotta, and K. Oka. 2017) There is however still very few detailed organogenesis studies on *C. intestinalis*, involving Ca^{2+}-signalling, compared to other invertebrates.

Moreover, recent studies have established the role of global calcium dynamics during *C. elegans* development. Calcium transients have for example been characterized to be important for muscle contraction, where the spread of a large Ca^{2+} wave is accompanied by contraction of one of the dorsal muscle bundles. Brain-wide calcium imaging has as well revealed high calcium activity in ventral nerve cord (VNC) motor neurons, where one of the cells is hypothesized to be involved in muscle contraction as well. Furthermore, a reversal in the eggshell was also found to correlate with the activity of calcium transients in pre-motor interneurons (AVA). (Ardiel, E.L., et al. 2017) Spontaneous long-range Ca^{2+} waves have additionally been visualized in developing butterfly wings. The waves displayed slow propagation over long distances in developing pupal wing tissue. Induced ectopic eyespots by physical damage, was also followed by Ca^{2+} waves spreading from the periphery of the damaged site. Additionally, pharmacological studies involving the wings and Ca^{2+}-ATPase inhibitors led to undeveloped wing scale and colour pattern abnormalities. (Ohno, Y. and J.M. Otaki. 2015) Corroborating these findings, studies of Drosophila extract have shown Ca^{2+}-signalling to be important for imaginal disc development as well. Complex calcium dynamics were described to occur as intercellular waves that traversed large tissue domains, in addition to calcium spikes that were confined to local domains of neighbouring cells. Ca^{2+}-signalling has also been suggested to take part in regulating the behaviour of epithelial cells through change in cell shape. For example, rapid oscillation of intercellular Ca^{2+} levels occurred in epithelial cells adjacent to a wound site in *D. melangolaster*. The latter changes were accompanied by local actomyosin flow and cell constriction, which contributed to formation of an actomyosin cable that sealed the wound site. Ca^{2+}-signalling might thus play an important role in regulating actomyosin networks with regards to cell shape changes and cell movements in muscle- and non-muscle cells. (Balaji, R., et al. 2017) In general, there is still a

growing effort to identify the molecular cascades generating Ca^{2+}-signalling, including the downstream targets and its function in various developmental processes.

1.4 *Ciona intestinalis* as experimental model

From an evolutionary perspective, *C. intestinalis* is regarded as the sister group of vertebrates, as both branches diverged from a common ancestor (Annona, G., N.D. Holland, and S. D'Aniello. 2015; Delsuc, F., et al. 2006). In recent years, *C. intestinalis* has thus emerged as a model system to study chordate development and genome organization. This is because the ~160 Mb genome of *C. intestinalis* is well annotated, and a high quantity of transcriptome data is also available from this animal (Aniseed database: https://www.aniseed.cnrs.fr/; Ghost database: http://ghost.zool.kyoto-u.ac.jp/cgi- bin/gb2/gbrowse/kh/) (Satoh, N., et al. 2014; Passamaneck Y.J. and Di Gregorio A. 2005).

There is additionally a great deal of characterized regulatory elements, i.e. promoters, which can be used to study the development of a particular organ. The invariant cell lineage of *C. intestinalis* is also well documented, making it easy to trace every cell in the developing embryos back to the zygote. (Delsuc, F., et al. 2006; Passamaneck Y.J. and Di Gregorio A. 2005) *C. intestinalis* has the additional advantage that several key Gene Regulatory Networks (GRNs) underlying developmental processes have been delineated. It is thus possible to map entire pathways involved in certain processes, such as notochord development. (Lemaire, P. 2011) *C. intestinalis* serves as an easy model to study notochord development also because it possesses only 40 notochord cells. It can additionally be labelled by means of electroporation with fluorescent proteins using transgenes, and easily imaged by means of fluorescent microscopy due to its transparent embryos. Given that both embryonic development and tubulogenesis take place within a short timescale, the entire process can be imaged live during a practical amount of time. When reared at 18°C for example, *C. intestinalis* larvae can become fully developed within 18 hours (**Figure 1.6**). (Passamaneck Y.J. and Di Gregorio A. 2005)
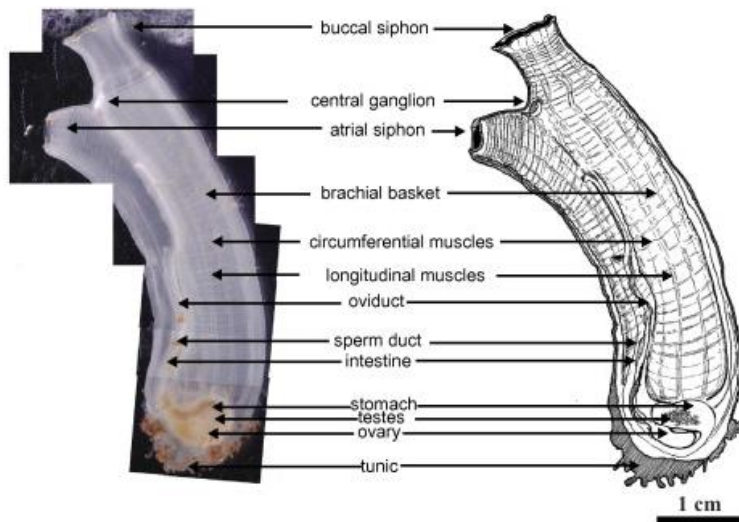
Figure 1.6 Adult *Ciona intestinalis* anatomy and its schematic view. The anatomical features are depicted in the figure. (Modified from; Colacci, M. et al. 2005)

The transparency of the embryos also makes it possible to perform in-situ hybridization to examine *C. intestinalis* gene expression (Satoh N, Satou Y, Davidson B, Levine M. 2003). Additionally, it is possible to examine gene function, by analysing potential phenotypic effects for example, through reverse genetics. The gene function can for instance be disrupted through RNA interference by introducing short hairpin RNA in *C. intestinalis* embryos. (Nishiyama, A. and S. Fujiwara. 2008) The effects of loss of gene function can be studied through CRISPR/Cas9-targeted genome editing as well (Stolfi, A., et al. 2014).

Nordic *C. intestinalis* additionally tolerate temperatures between -1°C to 18°C, where 8°C is the minimum temperature for spawning, over 3°C for egg production, and at 14°C-18°C for somatic growth. The animals also have an optimal salinity tolerance at ca. 38‰, and a pH at 8 or a little above. They additionally require daily algae at 3000 cells/mL, and light 16-18 hours per day or continuous light. In other words, the animals can tolerate much variation in environmental conditions, and lab facilities can be equipped for such thriving conditions (Carver et al. 2006; Petersen et al. 1995) With the latter in place, and the fact that *C. intestinalis* is a hermaphrodite (Lemaire, P. 2011), one can have access to sufficient amount of fertilized embryos for desired experiments. *C. intestinalis* can thus be used as an experimental model system to shed light on mechanisms underlying chordate development.

1.5 Thesis aims

In relation with the given background knowledge, the overall aim of this thesis is to elucidate the mechanisms underlying Ca^{2+}-signalling in developing *C. intestinalis* notochord, through four sub-aims;

1. Determine whether *C. intestinalis* notochord cells exhibit Ca^{2+}-signalling activity during development, by electroporation with Ca^{2+} indicators and in vivo live calcium imaging

2. Use pharmacology and live calcium imaging to determine the contribution of various subcellular compartments, known to store/release Ca^{2+}, to the observed Ca^{2+}-signalling activity

3. Initiate a screen to study the mechanisms underlying Ca^{2+}-signalling in *C. intestinalis* notochord cells, by electroporation with shRNAi constructs and live calcium imaging

4. Study the effects of calcium pathway on the actomyosin network, that mediates cell motility and cell shape changes, in *C. intestinalis* developing notochord by electroporation and pharmacology

2. Materials

2.1 Experimental animals

C. intestinalis were collected from the Norwegian west coast, mostly from Sotra Island and some from Hjellestad in Bergen. The collection period occurred while the animals underwent highly seasonal maturation and spawning, peaking around early spring and summer. SARS Embryology facility in Bergen took care of, and provided, the animals used for this thesis. Optimal condition at the facility were set to be at 10°C-12°C in the tanks, with salinity at 34‰-36‰, and pH at 8-8.2. The light conditions were set at continues warm light at 3000 K, and the FASW-T flow rate was kept at 3.5 L/min in average. All animals were continuously fed algae at 2000-3000 cells/mL every hour, prepared from a mixture of *Isochrysis*, *Chaetoceros*, *Rhinomonas sp.*, *Synechoccus sp.*, and Spirulina powder. The algae culture were kept under constant light, with continuous aeration, and swirled daily. The latter culture was additionally diluted with nutrient enriched seawater, consisting of vitamins and nutrients, twice a week. It was also monitored for good conditions, growth, cell activity and ciliate contamination, once a week.

2.2 Filtered artificial seawater buffered with TAPS (FASW-T)

FASW-T was provided by the SARS Embryology facility in Bergen. The ASW had been prepared from Crystal Sea Bioassay Laboratory Formula from Marine Enterprises International diluted and ddH$_2$O, with 34‰-36‰ salinity. This had been filtered through a 0.22 μM filter, before addition of 10 mL 0.5 M TAPS per liter FASW for a final concentration of 5 mM TAPS (pH 8.2). FASW-T was used in gamete collection, Dechorionation Solution preparation and dechorionation, Sperm-Activator Solution preparation fertilization, and wash of eggs and embryos.

2.3 Dechorionation and fertilization

Table 2.3 Dechorionation and fertilization solutions

Reagent name	Components	Manufacturer	Application
Dechorionation Solution	0.2 mg/mL NaTIO, 0.01 mg/mL pronase, in FASW-T	Own lab products	Dechorionation
Sperm-Activator Solution	0.047 M Tris-HCL, pH 9.5, in FASW-T	Own lab products	Fertilization

2.4 Fixation and in-situ hybridization

Table 2.4 Fixation and in-situ hybridization buffers/solutions

Reagent name	Components	Manufacturer	Application
Fixation Solution A	4% PFA, 0.1 M MOPS (pH 7.4), 0.5 M NaCl, 1 mM EGTA, 2 mM MgSO^4, 0.05% Tween, in ddH$_2$O	Own lab products	Fixing animals (for whole mount in-situ hybridization)
RNAse-free 1X PBS	0.01 M phosphate buffered saline (NaCl 0.138 M; KCl - 0.0027 M), pH 7.4, in RNAse-free ddH$_2$O.		Whole mount in-situ hybridization
PBT	0.1% Tween-20 in 1X PBS		
GB Solution	2 mg/mL glycine in PBT		
Post-Fix Solution	4% PFA in 1X PBS		
PreHB buffer	50% formamide, 6X SSC, 0.05% Tween20, in ddH$_2$O		
HB buffer	50% formamide, 1X Denhardt's, 6X SSC, 100 µg/mL yeast tRNA, 0.005% Heparine, 0.05% Tween-20, in ddH$_2$O		
Wash buffer 1	50% formamide, 50x SSC, 0.1% SDS, in ddH$_2$O		
Wash buffer 2	50% formamide, 2X SCC, 0.1% Tween-20, in ddH$_2$O		
Wash buffer 3	2X SCC, 0.1% Tween-20, in ddH$_2$O		
TNT buffer	0.1% Tris (pH 7.5), 150 mM NaCl, 0.1% Tween-20), in ddH$_2$O		
TNB blocking buffer	100 mM Tris (pH 7.5), 150 mM NaCl, 1% Blocking Reagent, 0.2% Triton-X100, in ddH$_2$O		
TMN buffer	100 mM NaCl, 50 mM MgCl$_2$, 100 mM Tris-HCl (pH 9.5), 0.1% Tween-20, in ddH$_2$O		
Staining Solution A	200 µL NBT + BCIP Solution from Sigma in 10 mL TMN buffer		
Mounting Solution A	50% glycerol and 2% DABCO, 1.5 µg/µL DAPI, in 1X PBS		

2.5 Fixing and mounting electroporated embryos

Table 2.5 Fixing and mounting solutions for electroporated embryos

Reagent name	Components	Manufacturer	Application
MEM-PA Stock	0.16 M MOPS (pH 7.4), 0.8 M NaCl, 3.2 mM $MgSO^4$, 0.8% Triton-X100, in ddH_2O	Own lab products	Fixing and mounting electroporated embryos
Fixation Solution B	0.1 M MOPS (pH 7.4), 0.5 M NaCl, 1 mM EGTA (pH 8.0), 2 mM $MgSO^4$, 3.7% formaldehyde, in ddH_2O		
Quenching Solution	1X PBS, 50 mM NH_4Cl, 0.35% Triton-X100, in ddH_2O		
Staining Solution B	1:1000 DAPI in PBT		
Mounting Solution B	50% glycerol and 2% DABCO, 1.5 µg/mL DAPI, in 1X PBS		

2.6 Buffers and chemicals

Table 2.6 Buffers and solutions

Reagent name	Components	Manufacturer	Application
1X TAE buffer	40 mM Tris, 20 mM acetic acid, 1 mM EDTA, pH 8	Own lab products	Agarose gel electrophoresis
LB-Medium	20 g LB Broth from Sigma in 1L ddH_2O		
LB-Medium-AMP	50 ng/mL Ampicillin in LB-Medium		

2.7 Commercial kits

Table 2.7 Utilized commercial kits

Name	Manufacturer	Application
Zymoclean^{TM} Gel DNA Recovery Kit	Zymo Research	DNA purification and recovery
GeneJET Plasmid Miniprep Kit	Thermo Fisher Scientific	Miniprep
Nucleobond Xtra Midi Kit	MACHEREY-NAGEL	Midiprep
TOPO® TA cloning Kits®	Invitrogen	Ligation with PCRII-TOPO vector

2.8 Primers

Table 2.8 Primers related to in-situ hybridization and RNAi

Name	Sequence (5→3)		Application
Ci-Brachyury (KH2012:KH.S1404.1)	Forward	TCGATTACGGGACTTGATCC	Polymerase chain reaction (in-situ hybridization)
	Reverse	TTCCAGGCTTCTGATTGGAC	
Ci-connexin-related-8 (KH2012:KH.C4.307)	Forward	CCGAACGTTTTCCTCCATAA	
	Reverse	GCTCTGACAAAACAGGCACA	
AT2B1;AT2B2;AT2B3 (KH2012:KH.C8.156)	Forward	GCTCTGACAAAACAGGCACA	
	Reverse	GGCCCATCATTTGTACCATC	
Ci-TRMP1/6/7 (KH2012:KH.C5.324)	Forward	CGAGTTGAAACAGTGGAGCA	
	Reverse	TGACAGCCTCAGTTGGATTG	
Ci-Cav1 (KH2012:KH.C4.795)	Forward	CACGCATGGAGAGAACTCAA	
	Reverse	GGAAGACCACCGTCCAGTAA	
KNCQ3;KNCQ4;KNCQ5 (KH2012:KH.C2.739)	Forward	TGCTGGTCACGTGGATATGT	
	Reverse	CGGTTCCCAGAAACACAACT	
Ci-TWIK5 (KH2012:KH.L9.36)	Forward	TTCGAGGGGTGGTCTTACAC	
	Reverse	TCTAGAATCCATGGCGAACC	
SERCA shRNA	Forward	agatctGCTGAAGAGGGTAAATCTTTG**gtgtgctgtcc**CAAAGATTTACCCTCTTCAGCTTTTTggatccG*	Ligation with U6 vector (RNAi)
	Reverse	AATTCggatccAAAAAGCTGAAGAGGGTAAATCTTTG**ggacagcacac**CAAAGATTTACCCTCTTCAGCag*	
Calmodulin shRNA	Forward	agatctGCAAGAGAAGTCGCGACAATA**gtgtgctgtcc**TATTGTCGCGACTTCTCTTGCTTTTTggatccG*	
	Reverse	AATTCggatccAAAAAGCAAGAGAAGTCGCGACAATA**ggacagcacac**TATTGTCGCGACTTCTCTTGCag*	

*Black thin capital letters = complementary sequence to the gene, small bold letters = loop, red capital letters= PolyA/PolT tail, small thin letters= sequence area for EcoRI and BseI enzymes.

3. Methods

3.1 Preparing fertilized *C. intestinalis* eggs

3.1.1 Gamete collection

To access the oviduct and sperm duct, animals were opened with scissors through their shorter siphon. After exposing both ducts, the oviduct was gently incised and the eggs collected with a glass Pasteur pipette. The pipettes had been previously washed by pipetting FASW-T up and down, in order to avoid gametes sticking inside. All collected eggs were then transferred into a tube containing cold FASW-T, and placed in cold running water to maintain a cool temperature. Afterwards, the sperm duct was gently incised, and the sperm was collected with a new glass Pasteur pipette into a 1.5 mL Eppendorf tube. The latter was stored at 4°C.

3.1.2 Dechorionation and fertilization

Following gamete collection, the eggs were dechorionated to enable a rapid fertilization. For this purpose, 10 mL Dechorionation Solution and 250 μL 1M NaOH were mixed in a 15 mL tube, in which the collected eggs were afterwards transferred into without excess water. The eggs were dechorionated by either pipetting continually for mechanical agitation, or by closing the tube and placing it on a shaker. The latter was performed for 6-7 minutes, while simultaneously examining the state of the eggs under a Nikon SZM645. After sufficient amount of eggs were dechorionated, a series of wash steps were performed with FASW-T until all debris and dechorionation solution was removed from the media. The eggs were then transferred into a 1% agarose-overlaid petri dish, to avoid embryos sticking to the dish surface, containing new FASW-T. The 1% agarose-overlaid petri dishes had been previously prepared by mixing UltraPure^TM Agarose from Invitrogen with FAWS-T, and poured into the dishes. All petri dishes used for this thesis were overlaid as such, unless stated otherwise.

Meanwhile, the 5-20 μL of the collected sperm was activated with Sperm-Activator Solution, from which 2-4 drops were added to the dechorionated eggs. When the eggs started to spin, they were left to fertilize for 6 minutes. If the eggs did not spin within 15-20 seconds, another drop was mixed in. Post fertilization, the eggs were washed with FAWS-T until all eggs stopped spinning. The fertilized eggs were then either stored at 14°C until ready to fix for in-situ hybridization, or immediately electroporated with exogenous DNA for live calcium imaging and other studies.

3.2 In-situ hybridization

3.2.1 Fixing embryos for in-situ hybridization

Embryos (Section **3.1.2**) from the late cleavage period to tailbud were selected to fix for an in-situ hybridization. Fixation Solution A was previously stored at 4°C in the dark, before transferring 0.75 mL into a 1.5 mL eppendorf tube on ice. Thereafter, embryos were carefully added to the fix and left to settle, followed by replacing the supernatant with 1.5 mL fresh Fixation Solution A after ca. 5 minutes. The embryos were then left to fix overnight at RT while rocking. Meanwhile, 1X fresh RNAse-free PBS was prepared and chilled on ice. Later on, the embryos were also kept on ice and left to settle, before starting dehydration. The supernatant was then replaced twice with 1 mL 1X ice cold PBS, with the tube still on ice. Afterwards, 500 µL 100% EtOH was added to the tube and rocked for 15 minutes. Later on, the embryos were left to settle, and 1 mL of the supernatant was removed. To the tube was then added 750 µL 50% and 250 µL 100% EtOH, with a final EtOH percentage at 50%, in order to reduce salt concentration and thus precipitates. The latter mixture was left to rock at RT for 15 minutes, followed by successively adding 750 µL 75% and 250 µL 100% EtOH, and left to rock again for 15 minutes. Finally, the embryos were left to settle and the supernatant replaced twice with 100% EtOH, and stored at -20°C.

3.2.2 Designing primers for polymerase chain reaction

To attain amplified amount of Ci-Brachyury (KH2012:KH.S1404.1), Ci-connexin-related-8 (KH2012:KH.C4.307), AT2B1 (KH2012:KH.C8.156), Ci-TRMP3 (KH2012:KH.C5.324), Ci-Cav1 (KH2012:KH.C4.795), KNCQ4/5 (KH2012:KH.C2.739) and Ci-TWIK5 (KH2012:KH.L9.36) genes, corresponding primers were designed for a PCR. More information about the genes can be obtained, by using the stated accession numbers at https://www.aniseed.cnrs.fr/aniseed/. The primers were designed based on the upstream and downstream nucleotide sequence of the stated genes above, by using the Primer3Plus website (http://www.bioinformatics.nl/cgi-bin/primer3plus/primer3plus.cgi). Each primer consisted of 20 bp, with a GC content at around 50% and a GC-clamp. Moreover, the melting temperature was kept between 57°C-61°C, and the expected PCR product sizes were indicated to be at 972, 1051, 991, 1400, 945, 1114 and 1062 bp, respectively.

3.2.3 Polymerase chain reaction

Amplification of the desired genes was performed by conducting a PCR. Each PCR sample contained 260 ng Ciona intestinalis cDNA template, 1X Green GoTaq Flexi buffer, 25 μM MgCl$_2$, 0.25 μM of each dNTP, 1 μM of each primer (Section **3.2.2**), 1.25 U/μL GoTaq@DNA Polymerase and ddH$_2$O in a total volume of 50 μL. The reaction was run as stated in **Table 3.1** using T100^{TM} Thermal Cycler from BIO-RAD.

Table 3.1 PCR protocol

Step	Temperature (°C)	Time (seconds)	Cycles
Initial denaturation	95	120	
Denaturation	95	60	
Annealing	57	30	35
Extension	72	90	
Final extension	72	300	
∞	4	∞	

3.2.4 Agarose gel electrophoresis and DNA recovery

In order to control the PCR products, an agarose gel electrophoresis was performed. For this purpose, a 1% gel was made by dissolving UltraPure^{TM} Agarose from Invitrogen in 1X TAE buffer and adding 0.5 μg/mL EtBr to the mix. The mixture was poured into a gel chamber and left to polymerize for 15 minutes at 4°C. Subsequently, the polymerized gel was submerged in 1X TAE buffer in a gel tank, followed by loading the PCR products into the wells. This was followed by also loading 0.9 μg 1 kb Plus DNA Ladder from Thermo Fisher Scientific, and running the electrophoresis at 125 V for 40 minutes. Later on, the gel was visualized through UV light by using the Molecular Imager$^®$ Gel Doc^{TM} EZ Imager from BIO-RAD. The DNA was then purified and recovered from the gel in accords with Zymoclean^{TM} Gel DNA Recovery Kit, from Zymo Research, except ddH$_2$O was used as the eluent.

3.2.5 Ligation with PCR^{TM}II-TOPO vector for blue-white screening

Ligation was performed to clone the purified genes into a vector. Each ligation sample consisted of 4.5 μL PCR product, 0.5 μl PCR^{TM}II-TOPO vector and 1 μL Salt Solution from Invitrogen TOPO$^®$ TA Cloning Kits$^®$, and left to ligate overnight at RT. PCRII^{TM}-TOPO

vector was selected due to its Lac, SP6, and T7 promoters. This is because the first stated promoter enables the possibility of a blue-white screening, while the other two promoters can enable sense/antisense sequence production of desired genes through in-vitro transcription.

3.2.6 Transformation (blue-white screening) and plasmid purification

The recombinant plasmid DNA was transformed by heatshock using *E. coli* competent cells. Hence, 25 µL *E. coli*® 10G DUOs Chemically Competent Cells from Lucigen was added to each ligated sample, and left on ice for 30 minutes. The samples were then put on a shaker at 42°C for 45 seconds, and on ice again for 2 minutes. Thereafter, 300 µL LB-Medium was added to each sample, followed by incubation at 37°C for one hour. The transformed samples were then plated on IPTG-X-Gal overlaid ampicillin plates, and left to incubate upside down at 37°C overnight. Later on, two white colonies were picked from each plate and were each inoculated in 4 mL LB-Medium-AMP medium, in 10 mL tubes. Thereafter, the bacterial cultures were left to grow overnight at 37°C on a shaker. Miniprep was then performed on 2 mL of each bacterial culture, to isolate the plasmid DNA from bacteria, while the remaining bacterial culture was stored at 4°C. Plasmid purification was performed as stated in Thermo Scientific GeneJET Plasmid Miniprep Kit, except ddH$_2$O was used as the eluent.

3.2.7 Digestion with EcoRI-HF and agarose gel electrophoresis

The purified plasmid was digested, followed by agarose gel electrophoresis, to select correct plasmids for sequencing based on DNA band size. Digestion samples consisted of 1 µL template DNA, 3 µL 10X CutSmart Buffer® and 0.25 µl EcoRI-HF® from NEB, and ddH$_2$O in a total volume of 24.25 µL. The latter were left to incubate overnight at 37°C, and then used to prepare agarose gel electrophoresis samples with. The gel electrophoresis samples consisted of each digestion sample mixed with 1X Purple Gel Loading Dye from NEB, and were loaded into a 1% agarose gel. Preparation of the agarose gel, loading 1 kb Plus DNA Ladder, and the electrophoresis itself was performed as stated in section **3.2.4**. The gel was then used to detect digested DNA band sizes, which were roughly equal to the expected PCR products (Section **3.2.2**) plus 50-100 bp more included from the digested vector. Thereafter, the purified plasmids related to each correct DNA band size were selected for sequencing.

3.2.8 Polymerase chain reaction with Big Dye and sequencing

Sequencing was performed to control whether the desired DNA was indeed present in the purified plasmids selected in **3.2.7**. First, DNA was amplified by PCR sequencing, where each sample contained 1 µL DNA template, 1 µL Big-Dye version 3.1 and 1 µL sequencing buffer from ThermoFisher, 1 µL M13 reverse primer Sigma, and 6 µL ddH$_2$O. The PCR reaction was run as stated in **Table 3.2**. Then, 10 µL ddH$_2$O was added to each PCR product, and sequenced by the staff at Sequencing Facility of MBI (UiB) using Applied Biosystems 3730XL DNA Analyzer. Later on, the sequences were examined by Ghost Database website (http://ghost.zool.kyoto-u.ac.jp/blast_kh.html) to check whether they were correct.

Table 3.2 Sequencing PCR protocol

Step	Temperature (°C)	Time (seconds)	Cycles
Initial denaturation	96	300	
Denaturation	96	10	
Annealing	50	5	25
Extension	60	4	
Final extension	60	1	
∞	4	∞	

3.2.9 DNA quantification and stock preparation

The concentrations of purified plasmid samples, with correct sequencing results, were measured by means of NanoDrop using a NanoDrop ND1000 spectrophotometer. ddH$_2$O was used as blank. For later use, the plasmids were transferred from 4°C to -20°C, and bacterial stocks were prepared by mixing 600 µL 60% glycerol with 300 µL bacterial culture. The latter mixture was stored at -60°C, to regrow cultures from again if needed.

3.2.10 Digestion with NotI-HF and agarose gel electrophoresis

Purified plasmids, with correct sequencing results, were treated with NotI-HF restriction enzyme to linearize the vector and cut after the insert sequence. The samples consisted of 3 ng DNA, 1X CutSmart Buffer and 5 U/µL NotI-HF® per ng DNA from NEB, and ddH$_2$O up to a total volume of 50 µL. Subsequently, the samples were left to incubate overnight at 37°C, followed by performing an agarose gel electrophoresis to examine the digestion success based

on possible bands at ca. 5 kb. Samples for the latter study contained 1 μL digested plasmid DNA and 1X Purple Gel Loading Dye from NEB, which were run on a 1% agarose gel with parameters stated as in section **3.2.4**.

3.2.11 DNA purification by phenol-chloroform extraction

Before starting the in-vitro transcription and subsequently proceeding with in-situ hybridization, the linearized plasmid DNA was purified by means of phenol-chloroform extraction. The purification was performed by adding nuclease-free water to the linearized DNA samples, each up to a total volume of 200 μL, and then transferring the mixture into 2 mL tubes containing silica columns. Thereafter, 200 μL UltraPure™ Phenol: Chloroform: Isoamyl Achohol (25:24:1, v/v, pH 8), from Invitrogen, was carefully added under a fume hood onto the diluted DNA, and afterwards centrifuged at 13000 rpm for 3 minutes. Then, another 200 μL Phenol: Chloroform: Isoamy Alchohol was added and centrifuged again as stated earlier. Subsequently, the upper liquid layer containing DNA was carefully transferred into a new eppendorf tube. Meanwhile, 3M NaOAc (pH 5.2) from Life Science, and 100% EtOH, were both cooled down to -20°C. 20 μL and 550 μL of the latter solutions, respectively, were gently mixed into the samples and then incubated for one hour in -20°C. The latter was followed by centrifugation at 14000 rpm for 15 minutes at 4°C. After centrifugation, the supernatant was removed and the pellet washed with 350 μL 70% EtOH, then centrifuged again at 14000 rpm for 5 minutes at 4°C. Later, the EtOH was removed and the tubes were left under the fume hood to evaporate any remaining EtOH. The dried pellet was then resuspended with 10 μL nuclease-free water, and concentrations measured by NanoDrop ND1000 with nuclease-free water as blank.

3.2.12 Large-scale in-vitro transcription

IVT was performed to produce RNA-probes complementary to mRNA transcribed by the desired genes. The chemicals used in this study belong to MEGAscript™ SP6 Kit from Invitrogen by Thermo Fisher Scientific, except; 70% RNAse-free EtOH, and Formamide and Digoxigenin-11-UTP from Sigma. IVT samples were each prepared by mixing 6 μL purified template DNA, 2 μL buffer, 2 μL ATP, 2 μL CTP, 2 μL GTP, 1 μL UTP, 3 μL Digoxigenin-11-UTP, and 2 μL Enzyme Mix in an eppendorf tube. The samples were then left to incubate

at 37°C for six hours. Later on, 0.5 μL TURBO DNase was mixed into each sample, and left to incubate for 15 minutes in 37°C. Then, 10 μL RNAse-free water and 10 μL Lithium Chloride Precipitation Solution was mixed in the sample and left to precipitate overnight at -20°C. The samples were afterwards centrifuged at 14000 rpm for 15 minutes at 4°C, followed by supernatant removal and pellet wash with 70% RNAse-free EtOH. Thereafter, the samples were centrifuged at 14000 rpm as stated earlier, and the supernatant removed before drying the pellet under a fume hood on ice. The pellet was then resuspended in room temperature (RT) with 60°C RNAse-free water, between 15-30 μL depending on the pellet size, and concentrations measured by NanoDrop ND100. Afterwards, the samples were diluted with 50% formamide, from Sigma, and stored at -60°C.

3.2.13 Whole-mount in-situ hybridization

Whole-mount in-situ hybridization was performed to enable expression analysis of ion channel genes in *C. intestinalis* notochord. Fixed embryos ranging from gastrula to larvae stages were transferred into 0.5 mL baskets, in a 48-well plate, for a whole-mount in-situ hybridization study. In a six series step, each at RT and for 20 minutes, the embryos were successively rehydrated in 100%, 70%, 50% and 30% MetOH, followed by the last step with PBT. Each buffer replacement was done at 500 μL for this step, and the later steps for the in-situ hybridization study unless stated otherwise. The embryos were then each washed twice with PBT for 5 minuts at RT, and treated with 4 μg/mL Proteinase K at 37°C for 25 minutes to permeabilize the embryos. Subsequently, the Proteinase K was stopped with GB Solution, and the embryos washed twice with PBT, at RT for 5 minutes each. Thereafter, the embryos were incubated with Post-Fix Solution for one hour at RT. The latter was followed by a series of three wash steps, each with PBT for 5 minutes at RT.

As a pre-hybridization (pre-HB) step, the embryos were first incubated with preHB solution for 10 minutes at RT, and then with 900 μL HB solution for 2 hours at 55°C. Meanwhile, the RNA probes were diluted to 0.1-1 ng/μL with HB solution, and denatured at 80°C for 5 minutes, where Ci-Brachyury would serve as control for in-situ hybridization. 50 μL from each of the latter mixture was added to the embryos, and left to hybridize at 55°C for ca. 16 hours with tin foil covering the wells. The latter was followed by a series of wash steps, with

a quick wash at RT by Washer buffer 1 (WB1) first. The other six wash steps were performed successively for 20 minutes at 55°C each; twice with WB1, twice with WB1:WB2 (1:1), and twice with WB2, respectively. The embryos then underwent further wash steps, once with WB3 for 5 minutes at RT, and then twice with WB3 but for 20 minutes at 55°C each.

Next, the embryos were incubated with TNT for 5 minutes, and then TNB blocking solution for 4 hours, both at RT. Thereafter, 1/5000 μL Anti-Digoxigenin-AP antibody from Fab fragments in TNB was added to the embryos. The latter was left to incubate for 2 hours at RT, and then left overnight at 4°C. Later on, the hybridized embryos went through another wash series with TNT at RT; once for 5 minutes, four times each for 20 minutes, and once for 40 minutes, respectively. While still at RT, the embryos were additionally washed three times with TMN for 10 minutes each, followed by staining with 1 mL Staining Solution A.

While still in the Staining Solution A, the embryos were examined using a Nikon SMZ645 microscope every 10-30 minutes to detect any signal every. When the Staining Solution A turned purple due to oxidation, the embryos were transferred into a new well containing new Staining Solution A. After detecting potential signal, and the embryos turning slightly pink, a series of six wash steps were performed with PBT at RT for 10 minutes each. The embryos were then transferred into individual 1.5 mL Eppendorf tubes, and left to settle down. Excess liquid was then removed, and three drops of Mounting Solution A was added to each tube. The embryos were then mounted on a microscope slide, stored at 4°C and imaged with Nikon Eclipse E800 microscope using a DAPI-filter at 20x (0.50 DIC M), and 40x (0.75 DIC M), where 10x (0.30 DIC L) was used to find the embryos.

3.3 Wild type *C. intestinalis* calcium imaging

3.3.1 Electroporation with GCaMP6 calcium indicators

Electroporation was performed to introduce exogenous DNA into newly fertilized *C. itenstinalis* eggs (section **3.1.2**), to examine possible notochord calcium signalling dynamics. With this in mind, the promoters for Ci-Cah3 and Ci-NFAT5 genes were selected for electroporation, as their gene expression had previously been described in the notochord. (Kugler, Passamaneck et al. 2008, Jose-Edwards, Kerner et al. 2011) Hence, 100-120 μg of

NFAT5>GCaMP6s and Cah3>GCaMP6s constructs were each diluted with ddH_2O up to a total volume of 100 µL, and mixed with 400 µL 0.96 M D-Manitol. The mixtures were added to separate tubes, which already contained fertilized eggs in 200 µL FASW-T, and mixed together. Subsequently, the mixtures were transferred into electroporation cuvettes, avoiding bubbles and any loss of liquid. The electroporation was performed with either the Time Constant Protocol or the Exponential Protocol, using GenePulser Xcell™ from BIO-RAD. For the Time Constant Protocol, the time constant was set at 15 ms, voltage at 50 V, and the cuvettes path length at 4 mm. As for the Exponential Protocol, the settings were sat at 50 V, capacitance at 800 µF, resistance at ∞, and path length at 4 mm.

3.3.2 Wash and spreading into petri dishes

Newly electroporated eggs were immediately transferred into petri dishes, containing FASW-T, to wash by replacing the FASW-T new FASW-T. This was repeated at least five times, until all traces of D-Manitol, debris and damaged eggs were removed from the liquid. And in order to avoid the eggs and developing embryos from sticking together in a crowded plate, the eggs were separated into multiple petri dishes containing FASW-T. The fertilized eggs were afterwards left to develop at 14°C.

3.3.3 Live wild type calcium imaging

To visualize notochord calcium dynamics, the embryos were imaged from developmental Hotta stages 22 to 26, where 5 images were taken every 5 seconds. This took place while the embryos were placed on agarose-less petri dishes in FAWS-T. All embryos were imaged by ZEISS Examiner.A1 upright microscope, using water immersion objective 40x with NA 0.75. The water immersion objective 5x with NA 0.16, on the other hand, was utilized for embryo identification. The images were taken by Hamamatsu ORCA-Flash 4.0 camera, with excitation filter at 460-470 nm, dichoric mirror at 493 nm LP, and emission filter at 505-530 nm. PhaseView ThunderScan was additionally used to image the embryos, as it enables high-speed volumetric imaging due to its digitally controlled tuneable lens. The lens power was controlled by PhaseView QTimage software, which enabled to select particular image plane at desired positions along the Z-axis. The latter software was utilized to set the other parameters as well, such as the quantity of images to take per time. Based on the first calcium imaging results, the best GCaMP6s construct was selected to continue wt calcium imaging with.

3.3.4 Wild type data-analysis

The images from live calcium imaging were concatenated into movies, using (Fiji) ImageJ win64 software, for analysis. This was performed by first max projecting the concatenated movies, and then using the max projections to select individual notochord cells as ROI. After all the ROI were selected in the given movie, one last ROI was selected from the background as background. Afterwards, the intensity-change measurements of the ROI were extracted using the same software, and the output data saved for further analysis. All data was gathered in a unified dataframe, to easily analyse and compare all experimental conditions. A background subtraction was then performed on each trace before applying a lab-made peakfinding algorithm using Python. $\Delta F/F$ values were calculated as (signal-mean)/mean. Locations were stored for all peaks that were higher than the mean deviation of its trace. If signal between two given peaks did not drop more than the standard deviation of the signal, the highest peak was then kept. Guassians were fitted to all found peaks in the dataset. The peak height was then defined as the signal height at the peak locations, and peak width defined as the sigma of the fitted Gaussian. Finally, the number of peaks per ROI per animal, mean peak height per ROI per animal, and mean peak width per ROI per animal, was plotted against *C. intestinalis* developmental stages 22 to 26. A non-parametric Mann-Whitney U test was also performed on the wt data, to detect potential statistical differences between the stated stages. P-values < 0.05 was set to indicate significant differences between two given stages.

3.4 Pharmacological study by drug perfusion

3.4.1 Determining drug concentrations

To study whether *C. intestinalis* notochord calcium signalling depends on IP_3R and SOCE, and/or cation channels, 2APB and $Gado^{3+}$ were selected as candidates for drug perfusions respectively. Carbenoxolone was additionally selected as a candidate to examine the importance of gap junctions. (**Table 3.3**) But first, drug concentrations for the perfusion were determined.

Table 3.3 Overview over inhibitors and inhibitor targets

Inhibitor	Inhibition target
Carbenoxolone	Gap junctions
$Gado^{3+}$	Cation channels
2APB	IP3R and SOCE

The concentrations were determined by incubating live Hotta stage-23 embryos with 10 μM, 100 μM, and 1 mM of each drug for one hour. The drugs were prepared with FAWS-T. Embryos were then washed with FAWS-T, and left to develop until late tailbud to larvae stage. The embryos were thereafter fixed as in section **3.6.3**, mounted as in section **3.2.13** but with Mounting Solution B, and stored at 4°C. Later on, they were imaged to detect any morphological effects of potential calcium signalling inhibition. The imaging was performed with Nikon Eclipse E800 microscope using a DAPI-filter at 20x (0.50 DIC M).

3.4.2 Embryo preparation for pharmacological study

The embryos for this study, prepared as stated in sections **3.3.1-2**, were electroporated with the best GCaMP6s construct. 1% low-melting agarose was then prepared by mixing Agarose (Low-Melting, <1kb DNA/RNA/Genetic Analysis Grade), from Fisher BioReagents, with FAWS-T and kept liquefied at 37°C. The latter was used to glue the embryos with on the agarose-less petri dishes. This was performed by first transferring the embryos into the petri dishes with as little liquid as possible. One drop of the agarose was then added onto the embryo, and the droplet cooled down before filling the petri dish with FAWS-T. The embryos were then used for a pharmacological study.

3.4.3 Pharmacological study while live calcium imaging and data analysis

The affect of 2APB, carbenoxolone, and $Gado^{3+}$ on *C. intestinalis* notochord calcium activity was examined by drug perfusions while performing live calcium imaging. Each drug was prepared with a final concentration of 100 μM in 200 mL FASW-T, where 2APB was dissolved in 500 μL 99.9% DMSO from Sigma, and carbenoxolone in 500 μL 70% EtOH, first. As a consequence, the running buffers for the latter two drugs were each prepared using equal amounts of 99.9% DMSO, and 70% EtOH, in a total volume of 200 mL FASW-T respectively. $Gado^{3+}$ dissolved in FAWS-T, hence the running buffer was only FAWS-T.

The drug perfusion was successively performed in three phases, each at 10 minutes, with a lab-made perfusion set-up while performing live calcium imaging (Section **3.3.3**). The first phase consisted of imaging a developing embryo from Hotta stages 22 to 26, while perfusing with running buffer. The second phases started immediately by imaging the embryo while perfusing the drug. The third phase was subsequently performed as a wash step, where the embryo was imaged while perfusing with running buffer again.

The images from the drug conditions were analysed as in section **3.3.4**, except mean peak height per ROI per ROI, mean peak width per ROI per animal, and number of peaks per ROI per animal, was plotted against wt and all drug-condition phases. Additionally, a non-parametric Mann-Whitney U test was also performed on this data, to find potential statistical difference between the three perfusion phases and wt.

3.5 RNA interference

3.5.1 Designing shRNA oligodeoxyribonucleotides

Downregulation via RNA interference (RNAi) was performed to disrupt the molecular pathway underlying calcium activity in the notochord, by introducing a short hairpin RNA (shRNA) into newly fertilized *C. intestinalis* eggs. RNAi oligodeoxyribonucleotides were thus designed against SERCA and calmodulin, with the tools at invivogen website (http://www.invivogen.com/sirnawizard/), using previously sequenced SERCA and Calmodulin sequences. The oligosequences were designed with a loop sequence in the middle, where the sequences to its right and left were complementary to each other and the respective gene (SERCA or calmodulin), with overhanging ends identical to BseI and EcoRI restriction enzyme sites. The GC content of these sequences was kept close to 50%, and each oligo consisted of 71 bp. In order to anneal, the oligopairs were each boiled at the concentration of 10 μM for 5 minutes at 100°C in 10 mM Tris (pH 7.5) and 50 mM NaCl. The annealed oligos were then left to cool at RT.

3.5.2 Ligation with U6 vector

shRNA constructs were prepared by ligating the designed shRNA oligodeoxyribonucleotides into a U6 vector, downstream of the U6 small nuclear RNA (U6 snRNA) promoter to drive their expression. Ligation was performed by first diluting the annealed oligos 1:1000 with ddH$_2$O, followed by adding 0.5 μL T4 DNA Ligase from NEB, and incubating the samples overnight at RT. The constructs will be referred to as shRNA-SERCA and shRNA-Calm.

3.5.3 Transformation and plasmid purification

The recombinant vector was used to transform competent cells with as stated in section **3.2.6**, except agar plates containing only ampicillin was used to plate the cells upon. The plasmids were also purified as previously described in section **3.2.6**.

3.5.4 Digestion with BseI and EcoRI

Purified plasmid DNA was linearized using EcoRI and BseI restriction enzymes from NEB. Each digestion sample contained 1 µg purified template DNA, 5U of each enzyme, 1X CutSmart Buffer from NEB, and ddH$_2$O in a total reaction volume of 5 µL. The samples were left to incubate overnight at 37°C.

3.5.5 Polymerase chain reactiong with BigDye and sequencing

To check whether the oligos were indeed present in the vector, the sequencing PCR and sequencing were performed in a similar manner as in section **3.2.8**.

3.5.6 Midi-culture from midiprep

Mini-cultures with correct sequences were used to prepare midi-cultures from, in order to amplify the amount of starting DNA for further experiments. This was prepared by transferring 2 mL of the mini-culture into 250 LB-medium, followed by incubation on a shaker overnight at 37°C. In order to extract and purify the DNA from bacteria, a midiprep was performed in accords with Nucleobond Xtra Midi kit from MACHEREY-NAGEL.

3.5.7 Co-electroporation and wash

The best GCaMP6s was co-electroporation with shRNA-SERCA and shRNA-Calm, to examine possible RNAi gene silencing affect on *C. intestinalis* notochord calcium signalling. The electroporation was performed as in section **3.3.1**, except 100 µg of each shRNA construct was mixed with 80 µg GCaMP6s, up to a total volume of 100 µL with ddH$_2$O, before adding 0.96 M D-manitol. Post electroporation, the electroporated eggs were washed as in section **3.3.2**.

3.5.8 Live calcium imaging and data-analysis

The signal was analysed in order to detect any gene silencing effect, by live calcium imaging as stated in section **3.3.3**. The data-analysis was performed as in section **3.3.4**, except the number of peaks per ROI per animal, mean peak height per ROI per animal, and mean peak width per ROI per animal, was plotted against wt and RNAi conditions. A non-parametric Mann-Whitney U test was also performed on the data, to detect potential statistical differences between the knock-downs and wt. P-values < 0.05 was set to indicate singicant difference between two given conditions.

Further analysis was performed on the data from shRNA-Calm RNAi condition. The number of peaks per ROI per animal, mean peak height per ROI per animal, and mean peak width per ROI per animal, of wt middle and anterior+posterior notochord locations were compared with respective shRNA-Calm affected notochord parts. A non-parametric Mann-Whitney U test was also performed on these data with the same principle as stated above.

3.6 Calcium operating channel drug screen

3.6.1 Co-electroporation and wash

Embryos were prepared (Sections **3.1.1**-**2**) and co-electroporated with Bra>MLC wt Mcherry and Bra>Lifeact GFP constructs. The electroporated embryos were then incubated separately with 2APB, Carbenoxolone and Gado^{3+}, to study their affect on *C. intestinalis* notochord actomyosin. Electroporation with Bra>Lifeact GFP can enable visualisation of notochord cells with respect to where brachyury drives expression of F-actin binding protein. The visualisation is enabled due to the latter protein being attached to green fluorescent protein in the Bra>Lifeact GFP construct. As for Bra>MLC wt Mcherry construct, it enables detection of myosin light chain (MLC) protein, due to Mcherry fluorescent protein attached to MLC. The co-electroporation and wash were performed as stated in sections **3.3.1**-**2**, except 100 μM of each construct was mixed together with ddH$_2$O up to a total volume of 100 μL.

3.6.2 Drug incubation and wash

The electroporated embryos for each drug were separated into two petri dishes containing FASW-T, where one was used to incubate with a given drug while the other was incubated

with the buffer of the drug as control. The drugs and their respective buffers were prepared as in section **3.4.3**. When the embryos reached early tailbud stage, they were incubated with the drugs, and their respective buffers, for one hour and left to develop in 14°C. The embryos were later on washed by replacing the media with new FAWS-T, at least five times, until all traces of the drugs were removed. Thereafter, the embryos were fixed every three hours.

3.6.3 Fixing electroporated embryos

Embryos were first submerged with 40 μL Fixation Solution B in a 50 μL tube, and left to settle down before supernatant removal. Then, 40 μL Fixation Solution B was added to the tube, and incubated for 15 minutes at RT while rocking. Later on, the supernatant was removed and embryos incubated with 40 μL Quenching Solution in a series of three steps, each for 20 minutes at RT. The liquid was afterwards removed, followed by a series of three wash steps each with 40 μL PBT. Next, the embryos were stained with 40 μL Staining Solution B, and incubated overnight at 4°C while the tubes were covered with tinfoil. The embryos were mounted as in section **3.2.13**, except Mounting Solution B was used.

3.6.4 Live confocal imaging and data-analysis

The fixed embryos were imaged to examine whether the drugs had an affect on notochord actomyosin network, by means of life confocal imaging using Leica TCS SP5 II LAS AF from Leica Microsystems. A sequential set-up was set up with ca. 24% red (PMT5) light and ca. 27% green (PMT3) light, where the frequency was at 700 Hz, frame average at 4, and line average at 1. Additionally, the number of Z-steps was kept at a constant 0.21 μM. The live confocal images were then visually analysed, to detect whether drug incubated notochord-actomyosin network differed from that of the wt condition.

4. RESULTS

4.1 Calcium signalling in wild type *C. intestinalis*

Newly fertilized *C. intestinalis* were electroporated with Cah3>GCaMP6s and NFAT5>GCaMP6s transgenes, in order to determine whether Ciona notochord cells exhibit calcium activity during embryonic development. These genes had previously been described to express in the notochord (Kugler, Passamaneck et al. 2008, Jose-Edwards, Kerner et al. 2011). 100-120 µg of NFAT5>GCaMPs and Cah3>GCaMP6s constructs were separately used for electroporations, and imaged by means of live calcium imaging from Hotta stages 22 to 26 (Sections **3.3.1-3**). Only embryos electroporated with Cah3>GCaMP6s construct exhibited calcium signalling (**Figure 4.1**). Hence, the latter was selected to continue wild type live calcium imaging with, as control for further calcium imaging studies in this thesis. After data-analysis (Section **3.3.4**), the results were illustrated as boxplots on top of violin plots, and p-values were obtained from the non-parametric Mann-Whitney U test.

4.1.1 Calcium signalling detected in the developing notochord cells

Ca^{2+}-signalling was observed in *C. intestinalis* notochord cells from Hotta stages 22 to 26, as depicted in **Figure 4.1**. The intensity of these signals varied between the notochord cells in all stages (**Figure 4.1**, **Stage 22**). Some of these signals were visualized as waves starting from an initiation point, which then traversed around individual notochord cells (**Figure 4.1**, **Stage 23**). These waves were most easy and clear to detect from stages 22 to 24. Moreover, the shape of the cells also varied from one stage to the other. At **Stage 22**, the notochord cells were visualized as thin coins. These coin shapes then appeared to be slightly thicker in size, and slightly smaller in diameter, at **Stage 23**. The same trend, i.e. thicker in size and smaller in diameter, continued to take place at **Stage 24** as well. Another event also took place around **Stage 24**, which was the lumen formation in-between neighbouring notochord cells. The lumens were visualized as dark spots that become enlarged as the embryo went through further developmental stages (**Figure 4.1**, **Stage 25-26**).
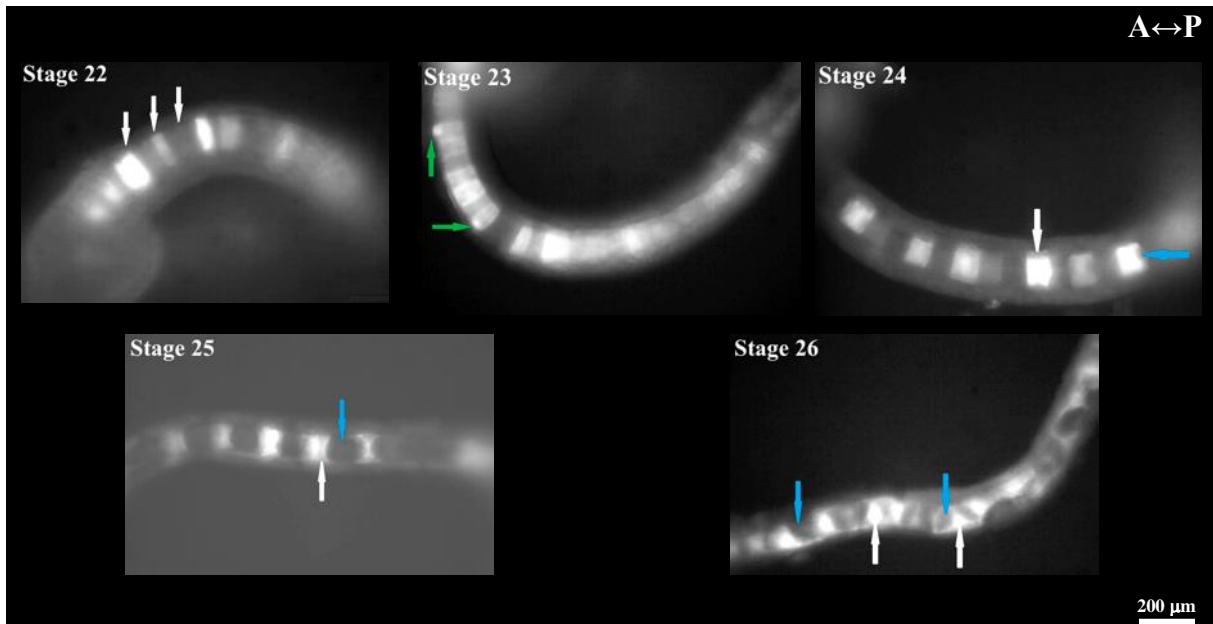
Figure 4.1 Live calcium imaging of wild type *C. intestinalis*. Newly fertilized embryos were electroporated with 100-120 μg Cah3>GCaMP6s, and imaged from Hotta stages 22 to 26 with 5 images/second. Arrows point at Ca^{2+}-signalling in individual notochord cells (white), initiation points of calcium waves (green), and lumens (blue). The three white arrows (**Stage 22**) point at three individual notochord cells with different signal intensity.

4.1.2 Calcium signalling as waves and/or blinks in notochord cells

The signal intensity of the waves, as described in Section **4.1.1**, would then occasionally increase to the point where it seemed like a sudden blink in an individual notochord cell (**Figure 4.2**, **E-F**). The blink would last around 1-3 seconds, followed by the signalling intensity decreasing back to the same intensity as before the blink was initiated. The blinks seemed to abruptly occur by themselves as well, and not necessarily as a result of a wave increasing in intensity. These blinks seemed to mostly occur stochastically. Notably, blinking patterns similar to the pattern in **Figure 4.2** were occasionally observed in some embryos from stages 22 to 26, most notably from stages 24 to 26. Furthermore, sometimes the signal from one notochord cell would occasionally travel to the neighbouring notochord cell, as illustrated in **Figure 4.2**, **H-J**. More so, signalling was usually also observed at the epidermal cells of the embryos (**Figure 4.2**, **G**).
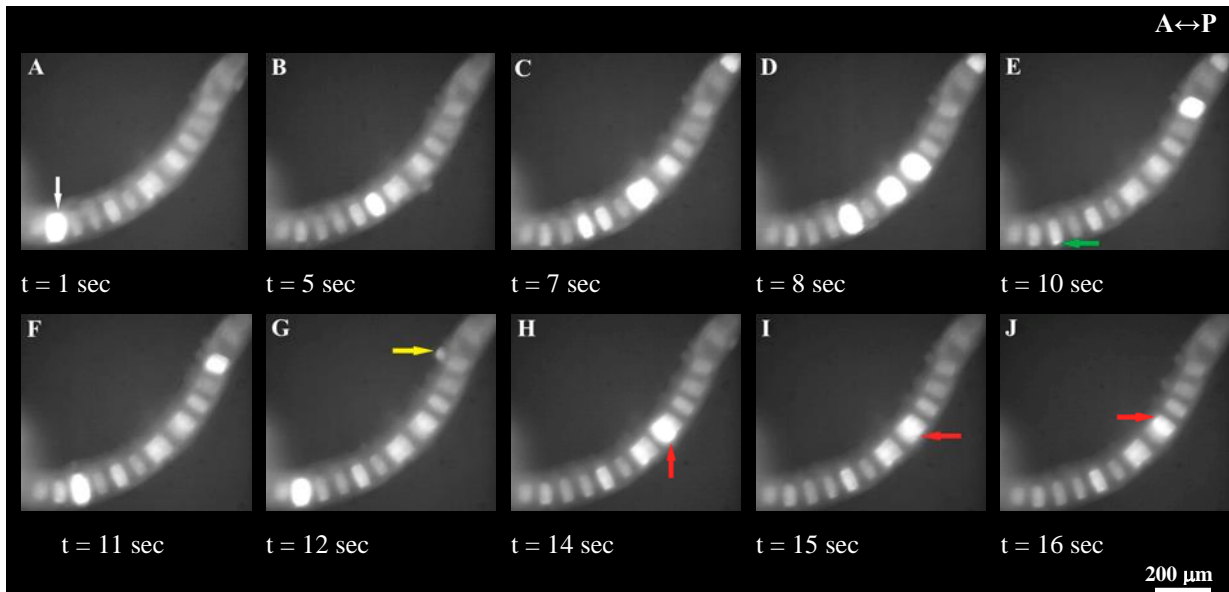
Figure 4.2 Signal fluctuations in *C. intestinalis* notochord cells. The figure illustrates signal dynamics at stage 24, where the animal was prepared and imaged as in **Figure 4.1**. The arrows point at individual notochord cell (white), initiation point of waves (green) in an individual notochord cell, signal travelling between two neighbouring notochord cells (red), and signal at epidermal cells (yellow).

4.1.3 Signalling in the epidermal and muscle accompanied by the embryo twitching

Calcium transients from the epidermal cells were often noticeably strong and highly dynamic. The epidermal signalling activity was often followed by either sudden blinks, or a relatively lasting signal, in certain notochord cells and regularly accompanied by the embryo twitching (**Figure 4.3**). Furthermore, there was almost always at least one strong signal that was generated more rhythmically as the embryo twitched. This activity was occasionally more pronounce at muscle cells at the posterior part of the embryo (**Figure 4.3**) and/or more at certain muscle cells all around the tail (Figure not included).
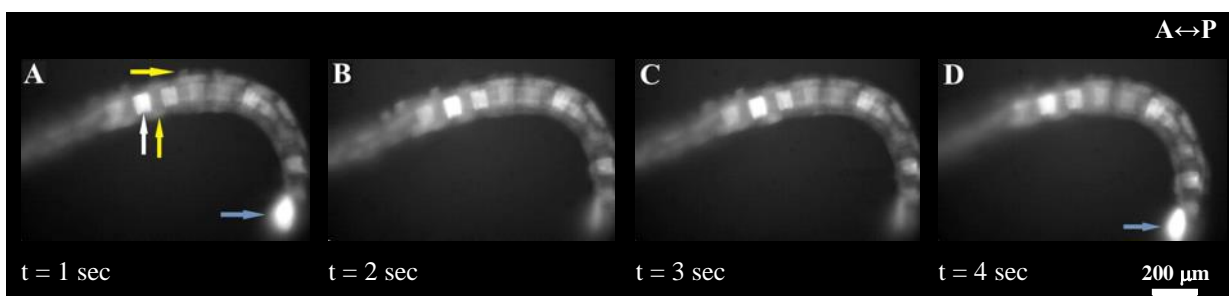
Figure 4.3 *C. intestinalis* embryo twitching. The figure illustrates signalling while stage 26 embryo twitches. The frame rate was 5 frames/second. The arrows point at individual notochord cell (white), signal at epidermal cells (yellow), and signal at muscle cell that is rhythmically accompanied with a twitch (teal).

4.1.4 Representation of raw data obtained by calcium imaging as signalling traces

The raw data of calcium imaging was illustrated as signalling traces (**Figure 4.4**) to better understand the dynamics of Ca^{2+}-signalling, and to use it for data quantification and further comparative analysis. For this purpose, the number of signalling peaks, peak height and peak width were defined. A peak was defined as a signal with intensity at least over the standard deviation of the noise in the given calcium imaging data. Gaussians were then fitted to all the found peaks in the dataset. For each peak, the peak height was defined as the signal height at the peak locations, and peak width as the sigma of the fitted Gaussian. The minimum distance between two peaks was at least 5 frames per second. (**Figure 4.4**)
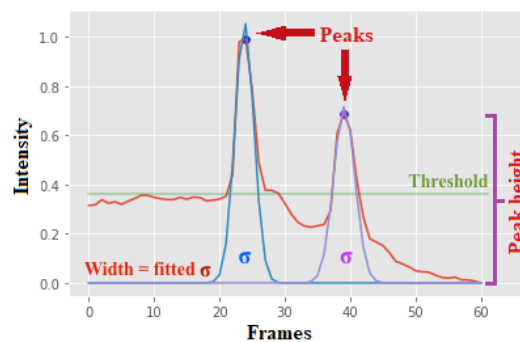
Figure 4.4 Ca^{2+}-signalling trace from a single notochord cell. Newly fertilized embryos were electroporated with 100-120 μg Cah3>GCaMP6 construct, and left to develop in 14°C. Live calcium imaging was performed on animals during Hotta stages 22 to 26, with 5 images per second. The raw calcium imaging data is depicted as the red trace in the figure, which illustrates Ca^{2+}-signalling from a single notochord cell. A signal was considered a peak if its intensity was at least over the standard deviation of the noise. This threshold is indicated in green in the figure. Gaussians were fitted to all found peaks in the dataset. For each peak, the height was defined as the signal height at the peak locations, and peak width defined as the sigma of the fitted Gaussian.

4.1.5 Different number of peaks per ROI per animal between most of the stages

The number of Ca^{2+} peaks, per ROI per animal, seemed different between certain developmental stages as the embryos developed (**Figure 4.5**). Likewise, the Mann-Whitney U test indicated a significant difference in peak number between certain stages, with p-values < 0.05 (**Table 4.1**). As the embryos developed, the number of peaks differed from stages 22 to 24, where stage 24 had similar peak numbers compared to stage 25. The peak number however differed between stage 25 and 26. Stage 22 and stages 24-26 possessed some outliers as depicted in **Figure 4.5**, which also illustrates the overall data distribution of each stage as violin plots behind respective boxplots.
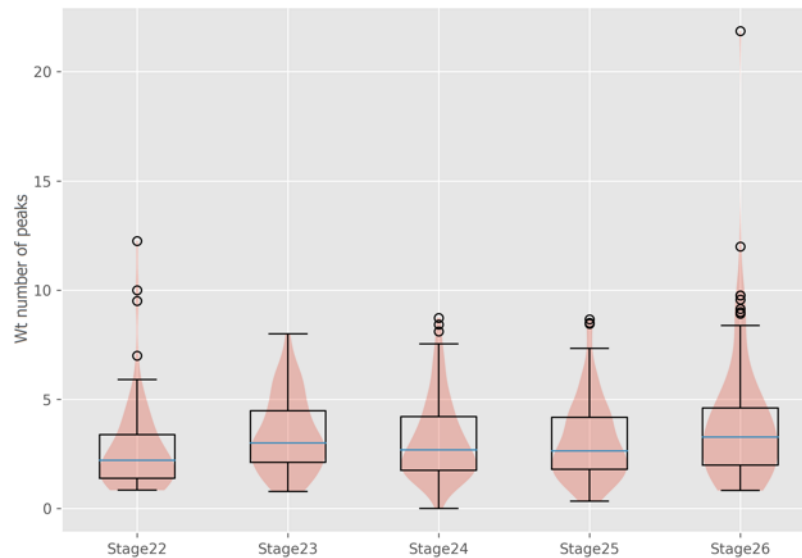
Figure 4.5 Wt Ca²⁺ number of peaks per ROI per animal per stage. Newly fertilized embryos were electroporated with 100-120 μg Cah3>GCaMP6 construct, and left to develop in 14°C. Live calcium imaging was performed on animals during Hotta stages 22 to 26, as depicted in the figure. The coloured violin plots, behind the boxplots, illustrate the overall data distribution within each stage. The number of peaks differed significantly from stages 22 to 24, but was similar between 24 and 25, and differed again from 25 to 26 (**Table 4.1**).

Table 4.1. P-values for wt Ca²⁺-signalling peak number per ROI per animal per stage

Developmental stages	22 vs. 23	23 vs. 24	24 vs. 25	25 vs. 26
(p-value)	0.003	0.018	0.100	0.016

Green = significant difference. Red = no significant difference.

4.1.6 Different mean peak height per ROI per animal between most of the stages

The wild type Ca²⁺-signalling mean peak height per ROI per animal seemed to differ between most of the developmental stages, as depicted by the boxplots in **Figure 4.6**. According to the p-values in **Table 4.2**, the peak numbers significantly differed from stage 22 to 23, but were similar between stages 23 to 24. The difference then continued from stages 24 to 26 as the embryo went through further development (**Figure 4.6**, **Table 4.2**). Based on **Figure 4.6**, all stages possessed some outliers, with stage 25 the most and stage 23 the least.
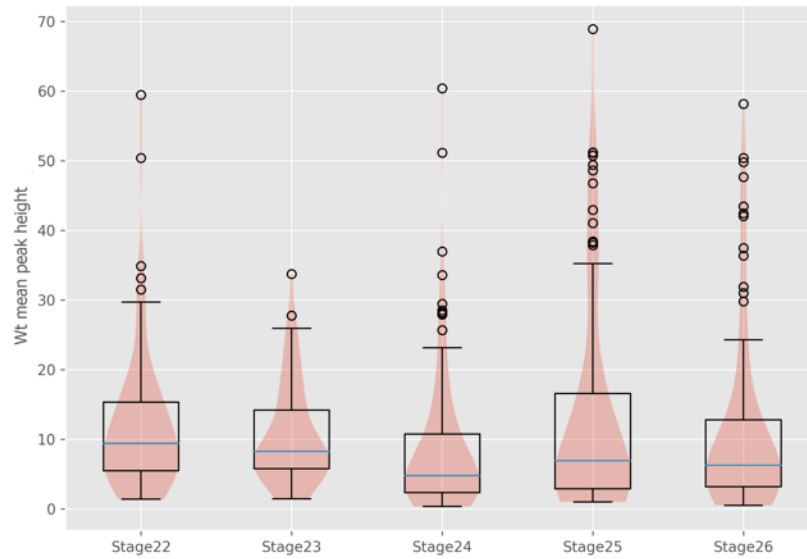
Figure 4.6 Wt Ca²⁺-signalling mean peak height per ROI per animal per developmental stage. Animals were prepared, and results illustrated, as in **Figure 4.5**. The mean peak height per ROI per animal differed from stage 22 to 23, was similar between stage 23 and 24, and differed again from stage 24 to 26 (**Table 4.2**).

Table 4.2. P-values for wt Ca²⁺-signalling mean peak height per ROI per animal per stage

Developmental stages	22 vs. 23	23 vs. 24	24 vs. 25	25 vs. 26
(p-value)	0.020	0.065	0.009	0.007

Green = significant difference. Red = no significant difference.

4.1.7 The change in mean peak height per ROI per animal differed for all stages

According to **Figure 4.7**, and the obtained p-values (**Table 4.3**), the change in mean peak height per ROI per animal differed from stage 22 to the successive stages, as the embryo underwent further developmental stages. All stages also possessed some outliers, with stage 22 outliers being the most distant from the mean (**Figure 4.7**).
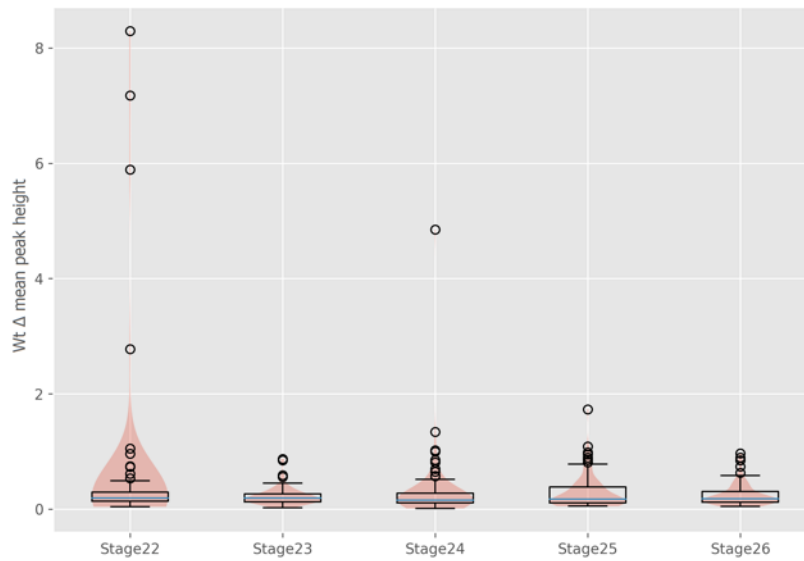
Figure 4.7 ΔF/F of Figure 4.6. The change in mean peak height per ROI per animal differed between all the stages as the embryo underwent developmental stages 22 to 26 (**Table 4.3**).

Table 4.3. P-values for the change in wt Ca^{2+}-signalling mean peak height per ROI per animal per stage

Developmental stages	22 vs. 23	23 vs. 24	24 vs. 25	25 vs. 26
(p-value)	0.001	0.004	0.047	0.007

Green = significant difference.

4.1.8 Mean peak width per ROI per animal differed for most of the stages

The mean peak width per ROI per animal was shown to differ between most of the stages, based on for example the interquartile range of the boxplots (**Figure 4.8**). This difference was also implied by the obtained p-values, which showed that the mean peak width values per ROI per animal differed from stage 22 to 23, but were similar between stage 23 and 24, and then differed again from stage 24 and onwards (**Table 4.4**). Notably, all stages possessed a few outliers, with stage 22 outliers being the most distant from the mean, and stage 26 outliers being the least (**Figure 4.8**).
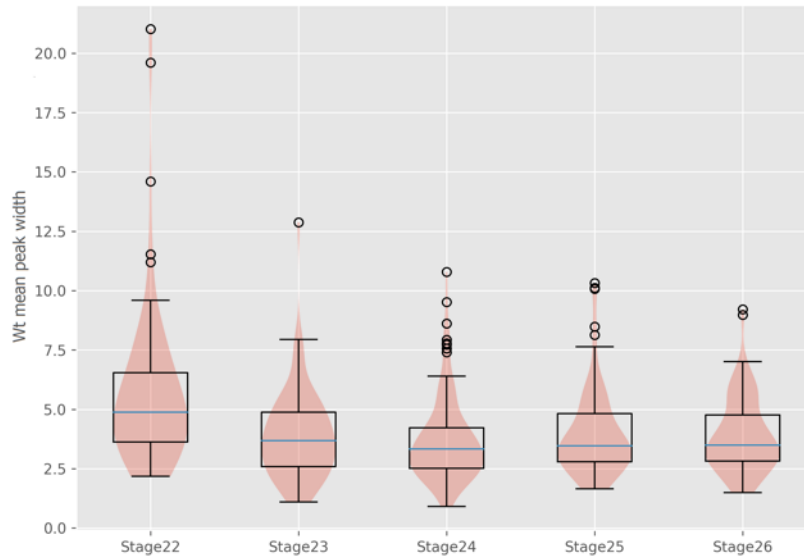
Figure 4.8 Wt calcium mean peak width per ROI per animal per stage. Animals were prepared, and results illustrated, as in **Figure 4.5**. Stage 22 and 23, and from stage 24 and onwards, differed from one another. Stage 23 and 24, however, did not. (**Table 4.4**)

Table 4.4. P-values for Ca^{2+}-signalling mean peak width per ROI per animal per stage

Developmental stages	22 vs. 23	23 vs. 24	24 vs. 25	25 vs. 26
(p-value)	0.013	0.440	0.017	0.005

Green = significant difference. Red = no significant difference

4.1.9 The change in mean peak width differed for most of the stages

The boxplots and violin plots describing the change in mean peak width, per ROI per animal per stage, resembled **Figure 4.8** and are excluded from the results section. Likewise, the p-values for the change in the mean peak width per ROI per animal per stage (**Table 4.5**) were also very similar to p-values found in **Table 4.4**.

Table 4.5. P-values for change in Ca^{2+}-signalling mean peak width per ROI per animal per stage

Developmental stages	22 vs. 23	23 vs. 24	24 vs. 25	25 vs. 26
(p-value)	0.020	0.430	0.013	0.005

Green = significant difference. Red = no significant difference

41

4.2 Pharmacological studies on *C. intestinalis* notochord

4.2.1 Morphological effects of Ca²⁺-signalling inhibition on *C. intestinalis*

Contribution from different submolecular compartments, known to store or release Ca^{2+}, to the observed calcium activity was determined by means of pharmacology combined with live calcium imaging. *C. intestinalis* embryos were incubated with 2APB and $Gado^{3+}$ separately, to detect morphological drug affect of calcium signalling inhibition in the notochord. 2APB is an inhibitor of IP_3R and SOCE, and $Gado^{3+}$ can convey information about cation channel importance for generation and propagation of calcium signalling in the notochord. Embryos at developing stage 23 were incubated separately with each drug for one hour, at three different concentrations (10 μM, 100 μM and 1 mM). They were afterwards washed and left to develop at 14 °C, followed by fixing at late taildbud or larvae stage (Section **3.4.1**). The control was embryos devoid of drug incubation.

4.2.1.1 Ca²⁺-signalling inhibition lead to deformed heads and/or notochord

Embryos incubated with 10 μM drug did not exhibit any morphological effects due to calcium inhibition in *C. intestinalis* notochord (Figures not included). As for incubation with 100 μM drug, the drug effect was evident in the notochord of some embryos, but the majority developed in a normal fashion (Figures not included). The results were however different for experiments using 1 mM drug. The control embryos (**A-B**) seem to develop a normal long tail and head, as presented in **Figure 4.9**. Embryos incubated with 2APB, on the other hand, lead to exploded heads, and deformed and short notochords (**C-D**). As for incubation with $Gado^{3+}$, some embryos seem to be both underdeveloped and deformed (**E**). The latter underdeveloped embryos have deformed flat heads, and short and twisted tails. The remaining $Gado^{3+}$ treated embryos seem to develop a more normal head, and a long tail. However, the tail of latter embryos appeared not have developed fully after initiation of lumen formation (**F**).
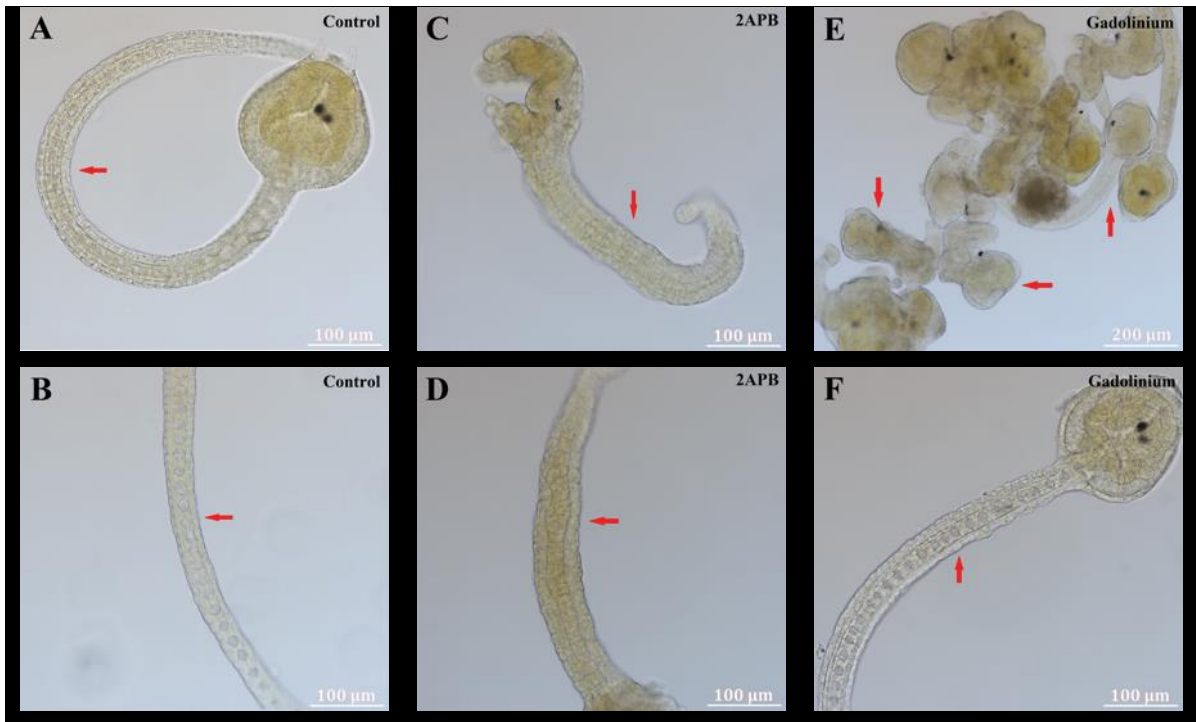
Figure 4.9 Inhibition of Ca^{2+}-signalling lead to deformed *C. intestinalis* embryos. Fertilized embryos were incubated at stage 23 developing stage for one hour with 1 mM of 2APB (**C-D**) and $Gado^{3+}$ (**D-E**) separately each. The control (**A-B**) that had not been incubated with any drug. In this figure, each condition is presented in separate columns, marked with letters and condition type. Red arrows indicate various location of drug affect. Drug affected embryos exhibit deformed morphology both in the notochord and head, compared to wt control.

4.2.2 Drug perfusion affect on *C. intestinalis* notochord during live calcium signalling

The effect of 2APB, carbenoxolone, and $Gado^{3+}$ on *C. intestinalis* notochord calcium activity was examined by drug perfusion, while performing live calcium imaging. In addition to 2APB and $Gado^{3+}$, Carbenoxolone was selected to determine the contribution of gap junction coupling to notochord calcium activity (Section **4.2.1**). Each drug was prepared with a final concentration of 100 μM. The perfusion buffer consisted of only FAWS-T for $Gado^{3+}$ condition. The perfusion buffer for 2APB and carbenoxolone conditions, on the other hand, consisted of FAWS-T with equal concentration of either DMSO or 70% EtOH that was used to dilute the respective drugs with (Section **3.4.3**). Drug perfusion was performed on live embryos from Hotta stages 22 to 26, which had previously been electroporated with 100-120 μg Cah3>GCaMP6s construct (Section **3.4.2**). The drug perfusion was performed in three phases: before = with respective perfusion buffer, during = with drug, and after = before. The control was wt *C. intestinalis* (Section **4.1**).

4.2.2.1 Visually decreased occurrence of waves and blinks in the notochord

Notochord Ca^{2+}-waves were detected in about half of the wt test embryos, but considerably lower during treatment with $Gado^{3+}$ (-70%), 2APB (-92%) and carbenoxolone (-54%). Moreover, majority of wt test embryos also exhibited notochord Ca^{2+}-blinks. The occurrence of these blinks were however lower in test embryos during $Gado^{3+}$ (-92%), 2APB (-29%) and carbenoxolone (-57%) treatment. (**Table 4.6**)

Table 4.6 Notochord Ca^{2+}-waves and -blinks detected per test embryo per condition

	Wt	**$Gado^{3+}$ treatment**	**2APB treatment**	**Carbenoxolone treatment**
Waves	52%	16%	4%	27%
Blinks	84%	7%	60	36%
Waves vs. wt		**-70%**	**-92%**	**-54%**
Blinks vs. wt		**-92%**	**-29%**	**-57%**

4.2.2.2 The number of peaks were effected differently by the drugs

Based on **Figure 4.10** boxplots, lower number of peaks per ROI per drug condition was detected during phase "before" compared to wt. But the interquartile ranges of the "before" phases vs. wt boxplots, and the respective p-values > 0.2 (**Table 4.7**), indicated similar peak number. According to the p-values (**Table 4.7**), animals perfused with carbenoxolone indicated similar number of peaks per ROI from phases B-D, but different from D-A and B-A. Perfusion with $Gado^{3+}$ on the other hand, resulted with different peak amount per ROI from phases B-D, but alike between D-A, and dissimilar again for B-A (**Table 4.7**). As for 2APB condition, the number of peaks appeared similar from B-D, D-A, and B-A, according to their respective p-values. In short, the drugs affected the number of peaks in a different manner.
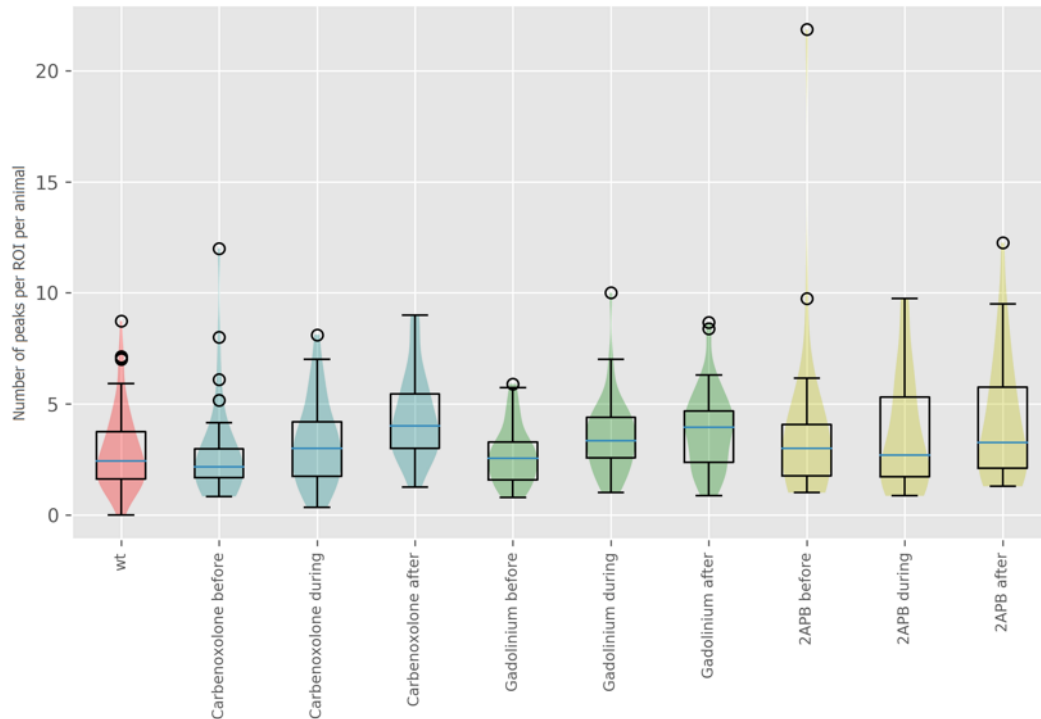
Figure 4.10 Drug effect on calcium peak amount per ROI per animal per experimental condition. Newly fertilized embryos were electroporated with 100-120 μg Cah3>GCaMP6s construct. While performing calcium imaging, the embryos were perfused with 100 μM carbenoxolone, Gado^{3+} and 2APB separately. Embryos were perfused during developmental Hotta stages 22 to 26 in three phases; before = perfusion with respective perfusion buffer, during = perfusion with drug, and after = before. (Section **3.4.2-3**) The control for this study was wt from wild type calcium imaging (Section **4.2**). The drug treatments resulted in different patterns, i.e. the number of peaks per ROI per animal was affected differently by each drug (**Table 4.7**).

Table 4.7 P-values for peak amount per ROI per animal per experimental condition

Condition	Before vs. wt (p-value)	B-D (p-value)	D-A (p-value)	B-A (p-value)
Carbenoxolone-treated		0.070	0.006	2.1×10^{-5}
Gado^{3+}-treated	> 0.200	0.006	0.160	0.001
2APB-treated		0.400	0.120	0.080

Green = significant difference. Red = no significant difference.

4.2.2.3 Mean peak height was affected similarly by carbenoxolone and Gado^{3+}

The mean peak height per ROI per animal was indicated to be similar between "before" phases and wt, according to the p-values > 0.1 (**Table 4.8**), even if not all the boxplot interquartile- and overall- ranges were completely alike (**Figure 4.11**). Perfusion with carbenoxolone led to differed mean peak height per ROI per animal between phases B-D, D-

A, and B-A (**Table 4.8**). Following the same pattern, Gado^{3+}-perfused animals also indicated different mean peak height between B-D, D-A, and B-A. Perfusion with 2APB also led to differed mean peak height between B-D, but then alike between D-A and different between B-A. In short, a similar pattern was observed for carbenoxolone and Gado^{3+} treated animals, where the mean peak height changed throughout the three phases. 2APB treated signalling pattern, however, differed from the other two drug conditions. (**Table 4.8**)

Figure 4.11 Drug affect on mean peak height per ROI per animal per experimental condition. Embryos were prepared, and the study performed, as in **Figure 4.10** with the same wt control. Carbenoxolone and Gado^{3+} affected mean peak height per ROI per animal in a similar fashion, which was not the same for 2APB-treated animals (**Table 4.8**).

Table 4.8 P-values for mean peak height per ROI per animal per experimental condition

Condition	Before vs. wt (p-value)	B-D (p-value)	D-A (p-value)	B-A (p-value)
Carbenoxolone-treated		0.003	0.004	9.1×10^{-8}
Gado^{3+}-treated	> 0.100	4.3×10^{-4}	0.002	1.1×10^{-7}
2APB-treated		0.009	0.110	3.3×10^{-4}

Green = significant difference. Red = no significant difference.

4.2.2.4 The drug treatments affected the change in mean peak height differently

The interquartile range of the "before" boxplots in **Figure 4.12**, and the p-value > 0.06 (**Table 4.9**), indicate similar change in mean peak height per ROI per drug treatment vs. wt. Carbenoxolone-perfused animals resulted with similar change in mean peak height per ROI from B-D, but not between D-A and B-A (**Table 4.9**). Gado^{3+} condition showed that the change was similar between B-D, B-A, and D-A (**Table 4.9**). As for 2APB-perfused animals, the change was dissimilar for B-D and B-A, but similar for D-A (**Table 4.9**). To summarize, the drugs affected the change in mean peak height differently.
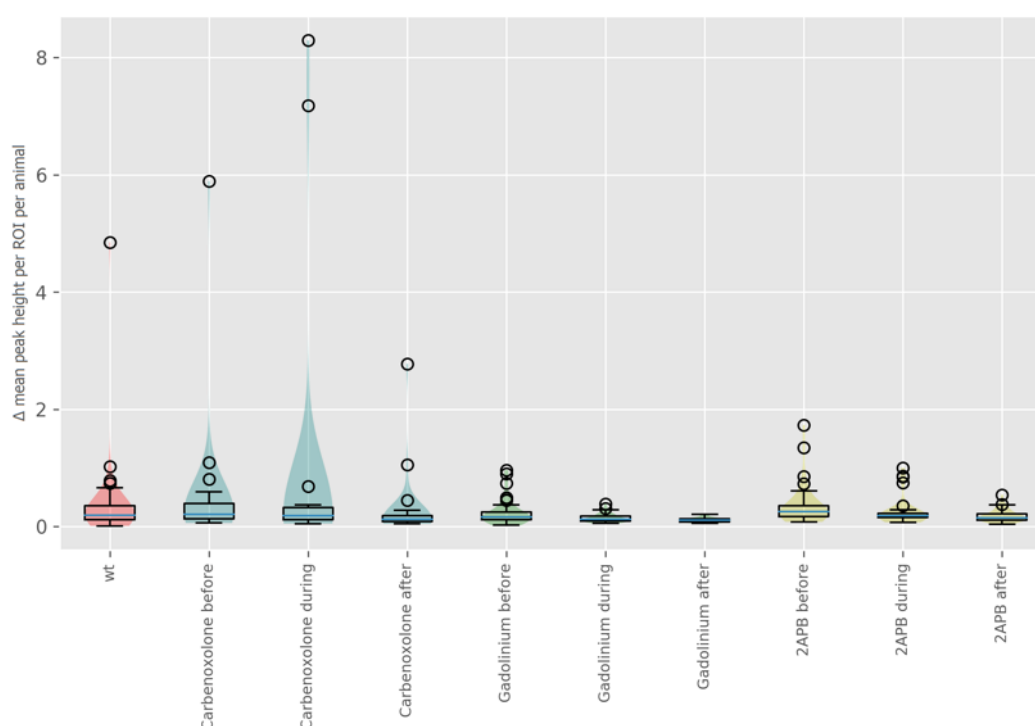
Figure 4.12 ΔF/F of Figure 4.11. The figure illustrates the change in mean peak height per ROI per animal per experimental condition, which was affected differently by the three drugs (**Table 4.9**).

Table 4.9 P-values for the change in mean peak height per ROI per animal per experimental condition

Condition	Before vs. wt (p-value)	B-D (p-value)	D-A (p-value)	B-A (p-value)
Carbenoxolone-treated	> 0.060	0.130	0.009	5.6x10^{-4}
Gado^{3+}-treated		0.008	0.023	1.6x10^{-5}
2APB-treated		0.020	0.070	0.001

Green = significant difference. Red = no significant difference.

4.2.2.5 The drug treatments affected the mean peak width in a similar manner

The p-values > 0.2 (**Table 4.10**), and the boxplots in **Figure 4.13**, show "before" mean peak width values of carbenoxolone and Gado^{3+} resembling wt condition. Notably however, 2APB-treated "before" phase differed from wt with a p-value at 0.001. It should also be noted that the wt condition differed both from 2APB phase "during" (p-value 0.02) and "after" (p-value 0.006) as well (Not included in the table). Interestingly enough, the mean peak width per ROI per animal was similar between B-A, D-A and B-A for all drug conditions, according to the p-values (**Table 4.10**).

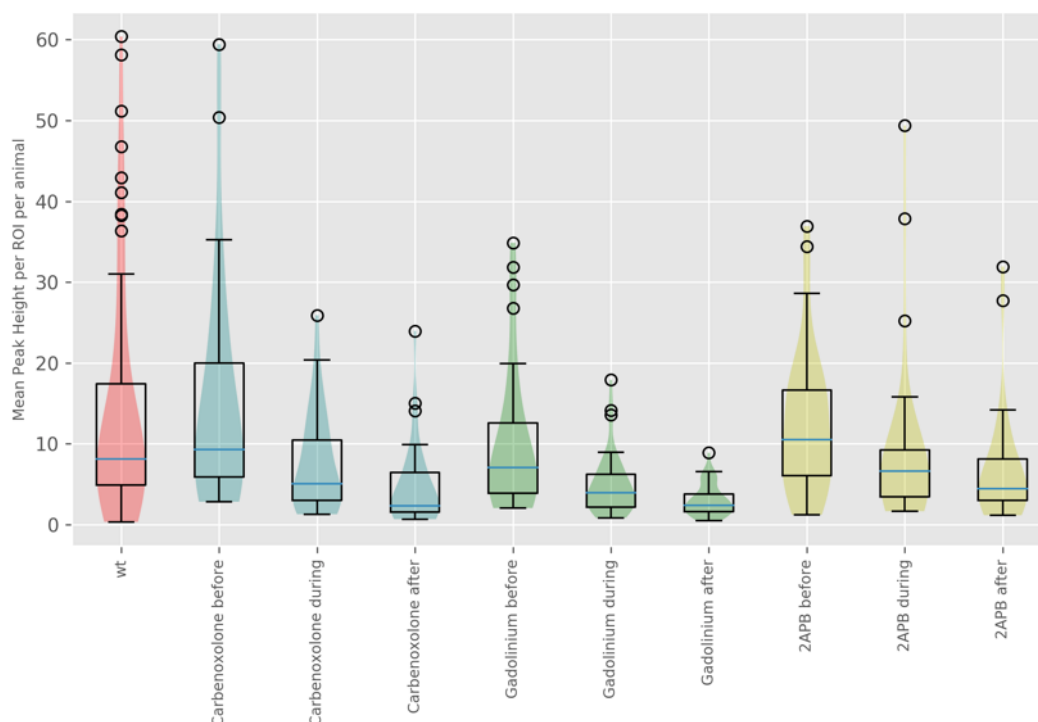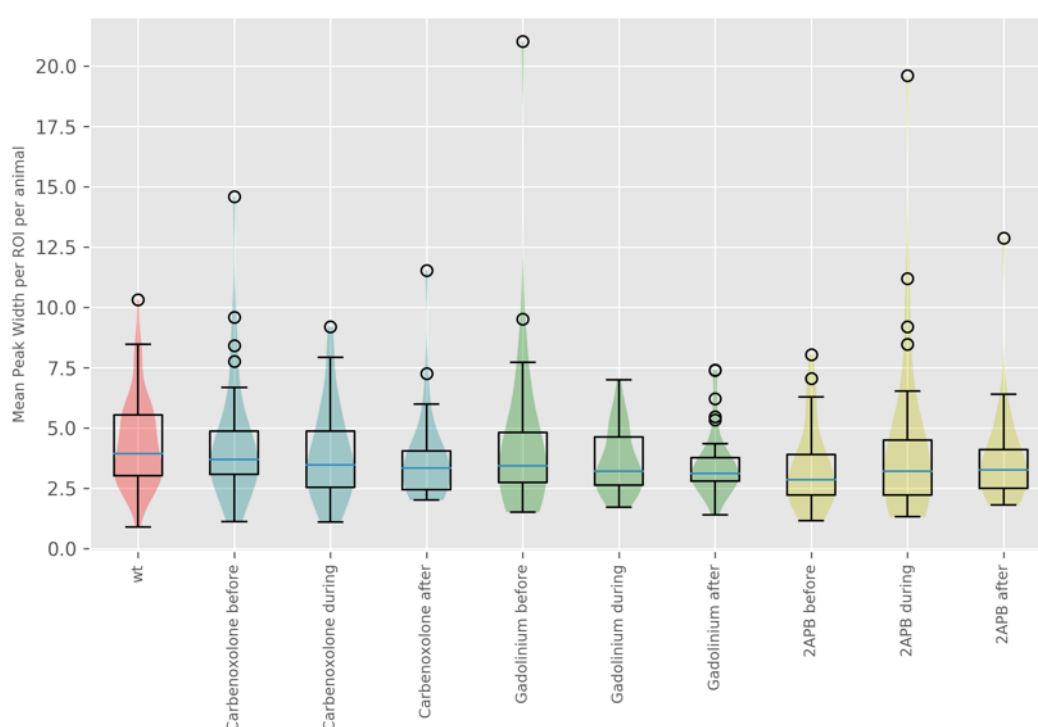**Figure 4.13 Mean peak width per ROI per animal per experimental condition**. Embryos were prepared, and the experiment performed, as in **Figure 4.10**. The mean peak width per ROI per animal was affected in a similar manner by all three drugs (**Table 4.10**). Notably, 2APB-treated "before" phase differed from (p-value 0.001).

Table 4.10 P-values for mean peak width per ROI per animal per experimental condition

Condition	Before vs. wt (p-value)	B-D (p-value)	D-A (p-value)	B-A (p-value)
Carbenoxolone-treated		0.230	0.310	0.070
Gado^{3+}-treated	> 0.070	0.270	0.410	0.180
2APB-treated	0.001	0.210	0.430	0.150

Green = significant difference. Red = no significant difference.

4.2.2.6 The drug treatments affected the change in mean peak width in a similar fashion

The boxplots and violin plots of the change in mean peak width per ROI, per animal per drug treatment, resembled **Figure 4.13** and is not included in the results section. The p-values are however included (**Table 4.11**), which indicates that the drugs affected the change in mean peak width per ROI per animal in a similar manner and followed the same trend as in section **4.2.2.5**. Also here, the change in wt mean peak width was different from that of 2APB phase "before" (p-value at 0.001), "during" (p-value 0.02) and "after" (p-value 0.006) (Not included in the table).

Table 4.11 P-values for the change mean peak width per ROI per animal per experimental condition

Condition	Before vs. wt (p-value)	B-D (p-value)	D-A (p-value)	B-A (p-value)
Carbenoxolone-treated		0.220	0.390	0.110
Gado^{3+}-treated	> 0.070	0.270	0.420	0.190
2APB-treated	0.001	0.210	0.430	0.150

Green = significant difference. Red = no significant difference.

4.3 Downregulation of *C. intestinalis* notochord calcium activity by RNAi

4.3.1 Downregulation of notochord calcium activity

This screen was initiated to study the mechanisms of calcium signalling in *C. intestinalis* notochord. With this purpose in mind, downregulation via RNAi was performed to disrupt the molecular pathway underlying calcium activity in the notochord. This was conducted by electroporating shRNA constructs into newly fertilized *C. intestinalis* eggs. The RNAi oligodeoxyribonucleotides were designed against SERCA and calmodulin (Sections **3.5.1-5**). 100 μg of either shRNA-SERCA, or shRNA-Calm, construct was mixed with 80 μg Cah3>GCaMP6s construct, to detect any downregulation through live calcium imaging (**3.5.6-7**). The wild type calcium imaging (Section **4.1**) was used as wt control for this study.

4.3.2 Overall similar number of peaks between the knockdown animals and wt

The number of peaks per ROI per knocked-down animal is indicated to be similar according to the p-values > 0.6, and the interquartile range of the boxplots in **Figure 4.14**, between both RNAi affected conditions and wt. The overall range of the shRNA-SERCA boxplot was however shorter than wt boxplots (**Figure 4.14**).

	p-value
shRNA-Calm vs. wt	0.130
shRNA-SERCA vs. wt	0.060
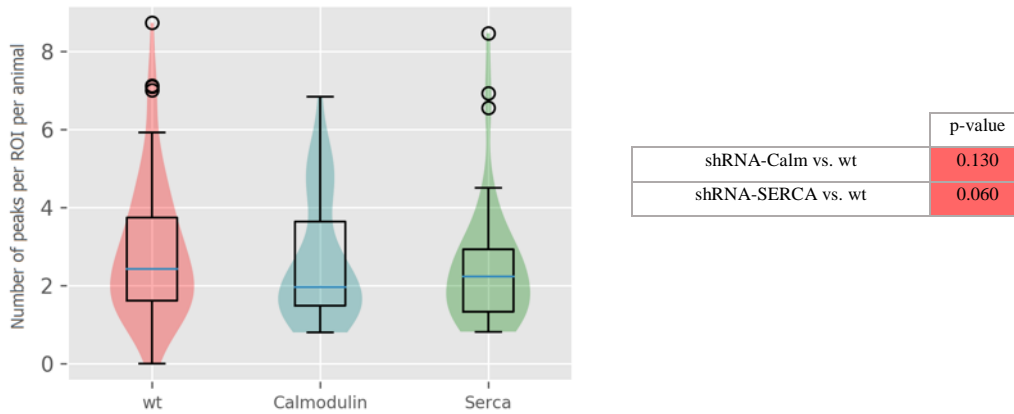
Figure 4.14 RNAi effect on overall calcium peak number per ROI per animal per experimental condition. Fertilized embryos were co-electroporated with 80 μg Cah3>GCaMP6s construct and 100 μg of either shRNA-SERCA or shRNA-Calm construct. The wt control condition is from wild type calcium imaging (Section **4.2**). The coloured violin plots, behind the boxplots, illustrate overall data distribution. P-values (red cells) indicate similar number of peaks per ROI per animal between the stated experimental conditions.

4.3.3 Stage 23 knocked-down animals possessed different peak numbers compared to wt

It is notable to mention that stage 23 wt animals exhibited different number of peaks, per ROI per animal, compared to shRNA-Calm and shRNA-SERCA knocked-down animals (**Figure 4.15**). In other words, stage 23 knock-downs differed from the other stages (Section **4.3.2**).

	p-value
shRNA-Calm vs. wt	0.020
shRNA-SERCA vs. wt	0.007
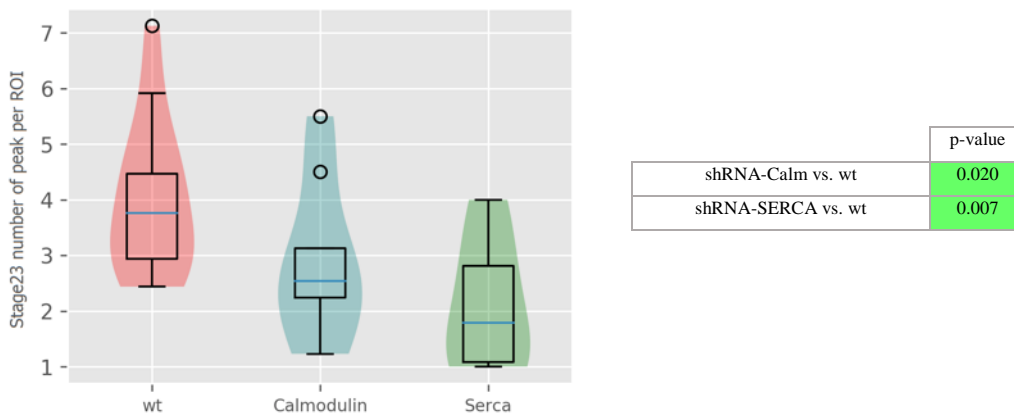
Figure 4.15 RNAi effect on calcium peak number per ROI per stage 23 animals per condition. Embryos were prepared, and the experiment performed, as in **Figure 4.14**. P-values in green cells indicate significant difference between the respective conditions.

4.3.4 Overall different mean peak height between knock-downs and wt

Figure 4.16, and the respective p-values, shows that the wt condition has different mean peak height per ROI per animal compared to both shRNA-Calm and shRNA-SERCA knock-downs.

	p-value
shRNA-Calm vs. wt	0.006
shRNA-SERCA vs. wt	0.003

Figure 4.16 RNAi effect on overall mean peak height per ROI per animal per experimental condition. Embryos were prepared, and the experiment performed, as in **Figure 4.14**. P-values in green cells indicate significant difference between the respective conditions.

4.3.5 Knock-downs at certain stages exhibited similar mean peak height relative to wt

Certain knocked down stages however possessed similar mean peak height compared to respective wt stages. These were stage 22, 24 and 26 of both RNAi conditions (p-value > 0.06), and shRNA-SERCA stage 25 (p-value 0.35), which had similar mean peak heights compared to wt condition. (Figures not included)

4.3.6 Overall differed change in mean peak height between knock-downs and wt

Dissimilarity was illustrated in terms of boxplots, and p-values, to show the change in mean peak height per ROI per animal between wt and both shRNA-Calm and shRNA-SERCA knock-downs (**Figure 4.17**).

	p-value
shRNA-Calm vs. wt	0.008
shRNA-SERCA vs. wt	0.011
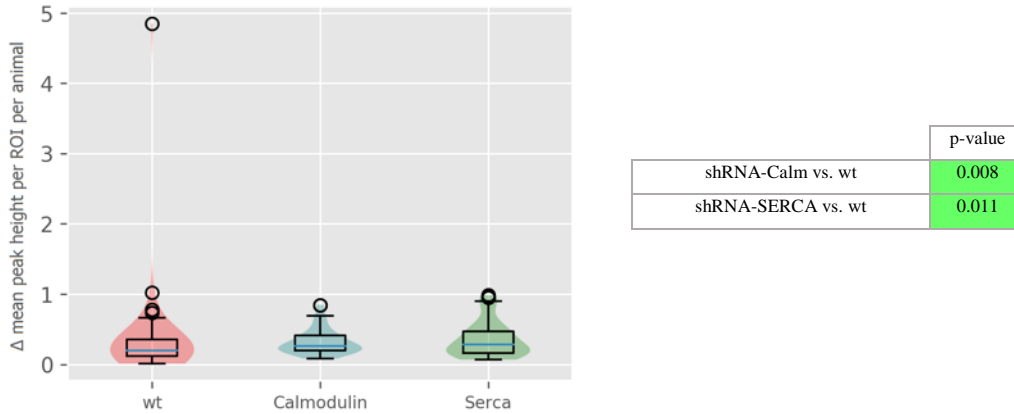
Figure 4.17 ΔF/F of Figure 4.16. Figure depicts the overall change in mean peak height per ROI per animal per experimental condition. P-values in green cells indicate significant difference between the respective conditions.

4.3.7 Knock-downs at certain stages exhibited similar change in mean peak height to wt

There was however also some similarities between certain development stages of RNAi conditions and wt, when it comes to change in mean peak height per ROI (Figures not included). Stages 22, 24, and 25 of both RNAi conditions had similar changes in mean peak height compared to respective wt stages (p-value 0.1-0.3). Moreover, wt animals and shRNA-SERCA knock-downs at stage 26 showed similar change in mean peak height (p-value 0.3).

4.3.8 Overall dissimilar mean peak widths in knock-downs compared to wt

The boxplots in **Figure 4.18** indicate that majority of the knock-downs possessed slightly lower mean peak width range compared to wt. This statement is also supported by the respective p-value > 0.04. Additionally, the change in mean peak width per ROI per animal per condition followed almost the exact same trend, with almost the same boxplots, p-values (+/- 0.001), and data distribution, as in **Figure 4.18**.

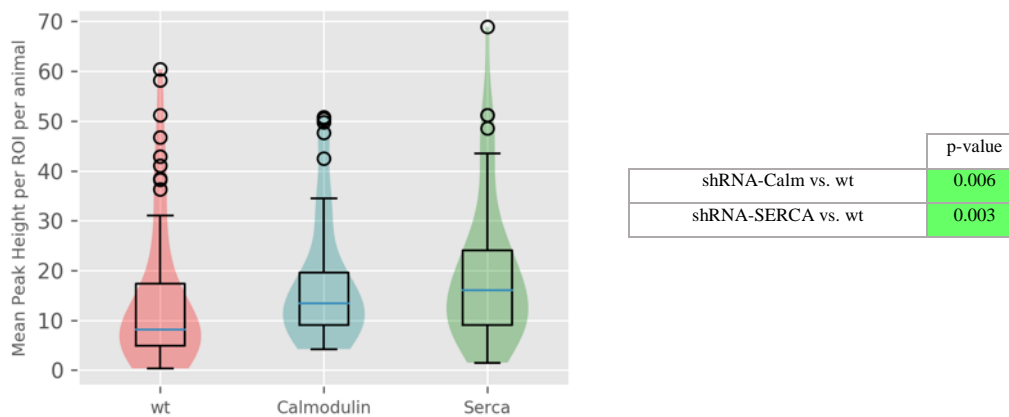|	p-value
shRNA-Calm vs. wr	0.020
shRNA-SERCA vs. wt	0.040
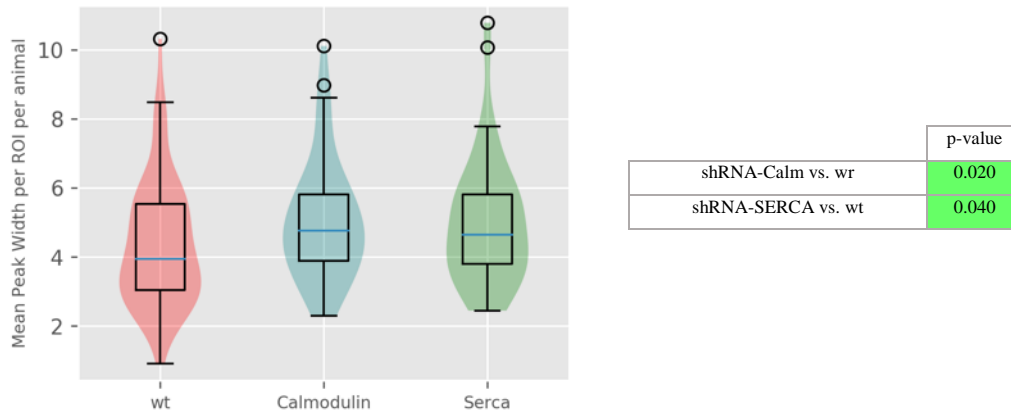
Figure 4.18 RNAi effect on overall mean peak width per ROI per animal per experimental condition. Embryos were prepared, and the experiment performed, as in **Figure 4.14**. P-values in green cells indicate significant difference between the respective conditions.

4.3.9 Certain knocked-down stages possessed similar mean peak width compared to wt

Regarding mean peak width per ROI per animal per experimental condition, there were also some similarities between certain development stages of both RNAi conditions compared to wt. shRNA-Calm and shRNA-SERCA knock-downs of stage 22 and 25 (Figures not included), and shRNA-SERCA stage 23 and 24 animals, had similar mean peak width compared to respective wt stages (p-values 0.07-0.3).

4.4 Difference in shRNA-Calm effected *C. intestinalis* notochord

4.4.1 Detecting difference in shRNA-Calm effected *C. intestinalis* notochord

Calmodulin has previously been described to express in the outermost part of *C. intestinalis* notochord (Reeves, W., Thayer, R., & Veeman, M. 2014). Further analysis on the data from shRNA-Calm knock-downs (Section **4.3**) was therefore performed to detect difference in the signalling located on different parts of the notochord. This was conducted by plotting calcium signalling data from wt anterior+posterior (AP) and middle (M) notochord cells against respective parts of animals down-regulated by shRNA-Calm.

4.4.2 Overall differed number of peaks at M and AP in shRNA-Calm condition vs. wt

Figure 4.19 illustrates shRNA-Calm knocked-down M and AP with decreased peak amount range, and interquartile range, compared to that of the wt. The p-values also indicated that the knocked-down M and AP differed from respective wt notochord parts.
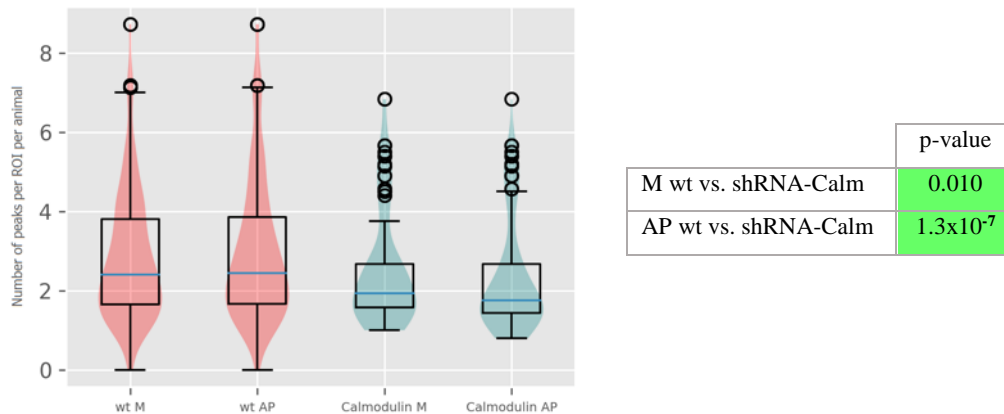
Figure 4.19 shRNA-Calm effect on overall number of peaks per ROI per animal in AP and M. Fertilized embryos were co-electroporated with 80 μg Cah3>GCaMP6s, and 100 μg shRNA-Calm, construct. The wt control condition is from wild type calcium imaging (Section **4.2**). P-values in green cells indicate significant difference between the respective conditions. The coloured violin plots, behind the boxplots, illustrate the overall data distribution within each notochord part.

4.4.3 Stage 22 and 24 knock-downs had similar number of peaks compared to wt

With regards to the mean peak amount values, there seemed to be some similarities at certain stages between shRNA-Calm affected notochord parts vs. wt. The latter applies to stage 22 M and AP of knocked-down animals vs. wt (**Figure 4.20**). Stage 24 RNAi affected M vs. wt M also possessed similar peak numbers (p-value 0.09) (Figures not included).

	p-value
M wt vs. shRNA-Calm	0.20
AP wt vs. shRNA-Calm	0.47

Figure 4.20. shRNA-Calm effect on calcium peak amount per ROI per stage 22 animals in AP and M. Embryos were prepared, and the experiment performed, as in **Figure 4.19**. P-values in red cells indicate no significant difference between the respective conditions.

4.4.4 Overall different mean peak height at M and AP vs. wt, except AP at stage 25

The boxplots of shRNA-Calm condition M and AP had both slightly different interquartile ranges, and mean peak height value ranges, compared to wt (**Figure 4.21**). Additionally, the p-values indicated different mean peak height per ROI per animal in M and AP between the RNAi and wt conditions. Moreover, the wt condition had more outliers compared to boxplots of RNAi knock-downs. Furthermore, only stage 25 shRNA-Calm effected AP had similar mean peak height per ROI compared to wt, with a p-value at 0.07 (Figure not included).

	p-value
M wt vs. shRNA-Calm	6.3×10^{-8}
AP wt vs. shRNA-Calm	3.5×10^{-11}
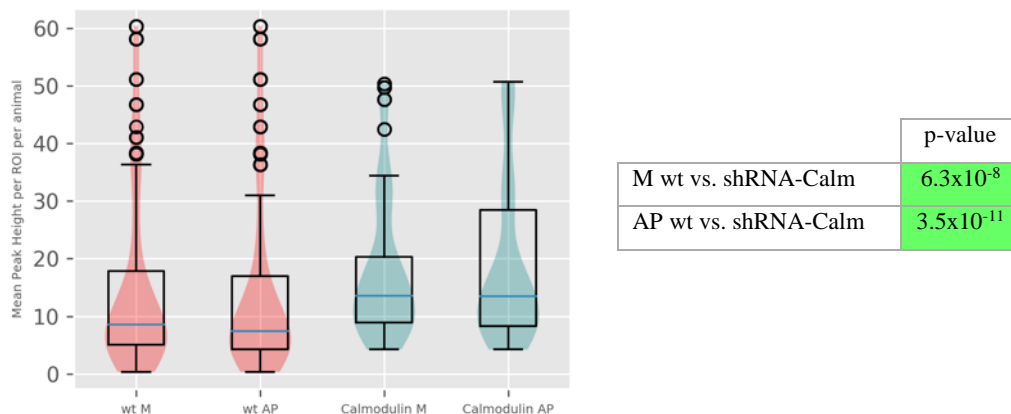
Figure 4.21 shRNA-Calm effect on overall mean peak height per ROI per animal in AP and M. Embryos were prepared, and the experiment performed, as in **Figure 4.19**. P-values in green cells indicate significant difference between the respective conditions.

4.4.5 Overall different change in mean peak height at M and AP of knock-downs vs. wt

Figure 4.22 illustrates different change in mean peak height per ROI per animal at M and AP between knock-downs and wt. In accord with the figure and p-values, there was a difference in the change in mean peak height per ROI at M and AP of shRNA-Calm knock-downs vs. wt.

	p-value
M wt vs. shRNA-Calm	2.0×10^{-9}
AP wt vs. shRNA-Calm	4.9×10^{-11}
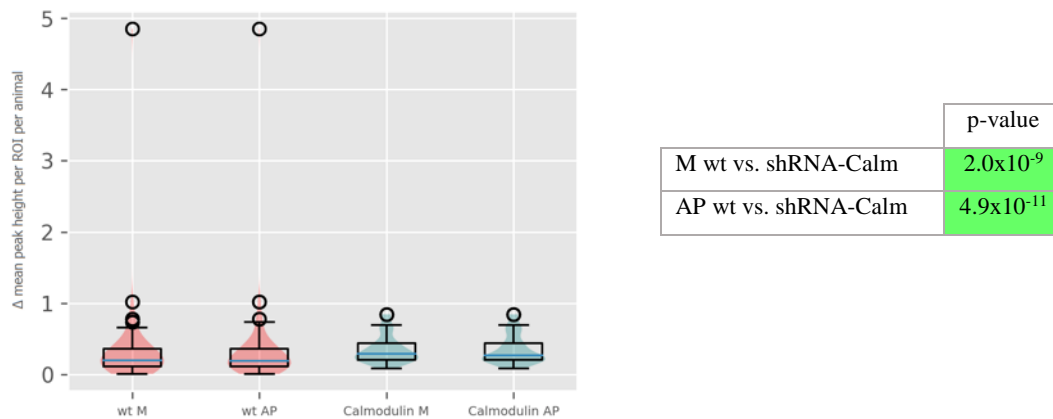
Figure 4.22 ΔF/F of Figure 4.21. The figure illustrates the overall change in mean peak height per ROI per animal in distinct anatomical locations. P-values in green cells indicate significant difference at M and AP of shRNA-Calm and respective wt notochord parts.

4.4.6 Stage 22 knock-downs exhibit similar change in mean peak height compared to wt

shRNA-Calm M knock-downs at stage 22 however, had similar changes in mean peak height per ROI per animal compared to respective wt parts (**Figure 4.23**). Stage 25 shRNA-Calm AP vs. wt AP also showed similar change in mean peak height with a p-value at 0.09 (Figure not included).

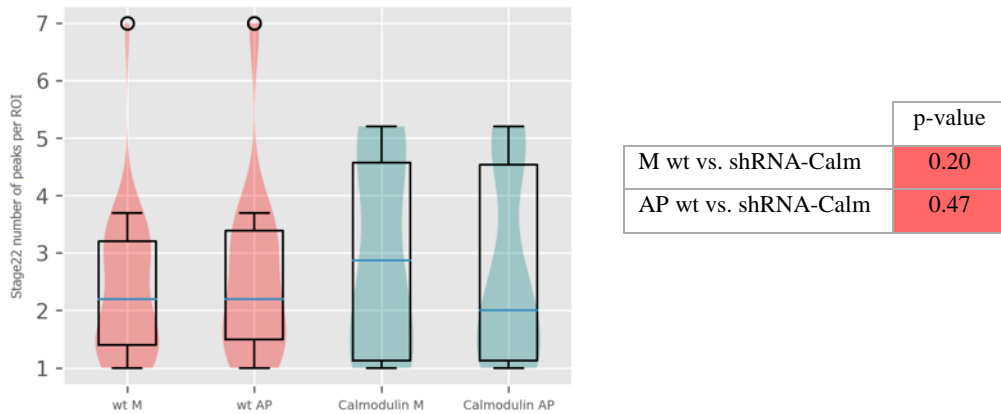|	p-value
M wt vs. shRNA-Calm	0.11
AP wt vs. shRNA-Calm	0.09
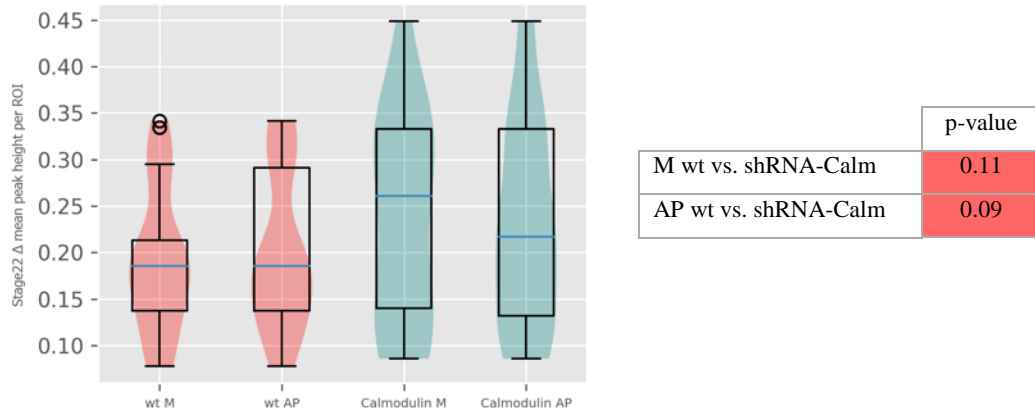
Figure 4.23 shRNA-Calm effect on change in mean peak height per ROI per stage 22 animals in AP and M. Embryos were prepared, and the experiment performed, as in **Figure 4.19**. P-values in red cells indicate no significant difference between the respective conditions.

4.4.7 Overall differed mean peak width at M and AP of knock-downs vs. wt

The mean peak width per ROI per animal in wt M and AP differed from RNAi effected M and AP (**Figure 4.24**). Moreover, the boxplots and p-values for the change in mean peak width per ROI per animal (Figure not included) resembled **Figure 4.24**, and is not included in the results section.

	p-value
M wt vs. shRNA-Calm	3.6×10^{-8}
AP wt vs. shRNA-Calm	1.2×10^{-11}
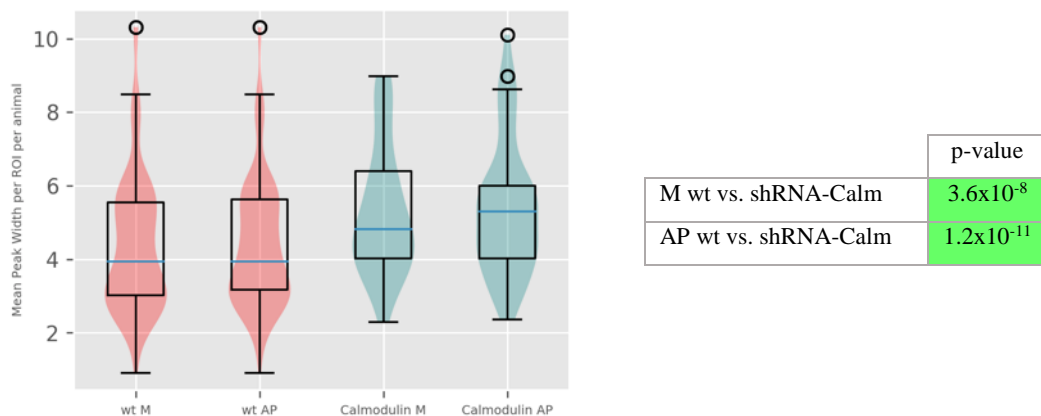
Figure 4.24 RNAi effect on overall mean peak width per ROI per animal in AP and M. Embryos were prepared, and data analysed, as in **Figure 4.19**. P-values in green cells indicate significant difference between the respective shRNA-Calm M and AP vs. wt M and AP.

4.4.8 Stage 22 knock-downs indicate similar mean peak widths compared to wt

Notably, stage 22 shRNA-Calm effected M and vs. wt M indicated similar mean peak width per ROI per animal with (p-values 0.37), and stage 25 knocked-down AP vs. wt AP (p-value 0.056) respectively (Figures not included).

4.5 In-situ hybridization

4.5.1 Expression analysis of ion channel genes in *C. intestinalis* notochord

This screen was performed to identify putative calcium signalling pathway components such as ion channels, cytosolic molecules, and effectors of this pathway based on published microarray data, in *C. intestinalis* notochord. First, amplified Ci-Brachyury, Ci-connexin-related-8, AT2B1, Ci-TRMP3, Ci-Cav1, KNCQ4/5 and Ci-TWIK5 genes (Sections **3.2.2-4**) were ligated into TOPO-TA vectors. Bacterial colonies were then selected for further processing using a blue-white screening approach (Sections **3.2.5-6**). Purified plasmid was then digested, followed by agarose gel electrophoresis, to select correct plasmids for sequencing based on DNA band size (Sections **3.2.7-8**). The samples with matching sequences to the reference cDNAs were later on purified (Sections **3.2.9-11**) and RNA antisense probes against mRNA of the genes were synthesized through in-vitro transcription (Section **3.2.12**). In-situ hybridization was performed using 1 ng/μL of each RNA antisense probe on fixed *C. intestinalis* embryos, from early gastrula to larvae stages, to detect their respective gene expression in the notochord (Section **3.2.12**). Previously described Ci-Brachyury was used as control for this study, due to its expression in *C. intestinalis* notochord cells (Takahashi, H. et al. 1999; Satoh, N., et al. 2014).

4.5.2 Ci-Brachyury expressed the most, whereas the other genes expressed weaker

As depicted in **Figure 4.25**, Ci-Brachyury expressed the most in the developing notochord cells, from gastrula to late tailbud stage (**A-C**). The expression of the latter gene seems to be strongest during gastrula, relatively strong during early tailbud, and weaker during late tailbud stage. Ci-connexin-related-8 and AT2B1 expressed weak and vaguely in the developing notochord cells from gastrula to early tailbud (**D-E**, **G-H**). The former did however express relatively strong behind the head, and in the tissue surrounding the notochord anterior, during late tailbud stage (**F**). As for AT2B1 during late tailbud stage, expression was strong near the neck in tissue surrounding the notochord, and in cells in mid-notochord (**I**). KNCQ4/5 on the

other hand did not express during gastrula, but vaguely expressed in the notochord cells during early tailbud, with strongest expression in tissues surrounding the notochord anterior during late tailbud (**J-L**).
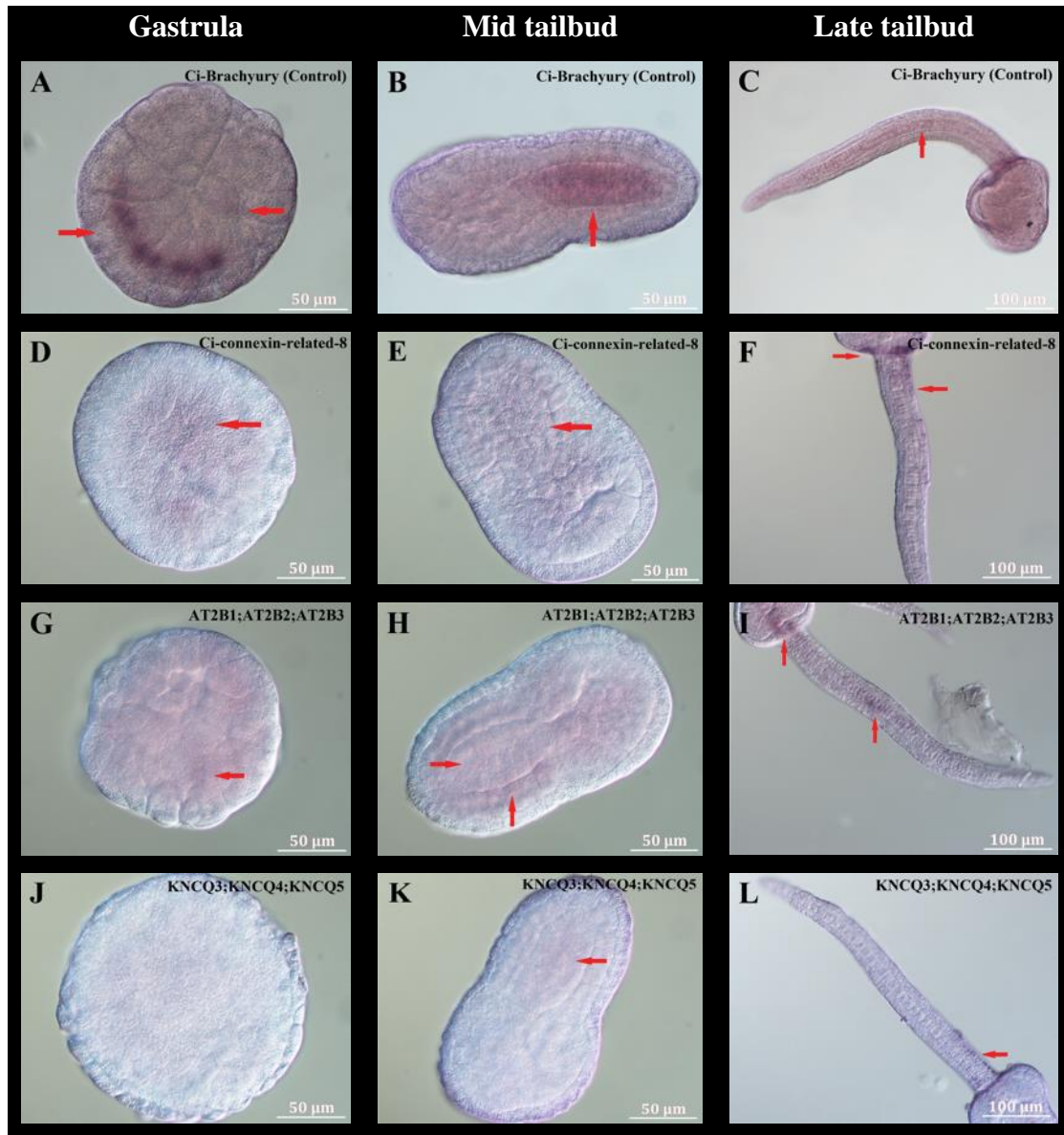
Figure 4.25 Ion channel gene expression in C. intestinalis notochord by in-situ hybridization. Antisense RNA probes against Ci-Brachyury (control), Ci-connexin-related-8, AT2B1, and KNCQ4/5 mRNA were synthesized by in-vitro transcription. 1 ng/µL of each RNA probe was used in in-situ hybridization on fixed C. intestinalis embryos. Imaged embryos from gastrula to late tailbud stage are depicted in individual columns, and marked with both letters and the gene that is being expressed. Red arrows point where expression is detected. Overall, the control expressed the most and decreased from gastrula to larvae, compared to the other genes.

4.6 Drug effect on *C. intestinalis* notochord cells actomyosin network

4.6.1 Structural analysis of drug effect on notochord cells actomyosin network

The actomyosin netword in *C. intestinalis* notochord mediates cell motility and cell shape changes in the developing embryo (Denker, E., and D. Jiang. 2012; Balaji, R., et al. 2017). With this in mind, the effects of calcium signalling on notochord actomyosin network were studied using pharmacology. Newly fertilized eggs were co-electroporated with 100 μg each of Bra>MLC wt Mcherry and Bra>Lifeact GFP constructs (Section **3.6.1**). The electroporated embryos were then incubated separately with 100 μM 2APB, carbenoxolone, and Gado^{3+} each, to study their effect on the notochord actomyosin network (Section **3.6.2**). The incubation occurred for one hour in 14°C, when the embryos were at early tailbud stage. Wt were incubated with the drugs individual perfusion buffer, which were prepared from FAWS-T with equal concentration of either DMSO or 70% EtOH used for drug preparation. The latter chemicals were used to dilute 2APB and carbenoxolone with, respectively. Gado^{3+} wt animals were incubated in only FAWS-T. Embryos were then washed, and left to develop at 14°C. They were later on fixed every three hours, and mounted on mounting slides for drug affect visualization by means of confocal imaging (Sections **3.6.3**-**5**).

4.6.2 The inhibitors effected the notochord actomyosin network slightly differently

The wt controls for this study did not differ from each other; **Figure 4.26** has therefore images of only one animal per fixation round for wt at three-hour intervals post drug incubation. Wt Bra>Lifeact GFP electroporated embryos (**A-C**) visualized brachyury driven expression of F-actin binding protein attached with green fluorescent protein. The latter signal was clear in all notochord cells at 3hpi (**A**) and 6hpi (**B**), with slightly declined expression and in fewer cells at 9hpi (**C**). It is notable to add that some embryos expressed in all notochord cells at 9phi as well (Figure not included). The same expression trend was detected in wt Bra>MLC wt Mcherry electroporated embryos (**A'-B'**), where brachyury drives the expression of MLC protein with attached Mcherry fluorophore.

Based on treatment with carbenoxolone; the embryos at 3hpi (**D, D'**) were similar to respective wt 3hpi (**A, A'**), both in terms of protein expression and notochord cell shape. At 6phi, however, drug incubated notochord cells expressed Lifeact-GFP and MLC wt Mcherry

in slightly fewer cells (**E, E'**), where the cells were also relatively smaller, compared to wt 6hpi (**B, B'**). Notably, at 9hpi, the drug incubated showed very weak expression in all notochord cells, where one cell was relatively bigger than the rest (**F, F'**). In other words, 3hpi wt and carbenoxolone had similar results. The differences started to show at 6hpi, where carbenoxolone treatment led to expression in fewer cells, but with equal intensity, relative to wt. At 9hpi, carbenoxolone incubated notochord cells showed expression in all cells, but weakly and mostly at cell edges, which was not the case for wt 9hpi.

As for incubation with $Gado^{3+}$, almost half of the notochord cells at 3phi (**G**) expressed Lifect-GFP as in wt 3hpi (**A**), while the other half had weaker protein expression. Meanwhile, MLC wt Mcherry expression at 3phi was weaker in some notochord cells (**D'**), and almost non-existent in others, compared to wt (**A'**). But the cells shapes at 3hpi were in general relatively similar to respective wt cell shape. At 6hpi (**H**), the $Gado^{3+}$ affect notochord cells had weaker Lifeact-GFP expression in some notochord cells, and even weaker in others, compared to wt (**B**). The MLC wt Mcherry expression seemed to be weaker and in even fewer notochord cells compared to both respective wt (**B'**) and the 6hpi Lifeact-GFP (**H**). Regarding notochord cells at 9hpi (**I, I'**), the cell shapes seemed similar to respective wt (**C, C'**), but with stronger protein expression. It is however notable to mention that there were also 9phi $Gado^{3+}$-inhibited cells that looked similar to **F** and **F'**.

Finally, 2APB treated notochord cells exhibited differences in both cell shape and protein expression already by 3phi (**J, J'**). The drug affected notochord cells at 3hpi seemed to have both some bigger, and smaller, cell shapes compared to respective wt (**A, A'**). 3phi drug incubated notochord cells additionally displayed somewhat similar Lifeact-GFP expression intensity, but weaker MLC wt Mcherry, compared to the wt. Furthermore, 6phi with $Gado^{3+}$ also led to notochord cells with even weaker (**K**), and in even fewer cells, compared to wt 6phi (**B**). MLC wt Mcherry was additionally expressed even less than Lifeact-GFP 6phi due to $Gado^{3+}$ (**K, K'**) compared to wt (**B'**). The clear expression in wt 9phi (**C, C'**) was also not present in 9hpi $Gado^{3+}$ treated notochord cells (**L, L'**) where Lifect-GFP was expressed weakly, and MLC wt Mecherry even weaker and in even fewer cells. To summarize, 2APB incubation affected the notochord cells already at 3hpi, and lead to fewer cells with expression that was weaker than wt.

Condition	3hpi	6hpi	9hpi
Wt	A Bra>lifeact GFP A' Bra>MLC wt 30 µm	B Bra>lifeact GFP B' Bra>MLC wt 30 µm	C Bra>lifeact GFP C' Bra>MLC wt 30 µm
Treatment with 100 µM carbenoxolone	D Bra>lifeact GFP D' Bra>MLC wt 30 µm	E Bra>lifeact GFP E' Bra>MLC wt 30 µm	F Bra>lifeact GFP F' Bra>MLC wt 30 µm
Treatment with 100 µM Gado³⁺	G Bra>lifeact GFP G' Bra>MLC wt 30 µm	H Bra>lifeact GFP H' Bra>MLC wt 30 µm	I Bra>lifeact GFP I' Bra>MLC wt 30 µm
Treatment with 100 µM 2APB	J Bra>lifeact GFP J' Bra>MLC wt 30 µm	K Bra>lifeact GFP K' Bra>MLC wt 30 µm	L Bra>lifeact GFP L' Bra>MLC wt 30 µm

Figure 4.26 Drug affect on myosin network of *C. intestinalis* notochord cells. In this figure, from left: the wt and drug conditions are stated in column one. All animals, except wt, were incubated with 100 µM of each drug separately, then washed with FASW-T, and left to develop at 14°C. The hours post drug incubation (hpi), which the animals were fixed at, is stated successively in the following columns. The wt was incubated similarly, but with mainly FAWS-T. Notochord cells coloured in green are caused by electroporation with Bra>Lifeact GFP (**A-L**), and red by Bra>MLC wt Mcherry (**A'-L'**). There are slightly different scale bars from image to image.

5. Discussion

The notochord is an essential structure for *C. intestinalis* embryonic development, where it serves as a structural support, enables locomotion during larval stage, and conveys position and fate information. In recent years, researchers have described Ca^{2+}-signalling/-channels as a key element in the development of many organisms. However, only one study has investigated the role and importance of Ca^{2+}-signalling in *C. intestinalis* more detailed (Akahoshi, T., K. Hotta, and K. Oka. 2017). My work aimed to elucidate the mechanisms underlying Ca^{2+}-signalling in Ciona notochord development. This overall aim was approached through four sub-aims by 1) determining whether the wild type notochord cells exhibit Ca^{2+}-signalling, 2) determining the contribution of various subcellular compartments, known to store/release Ca^{2+}, to the observed Ca^{2+}-signalling activity, 3) initiating a screen to study the mechanisms underlying Ca^{2+}-signalling, and 4) studying the effects of calcium pathway on the actomyosin network of notochord cells during embryonic development. The results from this study could thus expand on the current knowledge involving notochord development.

5.1 Wild type notochord cells exhibit Ca^{2+}-signalling during embryonic development

5.1.1 Ca^{2+}-signalling detected with Cah3>GCaMP6s construct

Newly fertilized embryos electroportated with Cah3>GCaMP6s construct enabled detection of Ca^{2+}-signalling in the notochord cells, but not with NFAT5>GCaMP6s construct. These transgenes have previously been described to express in the notochord (Kugler, Passamaneck et al. 2008, Jose-Edwards, Kerner et al. 2011), where Ci-Cah3 is shown to exclusively express in the notochord cells from 110-cell stage to late tailbud stage. Ci-NFAT5 however, has been detected from neurula to mid tailbud stages primarily in the notochord, but also weakly in the nerve cord (Jose-Edwards, Kerner et al. 2011). There is a possibility that the upstream regulatory region conferring the expression of NFAT5 in the notochord was not successfully identified by us. The latter could explain the absence of evident notochord Ca^{2+}-signalling by NFAT5>GCaMP6s construct. But if the cloning of the construct was performed correctly, the absence of detectable signals might also have been due to the promoter being very weak, given that it only needs to drive relatively limited expression. It should additionally be noted that the best GCaMP6s construct was selected based on only one electroporation round, which was also the first electroporation for this thesis, leaving room for manual error. With this in mind, the Ca^{2+}-signalling discussion will hereinafter refer to embryos electroporated with Cah3>GCaMP6s construct as the calcium indicator.

5.1.2 Ca^{2+}-signalling in developing notochord cells of wt *C. intestinalis* embryos

In accords with previously described morphogenesis of *C. intestinalis* notochord development during embryogenesis and tubulogenesis (**Figure 1.2-3**; Denker, E., and D. Jiang. 2012), the results of this thesis (**Figure 4.1**) present evidence of Ca^{2+}-signalling in the wt notochord cells. The signalling takes place during Hotta developmental stages 22 to 26, which was the selected stages for this thesis. With regards to the notochord, the stated stages mostly consist of cell shape changes (**Figure 4.1**) as the embryos go through further developmental stages, in addition to the process of lumen formation, as described previously (**Figure 1.3**; Denker, E., and D. Jiang. 2012). Ca^{2+}-signalling in Ciona notochord has recently been detected by one study (Akahoshi, T., K. Hotta, and K. Oka. 2017), where it was only detected between late neurula to initial tailbud stages. Our study however has detected significant signalling in later stages as well, as mentioned earlier. This might be due to the fact that Akahosi et al. performed transfection by mRNA injection, whereas our study was based on transgenesis by electroporation. In the case of mRNA injection, there is a finite amount of mRNA injected into unfertilized eggs that become diluted with every cell division post fertilization. In our case however, the expressed transgene continuously produces GCaMP6s mRNA. During stages 22 to 26 of our study, Ca^{2+}-signalling is detected within individual notochord cells as continuous blips in almost all notochord cells, while waves swirling around the cell, short and/or long lasting blinks within individual notochord cell, and/or blinks travelling in-between notochord cells, occur simultaneously (**Figure 4.1-3**). These wt Ca^{2+}-signalling characteristics are discussed below.

5.1.3 Ca^{2+}-waves and -blinks during cell shape changes and tubulogenesis

Calcium waves have been studied in for example *D. melanogaster* imaginal dics and butterfly wings (Balaji, R., et al. 2017; Ohno, Y. and J.M. Otaki. 2015) traversing across several cells. Similar waves, although not across several cells, have been detected in individual *C. intestinalis* notochord cells in our study (**Figure 4.1-2**). The repetitive waves start from a distinct initiation point and traverse around the individual Ciona notochord cells, from developmental stages 22 to 24. This feature is however harder to detect during stage 25, and it is almost undetectable at stage 26. During stage 25, it is however still possible to observe signalling blips and some subtle wave-effect, but almost never the waves or the initiation points. During stage 26 on the other hand, the blips are also detectable, but not the waves or the initiation points. While swirling waves dominate the majority of the notochord cells

during stages 22 to 24, it seems though signalling in the form short and/or long lasting blinks occur mostly from sometime late stage 24 to stage 26. Two types of blinks are observed in Ciona notochord cells; one being blinks suddenly occurring in cells that are either not signalling beforehand, or in cells where signalling blips are observed before the onset of the blink. As for the second blink type, it starts with a wave increasing in intensity to the point where the whole cell is saturated with a long lasting blink. The latter blinks will be referred to as <u>L</u>ong <u>L</u>asting <u>B</u>link (LLB), and sudden blinks as <u>S</u>udden <u>B</u>link (SB), hereinafter. Both types of blinks are visually more intense than the actual waves (**Figure 4.1-2**).

One could then argue that perhaps the cell shape changes and lumen formation events are related to the occurrence of waves mostly during stages 22 to 24, and blinks mostly appearing from sometime late stage 24 to stage 26. Seeing that cell shape changes and lumen formation are distinct events, although intertwined from stage 24, different signalling coordination may be more necessary for each event. It is then possible to consider that signalling in form of waves might be more important during stages 22 to 24 to promote cell shape changes, whereas lumen formation might rely more on intensive and strong signalling as blinks. It is also notable to mention that Michael J. Berridge (1997) argues that signalling such as blips/quarks are fundamental events, whereas puffs/sparks are elemental events and waves more global events. To further build upon his reasoning, LLBs might be an extension of such global event. As for SBs, it visually resembles puffs/sparks (Figure 3C in; Ward, Christopher & F. Schneider et. al. 2004). In Ciona notochord cells, the SBs sometimes arise from an initiation point in the cell that already is more intense than the rest of the cell. Other times, as mentioned earlier, the SBs takes place in cells that do not exhibit signalling before the onset of the SB. Furthermore, it is also the SBs that are more often observed travelling between two neighbouring cells (**Figure 4.2**). One could then also argue that the SBs in *C. intestinalis* might not be an elemental event, but perhaps more of a global event, or an intermediate event between these two. This is because the signalling is not confined to only one cell, but can travel from one cell to the neighbouring cell as an intercellular wave.

The occurrence of waves mostly during stages 22 to 24, and blinks during stages 24 to 26, can also be explained in terms of technical limitations in addition to morphogenesis during cell shape changes and tubulogenesis. These two events transform the cells coin-shape to more

cylindrical and elongated, and thinner, with fewer contact points between individual notochord cells (**Figure 4.1-2**; Denker, E., and D. Jiang. 2012). When the latter happens, it can be more difficult to distinguish individual cells and monitor the signalling. And since the initiation points seem to start at the same place in the cells during stages 22 to 24, the cell shape changes and lumen formation might further change the location of these initiation points at stages 25 and 26. This can then make it harder to detect both the initiation point and the waves in their entirety. Better softwares, perhaps with a tuneable lens capable of volumetric acquisition of the data, can overcome this technical limitation in the future. The experience gained in this study, for example, is currently being applied in developing softwares to overcome such limitations.

5.1.4 Calcium signalling dynamics during cell shape changes and tubulogenesis

As the embryos go through stages 22 to 26, the number of peaks per ROI per animal seams to differ between the successive stages, except between stage 24 vs. 25. These statements are supported by the representation of the boxplots, data distribution, and p-values (**Figure 4.5**; **Table 6.1**). The mean peak height representing signal intensity, on the other hand, is different between all successive stages except stage 23 vs. 24. The boxplots, data distribution and p-values support the latter statement for all stages except stage 23 vs. 24. This is because stage 23 and 24 boxplots have similar overall mean peak height range values, but the interquartile ranges (IQR) are not on the same y-axis region and stage 24 has more outliers. The latter could indicate dissimilarities between the two stages (**Figure 4.6**). The difference in appearance of the latter boxplots and the violin plots could be a result of different number of videos per ROI per animal within the two stages. Comparing the statistical values therefore seem to be a more reliable way of studying the mean peak height of stage 23 vs. 24. Moreover, there is no similarity for the change in mean peak height between successive stages, in accord with the boxplots, violin plots and p-values (**Figure 4.7**; **Table 6.1**). Furthermore, the mean peak width depicting the signal duration seems to differ between successive developmental stages, except for stage 23 vs. 24 (**Figure 4.8**; **Table 6.1**). The change in signal mean peak width follows the latter trend as well. Also here stage 23 vs. 24 boxplots and violin plots are slightly different, and so one would expect p-values indicating the same. But the same argument as earlier for stage 23 vs. 24 applies here, thus making the p-value to be more reliable. Furthermore, all wild type Ca^{2+}-signalling figures stated above

additionally have some outliers, but these are 1.5(IQR)>3rd-quartile (Q3), and therefore not statistically significant.

Table 6.1 Overview of p-values per stage for peak number, and mean peak height and width

Developmental stages	22 vs. 23	23 vs. 24	24 vs. 25	25 vs. 26
Number of peaks	0.003	0.018	0.100	0.016
Mean peak height	0.010	0.065	0.009	0.007
Δ mean peak height	0.001	0.004	0.047	0.007
Mean peak width	0.013	0.440	0.017	0.005
Δ mean peak width	0.020	0.430	0.013	0.005

Green = Significant difference. Red = No significant difference.

It is also interesting to consider whether the p-value trends (**Table 6.1**) are related to the cell shape changes and tubulogenesis events as well. The significant differences between stage 22 and 23 might be due to cell elongation along the anterior-posterior (AP) axis, which occur during these two stages. As the embryos develop from stage 23 to 24, where lumen secretion takes place, there might not be so many changes and activity in the cells. The latter could explain why the number of peaks and changes in mean peak height differ between stage 23 and 24, but not the mean peak height, mean peak width or the change in mean peak width of the signals. And as the embryos continue developing, there are significant changes between stage 24 and the successive stages, where only the number of peaks is not significantly different between stage 24 and 25. This might perhaps be due to big changes in cell shape remodelling, cell migration and lumen pockets fusing together. (Denker, E., and D. Jiang. 2012)

5.1.5 Ca^{2+}-signalling in epidermal and muscle cells during twitching

Ca^{2+}-signalling has previously been detected in muscle precursors at late gastrula stage, and in epidermal cells at mid tailbud stage in C. intestinalis. The latter signalling has been associated with relaxation of the tail, and named C̲a^{2+} T̲ransients of E̲pidermal C̲ells (CTECs). CTECs could also be associated with cell intercalation in the epidermis cells (Akahoshi, T., K. Hotta, and K. Oka. 2017) Akahoshi et al. also state that the CTECs were largely depending on the extracellular Ca^{2+}, which was artificially increased. This was not the case in our study. Not surprisingly, our study observed Ca^{2+}-signalling in the muscle and epidermal cells at later

stages as well, in addition to signalling in notochord cells (Figure 1A, Ryan, K. Lu, Z. and Meinertzhagen, I. A. 2016; **Figure 4.2-3**). The reasoning behind this observation is the same as discussed in Section **6.1.2**, regarding transfection with mRNA injection vs. electroporation.

In our study, signalling in the epidermal cells are often observed during tail relaxation and movement too, which seem to increase in intensity and number proportional to the movement. The latter resembles what Akahosi et al. observed in their study (SupplMov. 4., Akahoshi, T., K. Hotta, and K. Oka. 2017). As the embryos go through stages 25 and 26, the tail movements turn to twitching, where a twitch follows an increase in signalling intensity and number as well. In contrast to relaxation and movements however, a twitch is additionally almost always coupled to at least one strong signal generated at certain muscle cells (**Figure 4.3**). This signal regularly occurs at the tail end muscle cells on either side (**Figure 4.3**), and/or at certain muscle cells on each side of the anterior and/or middle part of the tail. It is however not evident exactly how many, and which, muscle cells exhibit signalling during twitching. The latter is due to time limitation, and actual aim of the study focusing on notochord, leading to lack of data on all signalling muscle cells. Nevertheless, it is likely that the muscle contraction leading to a tail twitch in *C. intestinalis* is related to Ca^{2+}-signalling. This is because calcium plays an important role in muscle contraction, and has for example been characterized to be important for muscle contraction in muscle bundles of *C. elegans* (Ardiel, E.L., et al. 2017).

As for the Ciona notochord cells during twitching, there often seems to be a lot of blinks occurring simultaneously as signalling takes place at the epidermal and muscle cells. This can lead one to speculate whether tail twitching during late tailbud stages, and perhaps larvae free-swimming stages, is also orchestrated by signalling in muscle cells alongside epidermal and notochord cells.

5.2 Various subcellular compartments contribute to the Ca^{2+}-signalling activity

By using pharmacology, while performing live calcium imaging, we also tried to determine contribution of various subcellular compartments to the observed Ca^{2+}-signalling activity. The targets of our pharmacological studies were subcellular compartments known to store/release Ca^{2+}, which were inhibited by $Gado^{3+}$, 2APB, and carbenoxolone (**Table 3.3**). 2APB and

Gado^{3+} inhibition have previously been studied in Drosophila imaginal dics, to determine whether they inhibit the observed calcium waves and spikes (Balaji, R., et al. 2017). Balaji et al. demonstrated that 2APB blocks the oscillatory waves in the wing discs, which implies that the waves might depend on IP$_3$R and SOCE, but not Gado^{3+}. The spikes were however not affected by 2APB, indicating IP$_3$R- and SOCE-indepentence. Balaji et al. also studied the importance of Ca^{2+}-signalling in cell-cell communication, which conveys information from one cell to the other through gap-junctions, by carbenoxolone treatment. The signal intensity over time was shown to not recover post carbenoxolone treatment, which suggests gap junction dependence. (Balaji, R., et al. 2017) One could then hypothesize whether these inhibitors have a similar effect on Ca^{2+}-signalling in *C. intestinalis* notochord cells as well.

5.2.1 Carbenoxolone, Gado^{3+} and 2APB morphologically affect *C. intestinalis* embryos

The embryos were incubated with 1 M, 10 μM and 100 μM of each drug separately, to determine concentrations that would give specific effects in terms of notochord development. The purpose of this was to determine potential inhibitor concentrations for the drug perfusions, based on morphological inhibitor effects. Our goal was to select a concentration that would only affect the calcium signalling, but not destroy it or the embryo itself. This is because we wanted to inhibit the signalling enough to see a difference, but not so much that it would be impossible to see a potential recovery post inhibitor treatment.

As presented in **Figure 4.9**, 2APB-treatment leads to severely deformed embryos in both the head and tail region. This deformity is shown as exploded heads, and short and deformed tails, compared to wt controls. Treatment with Gado^{3+} on the other hand, leads to some small and squeezed heads, and short tails, in some of the embryos compared to wt controls. The rest of Gado^{3+}-treated embryos seemed to develop more normally, i.e. with non-squeezed heads and longer tails, but seemed to cease developing around stage 25. This is because Gado^{3+} caused similar notochord morphology in all effected embryos that had longer tails, which was not a reoccurring feature in all wt controls. Since the morphological effects with 1 M inhibitor were very severe, we repeated the same drug incubation with 10 μM and 100 μM concentrations instead. Treatment with 10 μM did not show any effect (Figure not included). The study performed with 100 μM inhibitor led to some effects in the notochord, but majority

of all the embryos developed otherwise in a normal manner (Figure not included). We therefore selected 100 μM as the concentration for the pharmacology study.

5.2.2 Decreased Ca^{2+}-waves and –blinks, and cell-cell communication in notochord cells

In accords with **Table 4.6**, the occurrence of Ca^{2+}-waves decreases drastically in individual notochord cells during inhibitor treatment. It decreases considerably during treatment with 2APB (-92%) and $Gado^{3+}$ (-70%). The former percentage indicates that the waves might depend on IP_3R and SOCE; IP_3R releases Ca^{2+} from the ER to increase intracellular Ca^{2+} concentration, and SOCE enables Ca^{2+}-release activated current to replenishes the ER when depleted of Ca^{2+} (Clapham, D.E. 2007). As for $Gado^{3+}$ perfusion, it seems though that the waves might also depend on cation channels. The occurrence of blinks was also drastically decreased during $Gado^{3+}$ treatment (92%), implicating cation channel dependence in our study. The decrease in blinks were however not as drastic during 2APB-perfusion (29%), which indicates that the blinks might depend more on cation channels than IP_3R and SOCE. The embryos also exhibit decreased waves (54%) and blinks (57%) during carbenoxolone treatment in individual notochord cells. This indicates that perhaps about half of Ca^{2+}-signalling depends on cell-cell communication through gap junctions. The reliability of these visual-based conclusions, and potential signal recovery, is discussed in the sections below.

5.2.3 $Gado^{3+}$-treatment: Notochord cell Ca^{2+}-signalling might depend on cation channels

According to the p-values (**Table 6.2**), and boxplots and violin plots (**Figures 4.10-13**); there is no significant difference between Ca^{2+}-signalling of "Before" $Gado^{3+}$-treatment and wt. The "Before"-phase of this study can therefore be regarded as a control as well. The results indicate that the number of peaks, and (Δ) mean peak height, differ considerably between B-A. The latter implies different number of peaks and loss of peak intensity caused by inhibition. This fits well with the findings of Section **4.2.2.1**, to a certain degree, because $Gado^{3+}$ visually led to decreased occurrence of waves and blinks. But the duration of the peaks and the change in duration of the peaks, which are represented as mean peak width and Δ mean peak width, seem to recover post inhibitor treatment. In other words, the number of peaks, and (Δ) mean peak height seem to depend on cation channels. But the (Δ) mean peak width might be independent of cation channels. These findings did not correlate with what Balaji et al. (2007) observed, suggesting that cation chaneels might play a more important role

in Ciona than Drosophile. Furthermore, the figures stated above additionally have some outliers, but these are 1.5(IQR)>(Q3), and hence not statistically significant.

It is of course important to not exclude indirect inhibitor effects that might last beyond the time of the wash out phase. This would particularly influence data that could reveal a potential recovery. To exclude any potential indirect effects, one could then evaluate the inhibition effect by comparing the B-D data (**Table 6.12**). The latter data conveys information on whether the inhibitor does indeed affect the Ca^{2+}-signalling. In our case, the B-D data follows the same trend as the B-A; suggesting that the drug does affect the number of peaks and (Δ) mean peak height but not (Δ) mean peak width.

Table 6.2 Overview of p-values for Ca^{2+}-signalling dynamics of $Gado^{3+}$-treated notochord cells

	Before vs. wt	B-D	D-A	B-A
Number of peaks	> 0.200	0.006	0.160	0.001
Mean peak height	> 0.100	4.3×10^{-4}	0.002	1.1×10^{-7}
Δ mean peak height	> 0.060	0.008	0.023	1.6×10^{-5}
Mean peak width	> 0.070	0.270	0.410	0.180
Δ mean peak width			0.420	0.190

Green = Significant difference. Red = No significant difference.

5.2.4 2APB-treatment: Notochord cell Ca^{2+}-signalling might depend on IP_3R and SOCE

There is no significant difference between wt and "Before"-phase number of peaks, and (Δ) mean peak height (**Table 6.3**; **Figures 4.10-12**). The latter can thus be regarded as a wt control as well. With this in mind, the number of peaks seems to recover post 2APB-perfusion, but not the mean peak height or the Δ mean peak height. This implicates the later depending on IP_3R and SOCE. The number of peaks however do not seem to rely on these subcellular compartments releasing/storing Ca^{2+}. Moreover, the "Before"-phase (Δ) mean peak width have slightly different boxplots, violin plots, and p-values compared to wt (**Table 6.3**; **Figure 4.10-13**). The latter finding is slightly odd, because one would expect these "Before"-phases resembling the wt condition as well. Explaining this is a little challenging, as it is highly unlikely due to manual error. Given that a manual error has occurred during "Before"-phase, it would probably lead to differences in all "Before" phases. It is also highly

unlikely due to using DMSO to dissolve 2APB, because the final concentration of DMSO was only 0.0025% during perfusion. Balaji et al. also demonstrated that DMSO does not affect calcium oscillation (Figure S5D, Balaji, R., et al. 2017). We therefore decided to compare the (Δ) mean peak width directly with the wt condition (p-value 0.006 in both cases), instead of the respective "Before" phases. The more reliable p-values indicate that 2APB-treatment leads to differed (Δ) mean peak width; suggesting that the latter might depend on IP$_3$R and SOCE as well. One could then hypothesize that the visually drastic decrease in Ca^{2+}-waves (Section **4.2.2.1**) might be related to (Δ) mean peak height and (Δ) mean peak width not recovering. One could further hypothesize that the slightly less drastic decrease in Ca^{2+}-blinks might explain why there was no significant change in the number of peaks. Balaji et al. (2007) has for example studied that the waves are blocked by 2APB. Since we observed that both waves and blinks give rise to signalling in *C. intestinalis*, the stated two hypotheses seem plausible.

Table 6.3 Overview of p-values for Ca^{2+}-signalling dynamics of 2APB-treated notochord cells

	Before vs. wt	B-D	D-A	B-A
Number of peaks	> 0.200	0.400	0.120	0.080
Mean peak height	> 0.100	0.009	0.110	3.3x10^{-4}
Δ mean peak height	> 0.060	0.020	0.070	0.001
Mean peak width	0.001	0.210	0.430	0.150
Δ mean peak width				

Green = Significant difference. Red = No significant difference.

Likewise, the figures referred to in this section have some outliers that are 1.5(IQR)>(Q3), and not statistically significant. Moreover, the B-D data follows the same trend as the B-A (**Table 6.3**); the drug affects the (Δ) mean peak height, but not the number of peaks and (Δ) mean peak width.

5.2.5 Carbenoxolone-treatment: Cell-cell communication might depend on gap junctions
In lines with the p-values (**Table 6.4**), boxplots and violin plots (**Figures 4.10-13**); there is no significant difference between Ca^{2+}-signalling of "Before" carbenoxolone condition and wt. The "Before"-phase of this study can therefore be regarded as a control. The figures referred

to in section have statically not significant outliers as well. Furthermore, the results implicate a difference in B-A with regards to the number of peaks, and (Δ) mean peak height. The latter indicates differed number of peaks and peak intensity caused by carbenoxolone inhibition. But the duration of (Δ) mean peak width seems to recover post inhibitor treatment. In other words, cell-cell interaction between adjacent notochord cells may trigger calcium events and possibly contribute to the size of the peak, but not the signal duration. This could also explain the visually decreased occurrence of Ca^{2+}-waves and -blinks in the notochord cells at slightly over 50% (Section **4.2.2.1**). It would be interesting to study whether adjacent cells possess equal-amplitude peaks or if they are not related in any way, to find out if gap junctions play a role in triggering the calcium events and contributing to the peak size.

Interestingly, the B-D data follows the same trend as the B-A regarding (Δ) mean peak width and mean peak height (**Table 6.4**), but not with respect to the number of peaks and Δ mean peak height. The latter could be explained by 1) perhaps carbenoxolone not having an immediate effect on the number of peaks and the change in intensity, and/or 2) indirect inhibitor effects that might last beyond the time of the wash out phase.

Table 6.4 Overview of p-values for Ca^{2+}-signalling dynamics of carbenoxolone-treated notochord cells

	Before vs. wt	B-D	D-A	B-A
Number of peaks	> 0.200	0.070	0.006	2.1×10^{-5}
Mean peak height	> 0.100	4.3×10^{-4}	0.002	9.1×10^{-8}
Δ mean peak height	> 0.060	0.130	0.009	5.6×10^{-4}
Mean peak width	> 0.070	0.230	0.310	0.070
Δ mean peak width		0.220	0.390	0.110

Green = Significant difference. Red = No significant difference.

5.3 Mechanisms underlying Ca^{2+}-signalling in *C. intestinalis* notochord cells

The molecular pathway underlying notochord calcium activity was disrupted by downregulation through RNAi. This was performed by electroporating newly fertilized eggs with either shRNA-SERCA or shRNA-Calm construct, mixed with Cah3>GCaMP6s, and the notochord monitored by live calcium imaging. Calmodulin is a Ca^{2+} adaptor protein, which plays an important role in relieving protein autoinhibition, active site remodelling and protein

dimerization (Clapham, D.E. 2007). Moreover, it also facilitates PMCA Ca^{2+}-affinity and ATPase pump rate, (Clapham, D.E. 2007), and has been described to express in the outermost part of *C. intestinalis* notochord (Reeves, W. et al. 2014). SERCA on the other hand, is a sarcoendoplasmic reticular Ca^{2+} ATPase pump that facilitates Ca^{2+} extrusion into the ER (Clapham, D.E. 2007).

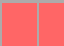### 5.3.1 Calmodulin might affect notochord Ca^{2+}-signalling dynamics differently
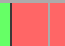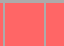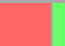
Presented by our research results (**Figure 4.14**), the number of peaks seem similar between the knock-downs and wt animals overall. Stage 23 embryos, however, indicate dissimilar number of peaks compared to wt stage 23 (**Figure 4.15**). This might be perhaps due to notochord cell elongation taking place during stage 23 (Denker, E., and D. Jiang. 2012), where calmodulin might play an important role in terms of number of peaks.

Furthermore, there is a significant difference in terms of mean peak height between the overall knock-downs and wt (**Figure 4.16**). Certain knocked down stages have however similar mean peak height compared to respective wt stages; stage 22, 24 and 26. This indicates that the signalling intensity might depend on calmodulin during stage 23 and 25, but not as much during generation of "stack of coins" configuration (~ stage 22), formation and expansion of extra- and intercellular lumen pockets (~ stage 24), and body extension (~ stage 26) (Denker, E., and D. Jiang. 2012). The overall data also indicates differences regarding the change in mean peak height (**Figure 4.17**). Contrary to the overall data though, stage 22, 24 and 25 embryos indicate similar change in mean peak height (Section **4.3.6**). This implicates that calmodulin might be more important for the change in signalling peaks during stage 23 and 26.

As for the mean peak width and the change in mean peak width, calmodulin seems to affect them in a similar manner relative to wt condition (**Figure 4.18**). The overall data indicates different (Δ) mean peak width as well. And also here, knocked down stages 22 and 25 resemble wt (Section **4.3.8**). This indicates that calmodulin might not be as important during stages 22 and 25 regarding (Δ) mean peak width, as much as during stage 23, 24 and 26.

Hence, the stage-specific data presented here is more informative than the overall data, and the latter data does not really match that of the stage-specific. Since our data is not normally distributed, this might have lead to false representation of the results; given that there is a very large difference between the median and the mean with regards to the overall data. Nevertheless, in short: the knock-downs implicate calmodulin playing an important role in different aspects of Ca^{2+}-signalling dynamics during different stages. Notably, stage 23 seems to consistently possess significantly different calcium activity compared to wt, suggesting that it might depend on calmodulin the most. Stage 22 on the other hand, behaved the opposite of stage 23. Furthermore, figures referred to in section do not have statically significant outliers. The overall results are straightforwardly presented as p-values in **Table 6.5**.

Table 6.5 Overview of p-values for calmodulin knock-downs per stage and overall

	Stage 22	Stage 23	Stage 24	Stage 25	Stage 26
C-K*	(colored cells)	(colored cells)	(colored cells)	(colored cells)	(colored cells)

Overall data				
	Number of peaks	Mean peak height	Δ mean peak height	Mean peak width	Δ mean peak width
C-K*	0.130	0.006	0.008	0.020	

C-K* = Calmodulin knock-downs vs. wt. Within each developmental stage; column 1) number of peaks, 2) mean peak height, 3) Δ mean peak height, 4) mean peak width, and 5) Δ mean peak width. Green = Significant difference (> 0.05). Red = No significant difference (< 0.05).

5.3.2 SERCA might affect notochord Ca^{2+}-signalling dynamics differently

The number of peaks are similar between the knock-downs and wt animals overall, except at stage 23 (**Figures 4.14-15**). This indicates that SERCA pumps are perhaps more important during stage 23, compared to the other stages. As for the (Δ) mean peak height, it seems to differ between overall wt and the RNAi knock-downs (**Figures 4.16-17**), indicating SERCA dependence. On the other hand, stage 22, and 24-26 knock-downs have similar (Δ) mean peak height relative to wt (Section **4.3.6**). One might argue that these pumps may be more important during stage 23, regarding peak intensity and the change in intensity, but not during other stages. Moreover, the mean peak width and the change in mean peak width seem to be affected similarity due to SERCA knocked down (**Figures 4.18**; Section **4.3.8**). This is because in both cases, the overall data indicates dissimilarities between knock-downs and wt, whereas stage 22-25 embryos imply similarities. The argument why this might be the case, is

the same as in section **6.3.2** regarding the different developmental events occurring at various stages. To summarize, SERCA might play an important role in different aspects of Ca^{2+}-signalling dynamics during different stages. Stage 22, 24 and 25 seem to not depend on SERCA at all, whereas stage 23 and 26 might to some degree. The overall results are straightforwardly represented as p-values in **Table 6.6**. Additionally, the stage-specific data is more informative compared to the overall data here as well. The same discussion, regarding mean and median of the overall data, of section **5.3.1** apply here.

Table 6.6 Overview of p-values for SERCA knock-downs per stage and overall

	Stage 22	Stage 23	Stage 24	Stage 25	Stage 26
S-K*	(red bars)	(green/red bars)	(red bars)	(red bars)	(red/green bars)
Overall data					
	Number of peaks	Mean peak height	Δ mean peak height	Mean peak width	Δ mean peak width
S-K*	0.060	0.003	0.011	0.040	

S-K* = SERCA knock-downs vs. wt. Within each developmental stage; column 1) number of peaks, 2) mean peak height, 3) Δ mean peak height, 4) mean peak width, and 5) Δ mean peak width. Green = Significant difference (> 0.05). Red = No significant difference (< 0.05).

5.3.3 Notochord M and AP affected differently by shRNA-Calm

Reeves et al. (2014) demonstrated that calmodulin is first detected as the embryos complete neurulation and proceed to notochord intercalation. Calmodulin seems to express mostly at the anterior and posterior notochord tips during stage 21. Their results reveal that gene expression however decreases at the anterior, relative to the posterior, as the notochord elongates post intercalation. The expression then becomes largely limited to the posterior part, as the embryos reach tailbud stage (stage 23). Reeves et al. (2014) also suggest that calmodulin might be involved in tip-specific expression and play a role in cell intercalation. Therefore, we investigated whether anterior-posterior (AP) and middle (M) knock-downs differ from that of respective wt notochord parts, by live calcium imaging.

Our overall data indicate significant differences in AP and M number of peaks between knock-downs and wt (Section **4.4.2**). The knocked down stage 22, and M of stage 24, however seem to possess similar number of peaks relative to wt (Section **4.4.3**). This suggests

that calmodulin is perhaps not that active during the latter stated stages, with respect to number of peaks. The mean peak height also seems dissimilar to wt according to the overall results (Section **4.4.4**), except AP stage 25. As for the change in mean peak height, the overall data suggest dissimilarities (Section **4.4.5**). The latter does not apply for mean peak height of stage 22, and stage 25 AP, in terms of p-values (Section **4.4.6**) even if the boxplots show clear difference (**Figure 4.19**). This contradictory result might be due to uneven number of videos per stage, and uneven number of selected ROI for AP and M, between wt and knock-downs. The latter could influence the shape of both the boxplots and violin plots. Furthermore, the mean peak width and the change in mean peak width follows similar trend; overall data imply significant difference compared to wt, except for stage 22. In other words, calmodulin seems to be more active at AP and M at almost all stages (that the embryos were imaged in this study) than during stage 22. These findings seem very contradictory to the study of Reeves et al. (2014).

Reeves et al. presented calmodulin expression in the notochord only at the anterior and posterior part. One would then expect our data to show dissimilar calcium dynamics at the AP between wt and knock-downs, but not at M. Since our data show differed signalling at M between the two conditions as well, it can either mean that 1) our study prove that calmodulin expresses in the notochord middle after all, but was not detected by the in-situ hybridization of Reeves et al. possibly due to low expression, 2) unexpected phenotypes such as feedback loop might have taken place, or 3) our analytical approach was not optimized enough. With regards to reason 1; a qPCR could confirm the knock down for each RNAi target, to measure the changes in gene expression post RNAi. But it is hard to imagine that our RNAi experiment has failed, because we do have positive results with respect to difference in AP between knock-downs and wt. However, the occurrence of an off-target effect, or cell non-autonomous effects, is also possible. With respect to reason 2; silencing calmodulin expression ubiquitously from early on could have led to unpredicted phenotypes, such as feedback loop. Given that there is a feedback loop between calmodulin expression levels in various cells, and with regards to calcium dynamics, the long-term perturbation would have a profound effect. In this case, we could perform a qPCR as well, and perhaps also conduct an in-situ hybridization to see if the expression is indeed as Reeves et al. stated. As for reason 3; we captured calcium images based on where the Ca^{2+}-signalling was clearest to image, without taking under consideration whether we imaged the whole notochord or particular

locations. This means that we have not captured calcium images of all AP and M notochord cells. The number of selected AP and M ROIs are also considerably unequal between wt and knock-downs. Moreover, since our data is not normally distributed, the p-values based on mean values might not be reliable enough given that the distribution is very skewed.

To obtain more conclusive results for this sub-study, the analysis approach could be optimized in a few ways. For instance, the statistics can be recalculated and be based on the median values instead of mean values, to attain more reliable p-values. It would also be better to select ROI for anterior and posterior separately, instead of treating them similarly, since Reeves et al. suggested that anterior and posterior vary in calmodulin expression. For future reference, it would be wise to keep the number of videos, ROIs, and length of videos equal between experimental conditions. It would also be wise to image all notochord cells. Our study did not focus on the latter, because the experimental part of the thesis was already finished when we considered this sub-study. To summarize, comparing wt AP and M with that of the knock-downs seem to give inconclusive results. Optimizing the experimental and analytical approach could therefore lead to a more reliable conclusion.

5.4 Potential Ca^{2+}-signalling pathway components to investigate in the future

We attempted to identify putative Ca^{2+}-signalling pathway components in *C. intestinalis* notochord (Section **3.2.2**). This was enabled by synthesizing RNA probes against mRNA of the genes through in-vitro transcription, and using the probes to analyse protein expression by in-situ hybridization (Section **3.2**). Brachyury was used as control, as it is known to express in the notochord (Satoh, N., et al. 2014).

5.4.1 Expression of Brachyury, Ci-connexin-related-8, AT2B1 and KNCQ4/5 vary

Due to limited time, and due to the fact that not all probes were ready at the same time, we only managed to perform in-situ hybridization for Brachyury, Ci-connexin-related-8, AT2B1, and KNCQ4/5. This is because the wrong Ci-TWIK5 and Cav1 bands were cut from the gel during DNA recovery (Section **3.2.4**), and Ci-TRMP3 was absent in the gel after NotI-HF digestion (Section **3.2.10**) perhaps due to manual error, during the first attempt. There are therefore no results presented for the latter three genes, as the in-situ was performed once.

Nevertheless, our results show that Brachyury expresses in the notochord, as expected (Satoh, N., et al. 2014). The expression is strongest during earlier stages, and decreases as the embryos reach late tailbud stage (**Figure 4.25**, **A-C**). Ci-connexin-related 8, AT2B1 and KNCQ4/5 however did not seem to express similarly. Ci-connexin-related 8 expresses weakly during gastrula and mid tailbud, but it is hard to decide exactly where, because of the weak expression (**D**-**E**). During late tailbud however, strong expression is detected in a few epidermal- and notochord cells near the head, including right behind the head (**F**). This could mean that integral membrane proteins, that form intercellular channels clustered at the gap junctions (Section **3.2.2**), might be expressed during late tailbud but perhaps not during gastrula and mid tailbud. AT2B1 seems to express similar to Ci-connexin-related-8 during gastrula and mid tailbud stage (**G-H**). At late tailbud stage however, AT2B1 expresses in the middle section of the notochord, and in muscle cells right behind the head (**I**). The latter suggests AT2B1 encodes plasma membrane Ca^{2+} ATPase at late tailbud stage, but maybe not during earlier stages. As for KCNQ4/5, no expression was detected during gastrula (**J**), but extremely weak to non-existing during mid tailbud in the notochord (**K**). During late tailbud however, some epidermal cells seem to express near the anterior part of the notochord (**L**). This could indicate that potassium channels are present during late tailbud, but not during earlier stages.

As stated earlier, these data are based on only one round of in-situ hybridization. This leaves room for manual errors, such as poorly staining and/or excessive washing, which could be crucial for genes that express very weakly. What would be interesting is to repeat this study to see whether the genes still follow the same expression-pattern.

5.5 Structural analysis of drug effect on actomyosin network of notochord cells

The notochord actomyosin network mediates cell motility and cell shape changes in the developing *C. intestinalis* embryos (Denker, E., and D. Jiang. 2012; Balaji, R., et al. 2017). Our sub-study aimed to study the effects of calcium signalling on the notochord actomyosin network. This was enabled by means of pharmacology, using embryos electroporated with Bra>MLC wt Mcherry and Bra>Lifeact GFP constructs (Section **3.6.1-5**).

5.5.1 Carbenoxolone-treatment: Ca^{2+}-signalling inhibition affects notochord actomyosin

The embryos at 3hpi resemble wt, both in terms of protein expression and notochord cell shape (**Figure 4.26, A-A', D-D'**). At 6hpi however, fewer cells exhibit expression, where the cells are relatively smaller in shape than wt (**E-E'**). The cell elongation process seems not to proceed properly at 6hpi, which could indicate that the actomyosin networks are not functioning normally. This is because equatorial contractile actomyosin rings, and other actin-binding proteins, mediate the cell elongation process (Denker, E., and D. Jiang. 2012). Interestingly, more cells seem are detected with protein expression at 9hpi compared to wt, but with weaker expression where some few big cells are detected between smaller cells (**F-F'**). In other words, Ca^{2+}-signalling inhibition appears to affect the notochord actomyosin network around 6hpi and onwards.

5.5.2 Gado^{3+}-treatment: Ca^{2+}-signalling inhibition affects notochord actomyosin

Already at 3hpi, Gado^{3+} inhibition leads to smaller cell shapes, where almost half of the cells show weaker Lifeact-GFP expression, compared to wt (**Figure 4.26, G-G'**). As for 3hpi MLC wt Mcherry, half of the cells express weaker than the inhibited Lifeact-GFP 3hpi, while the expression in the other half is almost non-existent. The same expression patterns, and smaller cell shapes, are also detected at 6hpi (**H-H'**). It is however even more extreme for MLC wt Mcherry, because expression seems to be absent in even more cells at 6hpi compared to 3hpi. Remarkably, not all inhibited notochord cells at 9hpi are affected similarly. This is because the cell shapes and expression of some inhibited embryos resemble wt (**I-I'**), while others resemble cells as seen in **F** and **F'**. This indicates that Ca^{2+}-signalling inhibition affects the notochord actomyosin network of all embryos at 3hpi and 6hpi, but the affects vary at 9hpi.

5.5.3 2APB-treatment: Ca^{2+}-signalling inhibition affects notochord actomyosin

The effects of 2APB-treatment seem very extreme. This is because some cells have abnormally thinner shapes, whilst others have larger shapes, compared to wt already at 3hpi (**Figure 4.26**, **J-J'**). The protein expression of Lifeact-GFP resembles wt, but not of MLC wt Mcherry, at 3hpi. Furthermore at 6hpi and 9hpi (**J-K, J'-K'**), the cell shapes appear to be thinner relative to wt 6hpi and 9hpi. As for the protein expression, it is drastically weak for Lifeact-GFP, and even weaker for MLC wt Mcherry (**L-L'**). In short, 2APB-inhibition seems to influence protein expression and thus cell shape changes considerably form 3-9hpi.

5.6 Conclusion

Our study presents evidence for the importance of Ca^{2+}-signalling in *C. intestinalis* notochord cells, from developmental stage 22 to 26. These signals take place in form of continuous blips within individual cells, while waves traversing around single cells, short and/or long lasting blinks within individual cells, and/or blinks that travel in-between cells, occur simultaneously. Moreover, cell shape changes occurring at earlier stages seem to rely more on waves, whilst tubulogenesis at later stages appear to rely more on blinks. There is also a significant difference in terms of number of peaks, peak intensity and duration, between stage 22 and 23 but not so much between stage 23 and 24. The former dissimilarities could be due to the cell elongation event, whereas the latter similarities might be due lumen secretion not leading to significant differences in signalling dynamics. The dissimilarities in signalling dynamics take place again from stage 24 and onwards, possibly due to big changes in cell shape, cell remodelling, and formation of lumen pockets in the notochord. The number of peaks seems to depend on cation channels, whereas the (Δ) peak intensity appears to rely on cation channels, IP_3R and SOCE. As for the cell-to-cell communications, our study suggests that gap junctions might affect the number of peaks and (Δ) peak intensity. With regards to (Δ) signal duration, they appear to depend on IP_3R and SOCE. Furthermore, calmodulin is indicated to be; 1) most important during stage 23, 2) least important during stage 22, 3) not important for number of peaks except for stage 23, and 4) its significance various for the different signalling dynamics from stage 24-26. With regards to SERCA, stage 22, and 24-25 suggest independence, whereas stage 23 and 26 seem to depend to some degree. In other words, the seemingly dynamic use of Ca^{2+}-signalling, and signalling components, at different developmental stages might be more important at one stage than the other. The latter might perhaps also be reflected in gene expression. Additionally, the stated RNAi effects might be due to cell non-autonomous behaviour, as it is hinted in calmodulin RNAi with regards to differences in both AP and M compared to wt. Inhibition of Ca^{2+}-signalling also seem to affect the notochord actomyosin network, where $Gado^{3+}$ and 2APB affected the cell structures and protein expression already from 3hpi. Carbenoxolone inhibition, lead to visual differences in the protein expression and cell shape from 6hpi. Our study further presents Ca^{2+}-signalling in epidermal and muscle cells, implying importance in tail relaxation, twitching, and movement, during embryonic development. We additionally attempted to identify putative Ca^{2+} pathway components for future studies; Ci-connexin-related-8, AT2B1, and perhaps KNCQ4/5.

5.7 Future perspectives

Our study has further paved the way for an interesting field of research regarding notochord Ca^{2+}-signalling dynamics in *C. intestinalis*. The more results we obtained during the course of our study, the more questions have been raised. Some of these questions can be answered by analysing the already gathered data for this thesis. For instance, the waves occurring in individual cells can be quantified to determine calcium dynamics such as; 1) how often the waves occur by measuring ISI, 2) whether the observed waves are initiated from a specific side of the cell, 3) whether the intercellular calcium events are initiated from a specific cell, or a couple of cells in a specific direction, 4) the speed of the intercellular and intracellular waves, or 5) to what extent the inhibition and RNAi affected waves differ from wt, for example. By further analysing our data, it is also possible to determine whether the blinks "travel" from anterior part of the notochord towards the posterior end, or vice versa, to detect if the overall signalling possess a general direction. It is additionally possible to quantify the cell shape changes caused by inhibition, by measuring the cell length, cell height and basal furrow location using the already collected data. Furthermore, in terms of experimental studies, once could 1) perform inhibition by thapsigargin to determine whether SERCA pumps contribute to the ER calcium stores, 2) treat the cells with ATP to determine if addition of ATP leads to a Ca^{2+}-signalling response in the notochord, or 3) inhibit actomyosin network with Blebbistatin to investigate if it affects Ca^{2+}-signalling response. It would also be wise to consider other methods to knock-down/knock-out SERCA, and especially calmodulin with regards to our AP/M study, to investigate the occurrence of cell non-autonomous behaviour, because the effects of the latter might be harder to distinguish by RNAi. These are just a few suggestions for further studies, as experience indicates that more questions will be raised the more we research Ca^{2+}-signalling in *C. intestinalis* notochord.

6. References

Abdul-Wajid, S., et al. 2015. 'T-type Calcium Channel Regulation of Neural Tube Closure and EphrinA/EPHA Expression', Cell Rep, 13(4): p. 829-39.

Akahoshi, T., K. Hotta, and K. Oka. 2017. 'Characterization of calcium transients during early embryogenesis in ascidians Ciona robusta (Ciona intestinalis type A) and Ciona savignyi', Dev Biol, 431(2): p. 205-214.

Andrew, D.J. and A.J. Ewald. 2010. 'Morphogenesis of epithelial tubes: Insights into tube formation, elongation, and elaboration', Dev Biol, 341(1): p. 34-55.

Annona, G., N.D. Holland, and S. D'Aniello. 2015. 'Evolution of the notochord', Evodevo, 6: p. 30.

Ardiel, E.L., et al. 2017. 'Visualizing Calcium Flux in Freely Moving Nematode Embryos', Biophys J, 112(9): p. 1975-1983.

Balaji, R., et al. 2017. 'Calcium spikes, waves and oscillations in a large, patterned epithelial tissue', Sci Rep, 7: p. 42786.

Berridge, M. J. 1997. 'Elementary and global aspects of calcium signalling', Journal of Phy8iology, 499.2, pp.291-306.

Bootman, M., et al. 1997. 'Imaging the hierarchical Ca2+ signalling system in HeLa cells', Journal of Physiology-London, 499(2): p. 307-314.

Bootman, M.D. and M.J. Berridge. 1996. 'Subcellular Ca2+ signals underlying waves and graded response in HeLa cells', Curr Biol, 1;6(7):855-65.

Carver, C. E., Mallet, A. L., and Vercaemer, B. 2006. 'Biological synopsis of the solitary tunicate Ciona intestinalis', Canadian Manuscript Report of Fisheries and Aquatic Sciences, 2746: 1488-538.

Cheng, H., W.J. Lederer, and M.B. Cannell. 1993. 'Calcium Sparks - Elementary Events Underlying Excitation-Contraction Coupling in Heart-Muscle', Science, 262(5134): p. 740-744.

Clapham, D.E. 2007. 'Calcium signaling', Cell, 131(6): p. 1047-58.

Colacci, M., et al. 2005. 'Characterization of the teneurin C-terminal associated peptide (TCAP) in the vase tunicate, Ciona intestinalis: A novel peptide system associated with energy metabolism and reproduction', ScienceDirect, 15;216:161-70.

Creton, R., J.A. Kreiling, and L.F. Jaffe. 2000. 'Presence and roles of calcium gradients along the dorsal-ventral axis in Drosophila embryos', Dev Biol, 217(2): p. 375-85.

Creton, R., J.E. Speksnijder, and L.F. Jaffe. 1998. 'Patterns of free calcium in zebrafish embryos', Journal of General Physiology, 112(1): p. 36a-36a

Delsuc, F., et al. 2006. 'Tunicates and not cephalochordates are the closest living relatives of vertebrates', Nature, 439(7079): p. 965-8.

Denker, E., and D. Jiang. 2012. 'Ciona intestinalis notochord as a new model to investigate the cellular and molecular mechanisms of tubulogenesis', Semin Cell Dev Biol, 23: 308-19.

Ferrari, M.B. and N.C. Spitzer. 1999. 'Calcium signaling in the developing Xenopus myotome', Developmental Biology, 213(2): p. 269-282.

Gilland, E., et al. 1999. 'Imaging of multicellular large-scale rhythmic calcium waves during zebrafish gastrulation', Proceedings of the National Academy of Sciences of the United States of America, 96(1): p. 157-161.

Hackley, C., et al. 2013. 'A transiently expressed connexin is essential for anterior neural plate development in Ciona intestinalis', Development, 140(1): p. 147-55.

Hotta, K., et al. 2000. 'Characterization of Brachyury-downstream notochord genes in the Ciona intestinalis embryo', Dev Biol, 224(1): p. 69-80.

Jose-Edwards, D. S., et al. 2011. 'The identification of transcription factors expressed in the notochord of Ciona intestinalis adds new potential players to the brachyury gene regulatory network', Dev Dyn 240(7): 1793-1805.

Kelu, J.J., et al. 2017. 'Ca(2+) release via two-pore channel type 2 (TPC2) is required for slow muscle cell myofibrillogenesis and myotomal patterning in intact zebrafish embryos', Dev Biol, 425(2): p. 109-129.

Kugler, J. E., et al. 2008. 'Evolutionary conservation of vertebrate notochord genes in the ascidian Ciona intestinalis', Genesis 46(11): 697-710.

Leclerc, C., et al 2008. 'An increase in intracellular Ca2+ is involved in pronephric tubule differentiation in the amphibian Xenopus laevis', Dev Biol, 2008. 321(2): p. 357-67.

Lemaire, P. 2011. 'Evolutionary crossroads in developmental biology: the tunicates', Development, 138(11): P.2143-52

Linask, K.K., K.A. Knudsen, and Y.H. Gui. 1997. 'N-cadherin-catenin interaction: Necessary component of cardiac cell compartmentalization during early vertebrate heart development', Developmental Biology, 185(2): p. 148-164.

Lipp, P. and E. Niggli. 1998. 'Fundamental calcium release events revealed by two-photon excitation photolysis of caged calcium in guinea-pig cardiac myocytes', Journal of Physiology-London, 510(3): p. 987-987.

Lu, P.F. and Z. Werb. 2008. 'Patterning Mechanisms of Branched Organs', Science, 322(5907): p. 1506-1509.

Lubarsky, B. and M.A. Krasnow. 2003. 'Tube morphogenesis: Making and shaping biological tubes', Cell, 112(1): p. 19-28.

Nishiyama, A. and S. Fujiwara. 2008. 'RNA interference by expressing short hairpin RNA in the Ciona intestinalis embryo', Development, Growth & Differentiation, 50(6): p. 521-529.

Ohno, Y. and J.M. Otaki. 2015. 'Spontaneous long-range calcium waves in developing butterfly wings', BMC Dev Biol, 15: p. 17.

Passamaneck Y. J and Di Gregorio A. 2003. 'Ciona intestinalis: chordate development made simple', Dev Dyn, 233(1):1-19.

Passamaneck, Y. J. et al. 2009. 'Direct activation of a notochord cis-regulatory module by Brachyury and FoxA in the ascidian Ciona intestinalis. Development', 136(21): 3679–3689.

Carver, C. E., Mallet, A. L., and Vercaemer, B. 2006. 'Biological synopsis of the solitary tunicate Ciona intestinalis', Canadian Manuscript Report of Fisheries and Aquatic Sciences, 2746: 1488-538.

Reeves, W. et al. 2014. 'Anterior-posterior regionalized gene expression in the Ciona notochord', Developmental Dynamics : An Official Publication of the American Association of Anatomists, 243(4), 612–620.

Reinhard, E., et al. 1995. 'Localized Calcium Signals in Early Zebrafish Development', Developmental Biology, 170(1): p. 50-61.

Ryan, K. Lu, Z. and Meinertzhagen, I. A. 2016. 'The CNS connectome of a tadpole larva of Ciona intestinalis highlights sidedness in the brain of a chordate sibling', eLife, pii: e16962.

Satoh N, Satou Y, Davidson B, Levine M. 2003. 'Ciona intestinalis: an emerging model for whole-genome analyses', Trends Genet, 19: 376–381.

Satoh, N., et al. 2014. 'On a possible evolutionary link of the stomochord of hemichordates to pharyngeal organs of chordates', Genesis, 52(12): p. 925-34.

Seville, R.A., et al. 2002. 'Annexin IV (Xanx-4) has a functional role in the formation of pronephric tubules', Development, 129(7): p. 1693-1704.

Speksnijder, J.E., C. Sardet, and L.F. Jaffe. 1990. 'Periodic Calcium Waves Cross Ascidian Eggs after Fertilization', Developmental Biology, 142(1): p. 246-249.

Stemple, D. L. 2005. 'Structure and function of the notochord: an essential organ for chordate development', Development, 132: 2503-12.

Stolfi, A., et al. 2014. 'Tissue-specific genome editing in Ciona embryos by CRISPR/Cas9', Development, 141(21): p. 4115-20.

Takahashi, H. et al. 1999. 'Brachyury downstream notochord differentiation in the ascidian embryo', Genes & Development, 13(12), 1519–1523.

Takahashi, H., et al. 1999. 'Brachyury downstream notochord differentiation in the ascidian embryo', Genes & Development, 13(12): p. 1519-1523.

Ward, Christopher & F. Schneider et. al. 2004. 'Expression of ryanodine receptor RyR3 produces Ca2+ sparks in dyspedic myotubes', The Journal of Physiology, 525, pp.91-103.

Webb, S.E. and A.L. Miller. 2011. 'Visualization of Ca(2)+ signaling during embryonic skeletal muscle formation in vertebrates', Cold Spring Harb Perspect Biol, 3(2).

Webb, S.E. and A.L. Miller. 2003. 'Calcium signalling during embryonic development', Nat Rev Mol Cell Biol, 4(7): p. 539-51.

Yagi, K., Satou, Y., Satoh, N. 2004. 'A zinc finger transcription factor, ZicL, is a direct activator of Brachyury in the notochord specification of Ciona intestinalis', Development, 131: 1279-1288.

Yao, Y., J. Choi, and I. Parker. 1995. 'Quantal Puffs of Intracellular Ca2+ Evoked by Inositol Trisphosphate in Xenopus Oocytes', Journal of Physiology-London, 482(3): p. 533-553.

Petersen, J., Schou, O., and T. Peter. 1995. 'Groth and enegetics in ascidian Ciona intestinalis', Marine Ecology Progress Series, 120: 175-184.
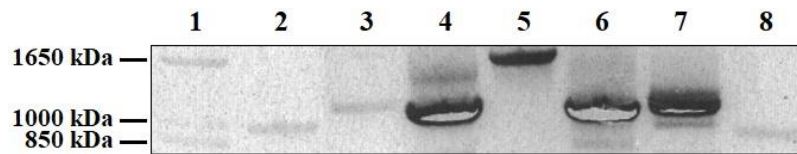
7. Appendix

Figure 1. Controlling PCR products by agarose gel electrophoresis. PCR samples contained 260 ng C. intestinalis cDNA template, 1X Green GoTaq Flexi buffer, 25 μM MgCl$_2$, 0.25 μM of each dNTP, 1 μM of each primer (3.2.2), 1.25 U/μL GoTaq@DNA Polymerase and ddH$_2$O in a total volume of 50 μL. The PCR products, and 0.9 μg 1 kb Plus DNA Ladder from Sigma, were loaded into a 1% agarose gel. PCR product bands at ca. 972-1114 bp were selected for DNA purification and recovery. Lanes; 1) 1 kb Plus DNA Ladder, 2) Ci-Brachyury, 3) Ci-connexin-related-8, 4) AT2B1;AT2B2;AT2B3, 5) Ci-TRMP1/6/7, 6) Ci-Cav1, 7) KNCQ3;KNCQ4;KNCQ5 and 8) Ci-TWIK5.